Universidad de Concepción
Facultad de Ciencias Físicas y Matemáticas

UV morphology of faint galaxies at z $<$ 0.3

Morfología ultravioleta de galaxias débiles en z $<$ 0.3

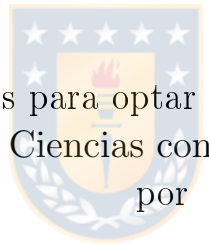

Tesis para optar al grado de
Magíster en Ciencias con Mención en Física
por

Nicole Edith Araneda Muñoz

Julio, 2019

Director de Tesis: **Dr. Sandro Villanova**

Agradecimientos

Primero, agradezco a mi madre por ayudarme a conseguir mis sueños y a seguir adelante, a mi hermana Jenny por apoyarme en los momentos difíciles y a mi padre por aceptar mis decisiones. A mi Sensei Hernán Beltrán y mi Senpai Patricia Beltrán, por enseñarme el arte de la meditación y a no rendirme jamás. A los exiliados del sexto piso (Nayda Guerrero, Jean Cortés, Gerald Neumann, papá Sebastián Pons) y a mis amigos de oficina (Carlos Torres, Antonio González, Sebastián Fuenzalida chino), por enseñarme el valor de la crítica constructiva y la amistad. A mi director de tesis, profesor Sandro Villanova, y mi tutora Paulina Assmann, por permitirme trabajar a mi ritmo y mostrarme grandes caminos. Al profesor Jiasheng, Cheng, Hai, Shumei y compañeros de la oficina de NAOC, por su simpatía y grandes aportes para mi vida. A mi esposo Luciano, por las conversaciones, consejos y apoyo incondicional. Por último, agradezco a toda persona que aportó al desarrollo de esta tesis, tanto con conocimiento, conversación, discusión y crítica.

Contents

List of Tables

List of Figures

Resumen

En esta tesis estudiamos galaxias enanas a z $<$ 0.3 con masas estelares entre 10^6 y 10^9 $M_\odot$, a partir de una muestra de 132 galaxias del campo GOODS-N de CANDELS [8, 9].

Nuestro objetivo es estudiar las galaxias enanas, su morfología y parámetros físicos para construir un catálogo y extender el límite inferior de la secuencia principal de formación estelar. Para ello, presentamos las relaciones entre la masa estelar y el tamaño de las galaxias usando el radio Petrosiano. Además, estudiamos las relaciones entre la masa estelar y la tasa de formación estelar, así como también la tasa de formación estelar específica.

Abstract

In this work, we study dwarf galaxies at z $<$ 0.3 with stellar masses in a range of 10^6 and 10^9 $M_\odot$, using a sample of 132 galaxies obtained from the GOODS-N field of CANDELS [8, 9].

The main goals of these project are to classify the morphology of dwarf galaxies, build a catalog with its physical parameters and finally make an extension of the lower limit of the main sequence of star formation. We present the relations between the stellar mass and the size of the galaxies using the Petrosian radius. Besides, we study the relations between the stellar mass, the star formation rate and specific star formation rate.

Chapter 1

Introduction

One of the most significant challenges of modern astrophysics is the understanding of how galaxies form and evolve. To face this problem, several theoretical models have been carried out assuming a Λ-CDM cosmology, where the hierarchical gravitational growth of the dark matter halos traces the large-scale structure of the observed baryonic matter. However, in the scale of galaxies, their evolution is controlled by non-linear and dissipative processes that are complex and unpredictable by theory. For such reason, it is necessary to observe different types of galaxies and clusters of galaxies to different redshifts, to allow the development of semi-analytical models of formation and evolution of galaxies. In this context, morphology plays an essential role in understanding galaxy formation and evolution, specifically correlating with the fundamental parameters such as color, luminosity, size, surface brightness, and star formation rate (SFR) [10–16]. Besides, the morphology of observed galaxies from the deep Hubble Space Telescope (HST) survey differs from that of the traditional Hubble scheme classified by local massive galaxies. High-redshift galaxies are dominated by irregular, peculiar, and merging galaxies, whereas the majority of nearby galaxies are in the form of elliptical and spiral galaxies [17–26]. On the other hand, to know the size of galaxies can help us to elucidate the history of galaxy formation and evolution. The change of size and stellar-mass relations over cosmic time would pose strong constraints on models of galaxy evolution. The observational relations between galaxy size and stellar mass have been studied in the local universe, based on the Sloan Digital Sky Survey (SDSS; [27, 28]. One other significant relation is

the called Star Formation Main Sequence (SFMS), which is a linear relation between the star formation rate and the stellar mass of star-forming galaxies. Star - forming galaxies have been studied for z $\leqslant$ 1 [5, 29, 30] and in different wavelengths, such as optical [31], infrared [32] and radio observations [33]. The tightness of the SFMS and the fact that most star-forming galaxies lie on it imply that the bulk of the star formation in the Universe occurs in a quasi-steady state [34]. Galaxies above the SFMS are called starbursts and which may or may not be merger-induced. All of these studies are limited to galaxies with stellar masses above the dwarf galaxy range 10^9 $M_\odot$.

Moreover, these studies have employed a range of different observing strategies to sample the galaxy populations as thoroughly as possible: e.g. [5–7, 33–44]. Massive galaxies have been well studied up to high redshift, but the information about the formation and evolution of galaxies at lower mass tail remain unclear. Therefore, if we want to understand the whole picture of galaxy formation is necessary to study the same properties of massive galaxies but now, for galaxies between $10^7 M_\odot$ and $10^9 M_\odot$. In this thesis, we aim to study the UV morphology of the galaxies at z < 0.3 and Absolute magnitude B > -18. As the UV emission mainly trace star-forming, we hope the UV morphology of those galaxies can help us to understand more about star formation history (SFH) or the stellar mass building history. We select 132 objects from GOODS-North of CANDELS at z < 0.3 with stellar masses between 10^7 $M_\odot$ and 10^9 $M_\odot$, we analyze their physical parameters, morphology, and make a catalog with them. Finally, this analysis lets us extend the current tail of mass-size relation and mass-SFR relation. This thesis is organized as follow: in chapter 2, we present a review of galaxy formation and evolution and the main physical and cosmographic parameters. In chapter 3, the selection of the sample and the used constraints are detailed. In chapter 4, the catalog and the results about the relations between size, SFR and stellar mass of the galaxies. Finally, we present the conclusions in chapter 5. We assume a cosmology of $(H_0, \Omega_M, \Omega_\Lambda) = (70\,\mathrm{km\ s^{-1}Mpc^{-1}}, 0.3, 0.7)$.

Chapter 2

Review of galaxy formation and evolution

The study of galaxy formation and evolution is related with the processes that formed a heterogeneous Universe from a homogeneous beginning, the formation of the first galaxies, how these galaxies change over time, and the processes that have generated the structures observed in nearby galaxies. Most of the visible matter in the Universe is concentrated in galaxies, which are the basic astronomical ecosystems in which stars are born, evolve, and die. The structural properties of galaxies and their distribution in space are determined primarily by the processes of galaxy formation. Other features such as the stellar and gas content of galaxies and their evolution with time depending mainly on the processes of formation and stellar evolution. So, for understanding the origin of the observed properties and their correlations must be considered the processes of galaxy formation and evolution. In this chapter, the overview of galaxies, their possible formation scenarios, the Hubble classification, their physical properties, and the main galaxy Surveys that helped to develop this thesis are detailed.

2.1 Galaxies

A galaxy consists of hundreds of millions or billions of stars, it can contain considerable quantities of interstellar gas and dust and can be subject to environmental influences through interactions with other galaxies and the intergalactic gas. Star formation takes place in dense regions of the interstellar gas. Also, dark matter, of nature unknown, dominate the dynamics of galaxies and clusters of galaxies. The two main types of galaxies are spirals (like the Milky Way) and elliptical galaxies. Besides, there are additional classes such as active galaxies, starburst galaxies, S0 galaxies, irregular and dwarf galaxies with significant amounts of gas. In addition to these dwarf galaxies, there is a class brighter whose morphology neither resembles a disk nor a smooth ellipsoid. These are called peculiar galaxies and include double or multiple sub-components linked by a filamentous structure and highly distorted with extended tails are usually associated with recent mergers or tidal interactions. Although peculiar galaxies only constitute a small fraction of the entire galaxy population, their existence conveys important information about how galaxies may have changed their morphologies during their evolutionary history. All these classes differ not only in their morphology, which forms the basis for their classification but also in their physical properties such as color (indicating a different stellar content), internal reddening (depending on their dust content), amount of interstellar gas, SFR, etc. Galaxies of different morphologies have evolved in different ways.

2.2 Galaxy formation scenarios

Two main theories of galaxy formation and evolution have been proposed. The classical, monolithic or "top-down" model suggests that galaxies form and evolve as isolated bodies in a single, rapid collapse of gas and dark matter, during which virtually all the gas was turned quickly into stars. In this scenario, galaxies evolve of a predetermined fashion dependent on the initial conditions and with little impact from the environment.

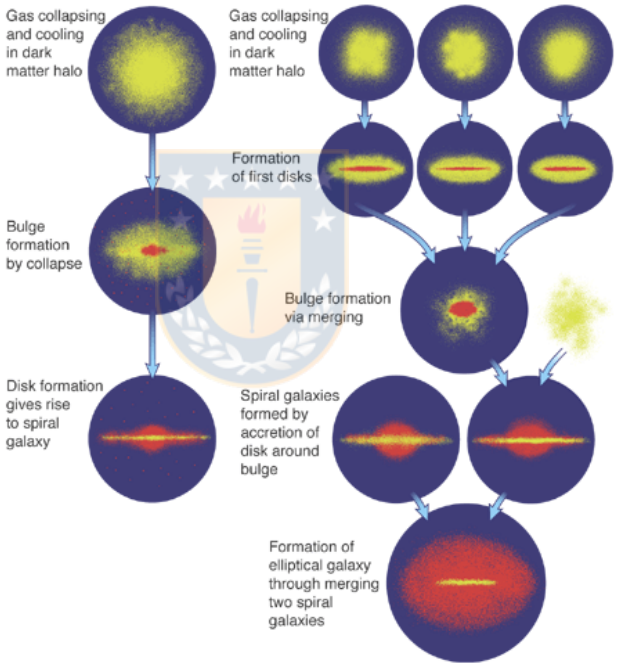

Figure 2.1: Leading models of galaxy evolution: Monolithic collapse model (left). Hierarchical model (right). Blue: dark halo, yellow: gas, red: stars. Source: [45].

The hierarchical or "bottom-up" model proposes that giant ellipticals form mostly through mergers of smaller galaxies that have already converted some of their gas into stars and their fate is more dependent on the environment which they inhabit. Each scenario of formation requires a particular type of dark matter that makes up a significant part of the Universe not visible to our instruments. These types of dark matter correspond to hot dark matter and cold dark matter.

Hot dark matter is composed of relativistic particles (e.g. neutrinos), so erases small-scale density fluctuations resulting in "top-down" formation of structure. Cold dark matter is composed of non-relativistic particles (e.g. axions or WIMPS), so density fluctuations at all scales survive, resulting in hierarchical structure formation. Cold dark matter is non-baryonic, unlike normal baryonic matter, with which it does not interact except by gravity. This component consists of the energy density of the current Universe. The observational evidence over time has demonstrated both present theories shortcomings.

2.2.1 Λ - CDM cosmological model

The Λ-CDM cosmological model is a hierarchical model which considers that galaxies form inside dark matter (DM) haloes. The cosmological constant is described in terms of Ω_Λ that correspond to the energy density ratio of a flat Universe.

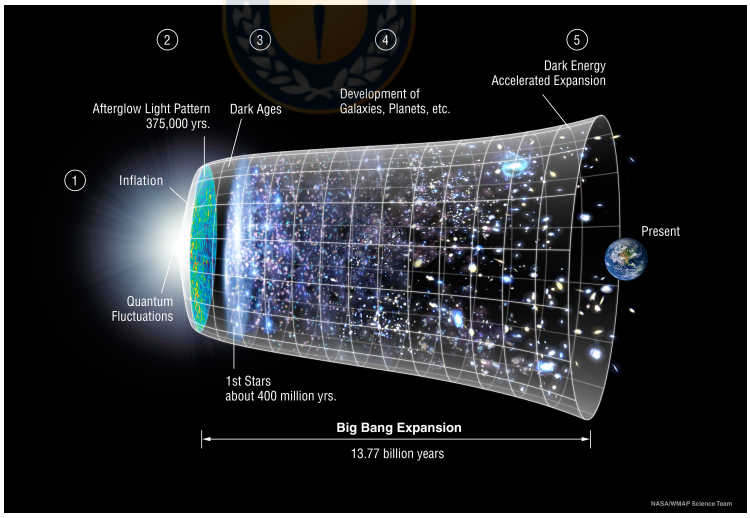

Figure 2.2: Λ-CDM cosmological model: a representation of the evolution of the Universe over 13.7 billion years. Source: NASA / WMAP Science Team.

In this model, larger DM haloes form through the merging of smaller DM haloes, a process which is driven by gravitational forces. These more minor DM haloes originate from fluctuations of the primordial density field and are amplified by the effect of gravity.

With the evolution of matter over time, these haloes eventually, transform into the known structures that we can observe today. High-resolution numerical simulations have been performed to study how matter evolves in the Universe according to the Λ - CDM model. Example of these are the Millennium simulations [46] and the Milky Way [47].

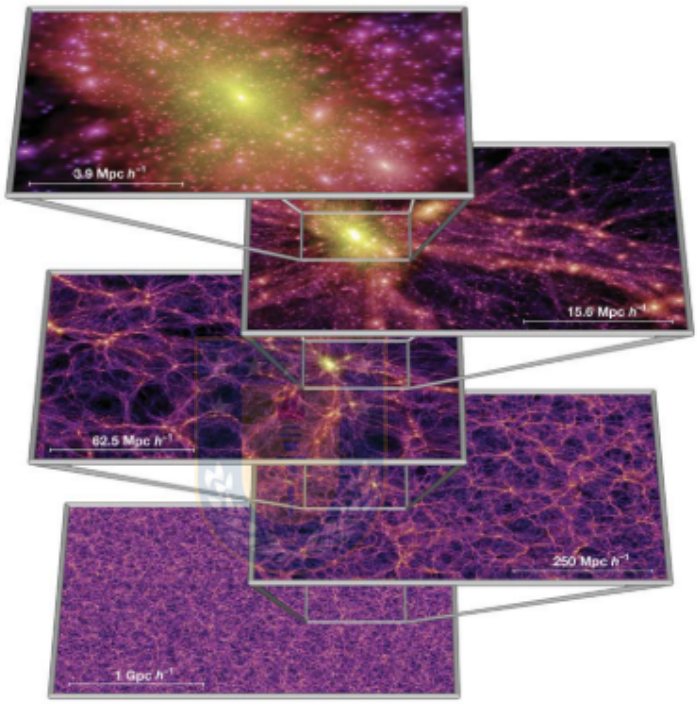

Figure 2.3: The Millennium simulations. This picture shows the dark matter distribution in the Universe at the present time, based on the Millennium Simulation, one of the largest N-body simulation carried out so far (more than 10^{10} particles). Source: [46].

A large number of observed objects, the measurements of the anisotropic microwave background radiation [48], and the detection of supernovae (SNe) of type Ia in distant galaxies [49–51] have significantly improved our understanding of the Universe. It is now widely accepted that the Universe is flat, with the cosmological parameters approximately given by: the Hubble constant $H_0 = h100$ [km s^{-1} Mpc^{-1}] with $h = 0.72$, the baryonic mass fraction $\Omega_b\, h^2 = 0.0227$ and the total mass fraction $\Omega_m\ h^2 = 0.133$ [52].

A problem related to the Λ-CDM model is that it predicts that the number of dwarf galaxies orbiting the Milky Way is larger than the number of observed galaxies [47, 53], even if we consider the recent observations of SDSS (Sloan Digital Sky Survey) between 2006 and 2007 through which the number of known dwarf galaxies doubled [54–58]. A possible explanation is found in [59], where they combine a dynamical model for the CDM sub-halo populations.

2.3 Galaxy morphology

The study of properties of galaxies is essential to develop a classification into morphology types because it shows different astrophysical properties and reflecting the various histories of formation and evolution of galaxies [60]. The first typically used method for studying galaxies morphology consists to visually look at individual galaxies and classify them into a previously established system. The second method is to quantify how a galaxy's light distribution changes from the center to its edge. If it is very concentrated in the center can be an elliptical galaxy and if it is extended can be a disk galaxy. The third technique consists of quantifying how asymmetric a galaxy is, rotating an image by 180 degrees and subtracting it from the original. The result indicates how asymmetric it is. This method is commonly used to identify galaxy mergers since they are typically irregular systems. Several attempts have been proposed for automated classification of morphologies [10, 61–63], but visual classification still serves as the most reliable method when we adopt the Hubble classification [64] for galaxies with large apparent sizes.

2.4 Hubble Sequence

In 1936, Edwin Hubble defined the "Hubble Sequence of Galaxies", described in Hubble's monograph The "Realm of the Nebulae" [65]. This Hubble sequence sometimes referred to as a tuning-fork diagram, arranges galaxies into a continuous sequence with elliptical galaxies at the left-hand end and spirals at the right-hand end.

The spiral galaxies are ordered into two branches named normal and barred spirals. Conventionally, galaxies of the left-hand end of the sequence are referred to as early-type galaxies and of the right-hand end as late-type galaxies. Spiral galaxies (late-type galaxies) are systems in which star formation is active.

The S0 galaxies, of intermediate type, show a disk similar to that of spiral galaxies but they consist mainly of old stars, i.e., stars of low mass and low temperature.

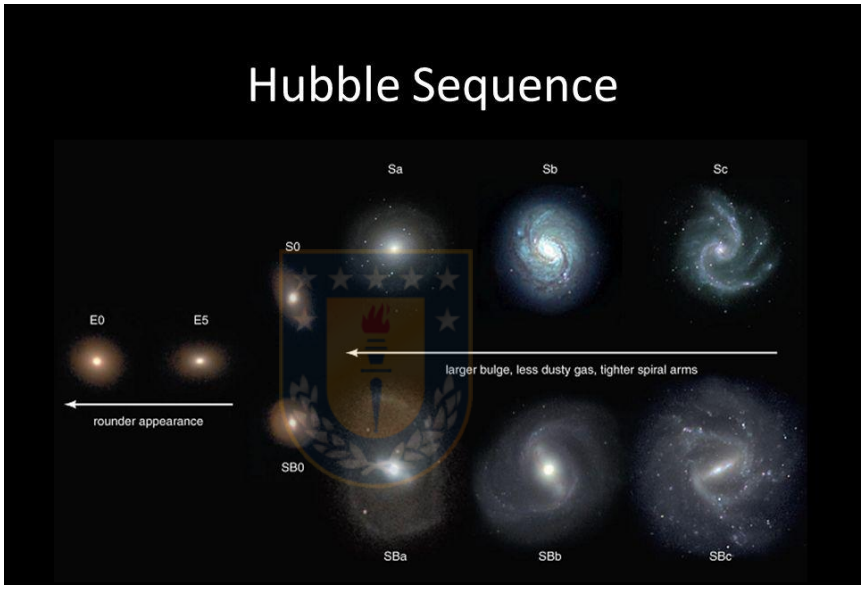

Figure 2.4: Hubble sequence of galaxies. Source: Barbra Shelton.

On the other hand, elliptical galaxies (early-type galaxies) are systems in which star formation finished a long time ago, so present mainly old stars. The majority of galaxies can be accommodated within the revised Hubble Sequence of galaxies, which is described in detail by [66–70]. Van den Bergh emphasized that the classical Hubble types refer primarily to intrinsically luminous galaxies and that, besides, there exists a large population of intrinsically low luminosity dwarf galaxies which can only be observed relatively nearby. The important aspect of the Hubble sequence is that many intrinsic properties of galaxies, such as luminosity, color and gas content, change systematically along this sequence and is probably disks and ellipsoids have very different formation mechanisms.

Therefore, the morphology of a galaxy, or its location along the Hubble sequence, is directly related to its formation history. Besides of visible matter, the galaxies contain a large amount of dark matter. However, we can only get rough estimates of the extent of its halo, although there are strong indications that it is substantially larger than the extent of the visual matter. Next, we present the main types of galaxies of the Hubble Sequence.

2.4.1 Elliptical galaxies

Elliptical galaxies have very little gas and dust, so are formed by old stars (Population II stars) and have smooth light distributions, where the isophotes, lines of constant surface brightness, have elliptical shapes.

Figure 2.5: Elliptical galaxy IC 2006. Source: Hubble Space Telescope.

These galaxies are classified according to its ellipticity that is denoted as En, where $n = 10(1 - \frac{b}{a})$, and a and b are the semi-major and semi-minor axis of the ellipse respectively. Thus, a galaxy with ellipticity E0 is round, and with E7 is flattened. A 3D ellipsoidal shape, with semi-axes a, b and c (ordered as $a \geq b \geq c$), is called oblate when $a = b > c$ (a pancake), prolate when $a > b = c$ (a cigar), and tri-axial when $a > b > c$ (a squashed American football ball). Elliptical galaxies have not current star formation.

Besides, these are preferentially produced in clusters of many ellipticals and have little evidence for rotation, so the stars must have large random motions to keep the system from collapsing (also called a hot stellar system).

2.4.2 Spiral Galaxies

Spiral galaxies have three main components: bulge, disk and halo. The bulge is a spherical structure that is located in the center of the galaxy and mostly contains old stars. In the disk is formed the spiral arms that contain dust, gas and young stars. The halo is a spherical structure located around the bulge and some disks. It contains old star clusters, known as globular clusters. Its diameter (measured on the extent of the starlight) is between 10 and 50 kpc. Spiral galaxies are classified

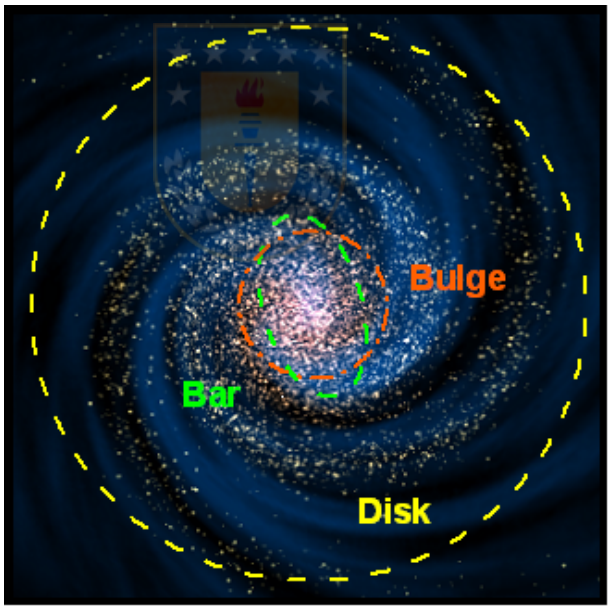

Figure 2.6: Spiral galaxy: a face-on view of a disk galaxy with spiral arms, bar and bulge. Source: Jakub Schwarzmeier.

into two groups, normal and barred. The first group is designated by S or SA and the second group by SB. In the normal spirals, the arms originate directly from the nucleus, while in the spirals with bars the arms emerge of a bar of material that crosses the nucleus. These two types are assigned a classification according to the narrowness with which they wrap their arms.

The classifications are a, b, c and d. Letter "a" indicate tighter arms, are usually not well defined and form an almost circular pattern. If the classification of a galaxy presents two lowercase letters, it means that the tension of the spiral structure is halfway between these two letters.

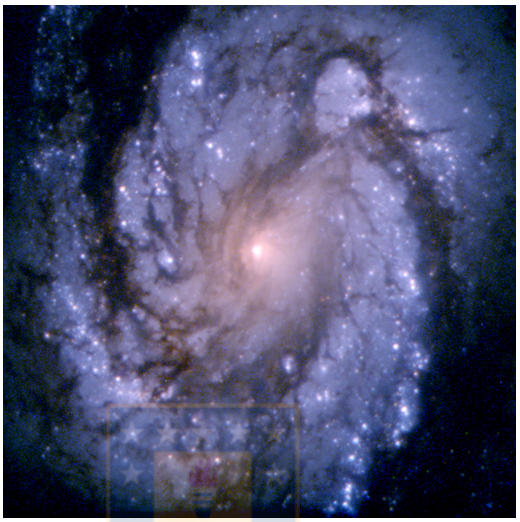

Figure 2.7: Normal spiral galaxy NGC 4321. Source: Hubble Space Telescope.

Figure 2.8: Barred spiral galaxy NGC 1365. Source: SSRO/PROMPT and NOAO/AURA/NSF.

2.4.3 Lenticular galaxies

Galaxies with smooth light distributions and axial ratios $b/a < 0.3$ show evidence of a disk-like component and these are called lenticular (lens-like) or S0 galaxies. They differ from ellipticals because they have a bulge and a thin disk, but are different from spirals because they have no spiral structure. The lenticular galaxies appear intermediate in morphological type between elliptical and spiral galaxies.

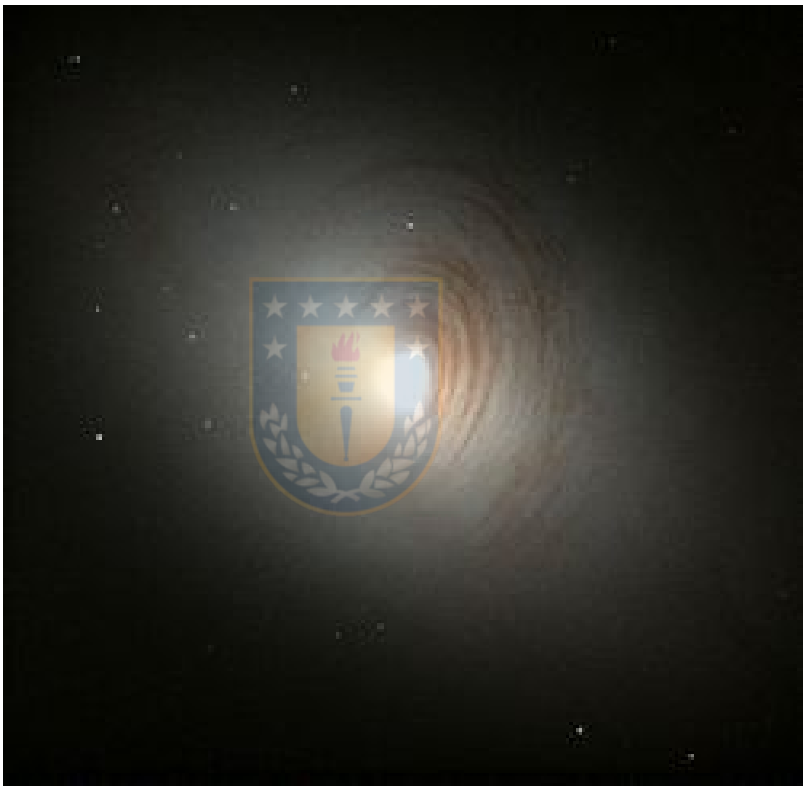

Figure 2.9: NGC 2787: the SB0 or lenticular galaxy NGC 2787. Source: NASA, ESA and the Hubble Heritage Team (STScI/AURA).

Just like spiral galaxies, some lenticular galaxies have a bar. They are called barred lenticular galaxies and are denoted SB0. Normal lenticular galaxies are denoted S0.

2.4.4 Irregular Galaxies

In Hubble's original classification, irregular galaxies were systems "lacking both dominating nuclei and rotational symmetry"and the class included everything which could not be readily incorporated into the standard Hubble sequence. Many of these irregulars were similar to neighbor galaxies of our own Galaxy as Magellanic Clouds, and these were designated Irr I or Magellanic irregulars. Galaxies such as M82, NGC 520 and NGC 3077, in which there was no evidence of resolution into stars, were classified Irr II galaxies.

Figure 2.10: Magellanic clouds: the Large and Small Magellanic Clouds (the LMC and SMC, respectively) are classified as irregular dwarf galaxies. Source: ESO/S. Brunier.

2.5 Fundamental parameters

The important observational properties of galaxies are color, internal reddening, amount of interstellar gas, SFR, SFH and stellar mass. The studies about the relation between SFR, stellar mass and size of the galaxies are presented. Besides, cosmographic parameters as redshift, angular diameter distance, luminosity distance and K-correction are described.

2.5.1 Stellar mass and size

The scale size of galaxies is one of the fundamental parameters to study the history of galaxy formation and evolution. Many studies have investigated sizes of massive galaxies at a higher redshift using rest-frame optical bands, which presumably trace the distribution of stellar mass ($M_* \gtrsim 10^{10}$ $M_\odot$). Besides, [71] studied the stellar mass and size relation in late-type galaxies at $0.2 < z < 1$ and [72, 73] in early- type galaxies. For other hand, [74] and [75] gave size-mass relations in massive galaxies ($M_* \gtrsim 10^{10.5}$ [$M_\odot$]) at $z \sim 1.5$, while [76] studied the relation with large samples of galaxies at $z \lesssim 2$. For higher redshifts $z \sim 3$, size-mass relations have been obtained for galaxies with $M_* \gtrsim 10^{10}$ [$M_\odot$] [77–79]. Many studies have corroborated that massive galaxies at high redshifts were much smaller than local galaxies with comparable mass [23, 74, 79–92]. At a fixed stellar mass, spheroidal galaxies were significantly more compact at high redshift and evolved with a rapid increase of the effective radius by a factor ~ 4 or even larger from $z \sim 2$ [85, 90] and by a factor ~ 2 from $z \sim 1$ [73, 93]. The findings demonstrate that massive galaxies have increased their size dramatically since $z \sim 3$ of a different manner from the evolution of less massive galaxies. However, other studies have reached contradictory conclusions. There is significant disagreement between the results of different investigations. [71] found weak or no evolution in the relation between stellar mass and effective disk size for galaxies with $M_* > 10^{10}$ [$M_\odot$] since $z \sim 1$. Very deep observations e.g., [23, 91, 94] or stacking methods to enhance the faint envelope of galaxies e.g., [84, 86, 88, 93] have claimed that it is not the case.

For studying galaxies of low surface brightness or galaxies which are dimmed due to the cosmological expansion at high redshift to measure the radius at the faint outskirt of galaxies, the depth is crucial.

Petrosian Radius

Since the galaxies have not the same brightness profile of radial surface nor defined edges, is difficult to measure their flux. To overcome this problem, SDSS has adopted a modified form of the [95] system, which measures the fluxes of galaxies within a circular aperture whose radius is defined by the shape of the azimuthally averaged light profile. Petrosian ratio $\mathcal{R}_P$ is defined as a radius r from the center of an object to be the ratio of the local surface brightness in an annulus at r to the mean surface brightness within r, as described by [96, 97],

$$\mathcal{R}_{P(r)} = \frac{\int_{0.8r}^{1.25r} dr' 2\pi r' I(r') / [\pi(1.25^2 - 0.8^2) r^2]}{\int_0^r dr' 2\pi r' I(r'/\pi r^2)}, \tag{2.1}$$

where $I(r)$ is the azimuthally averaged surface brightness profile.
The Petrosian radius r_P is defined as the radius at which $\mathcal{R}_P(r_P)$ equals some specified limit value $\mathcal{R}_{P,lim}$, set to 0.2, 0.5 or 0.9 in our case. The solution of the following equation represent Petrosian radius,

$$I(\mathcal{R}_P) = \eta \frac{\int_0^{\mathcal{R}_P} I(r) 2\pi r dr}{\pi {R_P}^2}, \tag{2.2}$$

where the integral represents the sum of the intensity of light in a circular aperture of radius r_P, the denominator is the area of the aperture and the result of the division is the uniform superficial density of intensity for the circular aperture.

Since the observed intensity coincides with calculated uniform intensity, the Petrosian radius is designed to measure a constant fraction of the total light independent of the surface brightness limit. Petrosian ratio is a good way to get a sample of irregulars galaxies or some galaxies we don't know if are regulars because this method allows measuring a constant fraction of the total light, regardless of the position and distance of the object.

2.5.2 Stellar mass and SFR

The SFR and stellar mass are the main parameters estimated from large samples of galaxies. The SFR is the total mass of stars formed per year, often given as solar masses per year. This parameter also is symbolized by $\dot{M}_*$, often with units of solar mass per year or solar mass per million years, and its meaning depends on how much averaging over time and space is involved. Numerous works found a tight relation between the SFR and stellar mass both at low and high redshift, often called the Main Sequence (MS) of galaxies [34, 98]. The slope and the scatter of this relation, as well as its evolution with redshift, put constraints on the SFH of the galaxies as a function of their mass: the galaxies located on this MS may experience a rather smooth star formation evolution during several Gyr and the starburst mode seems to play a minor role in the production of stars [98]. Major progress has been made in the measure of the SFR inside the disk of nearby galaxies, with a strong relation found between the SFR and the molecular gas content [99], and measurements of the star formation efficiency in galaxies are now possible up to large redshifts [100]. Besides, these studies aimed at understanding the process of star formation, the global amount of star in the Universe is measured by building statistical samples, with observables related to the recent star formation [101]. To understand the relation between the star formation and stellar mass, one simple method is to compare the ultraviolet (UV) and Near-infrared (NIR) bands images under a similar resolution. The UV image shows the hint of the star formation morphology while the NIR image can be used to trace the stellar mass distribution. SFR is a key parameter to understand galaxy formation and evolution due to its fundamental relation with the stellar mass and the gas reservoir on which our understanding of galaxy formation and evolution is based. Yet, despite its considerable importance, measuring star formation accurately remains difficult [1].

Star Formation History

One of the key assumptions to measure the SFR of a galaxy is its SFH. The SFH is how stars formed over time and space, whether in short bursts or over longer periods. Most classical estimators are based on the assumption of a constant SFR over a period of 100 [Myr] e.g. [102].

If this assumption may seem reasonable for low redshift spiral galaxies evolving secularly, it is unlikely to hold true for interacting systems or at higher redshift where the SFR necessarily varies on timescales that can be similar or shorter than 100 [Myr]. With the increasing availability of observations spanning a broad range of wavelengths, one possibility to waive the assumption on the SFH is to carry out multi-wavelengths spectral energy distribution (SED) modeling. The SFH can then be left as a free parameter to compute the SFR,

$$\text{Exponential tau Model SFH}(t) \propto e^{\frac{-t}{\tau}} \tag{2.3}$$

$$\text{Delayed tau Model SFR}(t) \propto te^{\frac{-t}{\tau}} \tag{2.4}$$

$$\text{Constant Model SFH}(t) = \text{Constant}, \tag{2.5}$$

Unfortunately, the SFH is degenerate with other parameters such as the attenuation. For instance, a galaxy can exhibit a red UV slope because it is dusty and actively forming stars, or because it is not forming stars anymore. If multi-wavelengths data partly alleviate this problem when UV and IR (infrared) data are simultaneously available, the SFH still remains poorly constrained.

2.5.3 Stellar mass and SSFR

In recent years, it also has become common to compare galaxies in terms of their SFR per unit galaxy mass, or Specific Star Formation Rate (SSFR).
SSFR is represented by,

$$\text{SSFR}[yr^{-1}] = \frac{\text{SFR}[M_\odot/yr]}{M_*[M_\odot]}. \tag{2.6}$$

In [103] investigated the SSFR (SFR per unit galaxy stellar mass) as a function of galaxy stellar mass and redshift and they found that, at all redshifts, the SSFR decreases as stellar mass increases. This indicates a higher contribution of SF to the growth of low-mass galaxies since z = 1.5 and suggests that high mass galaxies formed the bulk of their stellar content earlier than z = 1. Besides, in [7] confirm that the mass-SFR relation has a slope close to unity (see also [5, 6, 33, 38, 104]).

Such a slope can be obtained by fitting either the entire star-forming galaxies (SFG) sample dominated by low-mass ones or the mean/median SFRs at given stellar masses. Is important noting that the slope is sensitive to the sample selection. A slope of unity for the mass–SFR relation means that SFGs of different stellar masses have a nearly constant SSFR in the population average sense. Together with the fact that the slope of the mass–SFR relation does not change much from z $\sim$ 2 to the present day [33], this supports the picture that star formation in SFGs is generally driven by gas accretion from a gradually decreasing gas reservoir in galaxy halos from high to low redshift [105, 106].

2.6 Cosmographic Parameters

We provide detailed information regarding the cosmological parameters that we use during the development of this thesis, using as reference [107].

2.6.1 Redshift

The redshift z of an object is the fractional Doppler shift of its emitted light resulting from radial motion,

$$z \equiv \frac{\nu_e}{\nu_o} - 1 = \frac{\lambda_o}{\lambda_e} - 1, \tag{2.7}$$

where ν_o and λ_o are the observed frequency and wavelength, ν_e and λ_e are the emitted. In special relativity, redshift is related to radial velocity v by

$$1 + z = \sqrt{\frac{1 + v/c}{1 - v/c}}, \tag{2.8}$$

where c is the speed of light.

Spectroscopic and photometric redshift

Spectroscopy measures the spectrum of electromagnetic radiation, including visible light and radio, which radiates from stars and other celestial objects.

A stellar spectrum can reveal properties of stars, such as their chemical composition, temperature, density, mass, distance, luminosity and relative motion using Doppler shift measurements. The process to get a stellar spectrum consists in pass the light through a dispersive element and then record the dispersed light. Thus, we have a record of the intensity of the light as a function of wavelength. The main advantage is that we can record the light of one or more objects over a very wide wavelength range, have excellent fine discrimination between different wavelengths and look for individual spectral features. The disadvantage is that spread the light from the source thinly over the detector and it can be difficult to get spectra of many sources in one go (maybe 10 s to 100 s if it uses multi-slit of multi-fibre spectrographs). To get a redshift from a spectrum, it must try to do match the positions of known spectral features and measure the wavelength shift from the rest-frame.

Photometry consists in measuring the flux or intensity of electromagnetic radiation of an object. Typically, photometric measurements of multiple objects obtained through two filters are plotted on a color-magnitude diagram. The process consist in record images of interest sources where the light is allowed to pass through colored filters. The only wavelength information we have is the intensity of light admitted through the filter (and also modified by the detector response). The main advantage is that the light from a source over our filter band is concentrated on a spot in the detector, giving better signal-to-noise ratios. We also get data for as many sources are in the image. The disadvantage is that the effective wavelength resolution is only as good as how narrow the filter band-passes are. It loses the ability to see individual spectral features. Estimating a redshift from Photometry needs images taken through several filters and the spectral energy distributions SED (the crude intensity vs wavelength relation defined by the few photometric brightness measurements) are matched with those predicted from a library of model galaxies redshifted by differ-

ent amounts. The detectors used for both techniques is usually a CCD camera. So what differs is what is in the instrument prior to the CCD. For spectroscopy, it is a dispersive element, for Photometry a colored filter. Albeit is less accurate than spectroscopy, photometric redshifts provide a way to estimate distances of galaxies too faint for spectroscopy or samples too large for complete spectroscopic coverage. The photometric redshift technique is usually divided into two groups, template fitting and empirical fitting. Template fitting technique derives the photometric redshift by minimizing the value χ^2 when comparing an observed SED with the SED computed from a template library that includes spectral-energy distributions for a variety of galaxy types (representing different redshifts, SFH, chemical abundance and mixtures of dust and stars). Empirical technique uses a training set of galaxies with known spectroscopic redshifts to derive a relation between observed Photometry and redshifts. Photometry redshift accuracy for the low redshift galaxies are not as good as the photometric redshift at higher redshift [108].

2.6.2 Angular diameter distance

The angular diameter distance D_A is defined as the ratio of an object's physical transverse size to its angular size (in radians). It is used to convert angular separations in telescope images into proper separations at the source. Angular diameter distance is related to the transverse co-moving distance by

$$D_A = \frac{D_M}{1+z} \tag{2.9}$$

where D_M is comoving distance, defined as the ratio of the actual transverse velocity (in distance over time) of an object to its proper motion (in radians per unit time) [109–111].

2.6.3 Luminosity distance

The luminosity distance D_L is defined by the relationship between bolometric (i.e, integrated over all frequencies) flux S and bolometric luminosity L,

$$D_L \equiv \sqrt{\frac{L}{4\pi S}}. \tag{2.10}$$

It turns out that this is related to the transverse comoving distance and angular diameter distance by

$$D_L = (1+z)D_M = (1+z)^2 D_A \tag{2.11}$$

[109, 110]. The latter relation follows from the fact that the surface brightness of a receding object is reduced by a factor $(1+z)^{-4}$, and the angular area goes down as D_A^{-2}.

If use differential flux S_ν and luminosity L_ν, then k-correction, must be applied to the flux or luminosity because the redshifted object is emitting flux in a different band than that in which we are observing. The k-correction depends on the spectrum of the object in question and is unnecessary only if the object has spectrum $\nu L_\nu =$ constant. For any other spectrum, the differential flux S_ν is related to the differential luminosity L_ν by

$$S_\nu = (1+z)\frac{L_{(1+z)\nu}}{L_\nu} \tag{2.12}$$

where z is the redshift. The ratio of luminosities equalizes the difference in flux between the observed and emitted bands, and the factor of (1 + z) accounts for the redshifting of the bandwidth.

2.6.4 K correction

The K corrections for galaxies of different morphological types are necessary to interpret the magnitude-redshift relation, the luminosity function of galaxies and for most of the spectrophotometric studies of distant objects. The K correction is defined as the corrective term that needs to be applied to the observed magnitude in a certain band due to the effect of redshift. In other words, the transformations between observed and rest-frame broad-band photometric measurements involve terms known as "K corrections" [112, 113]. In [114], they consider a source observed at redshift z, meaning that a photon observed to have frequency ν_o was emitted by the source at frequency ν_e with

$$\nu_e = (1+z)\nu_e. \tag{2.13}$$

The apparent flux of the source is imagined to be measured through a finite observed-frame band-pass R and the intrinsic luminosity is imagined to be measured through a finite emitted-frame band-pass Q. The K correction is used in relating these two quantities. If we consider a source observed have apparent magnitude m_R when observed through photometric band-pass R and one wishes to know its absolute magnitude M_Q in emitted-frame band-pass Q, the K correction $\mathrm{K_{QR}}$ for this source is defined by

$$m_R = M_Q + DM + K_{QR} \tag{2.14}$$

where DM is the distance modulus, defined by

$$DM = 5 \log_{10} \left(\frac{D_L}{10[\mathrm{pc}]} \right) \tag{2.15}$$

and D_L is the luminosity distance [114]. The apparent magnitude m_R of the source is related to its spectral density of flux f_ν (ν) (energy per unit time per unit area per unit frequency) by

$$m_R = -2.5 \log_{10} \left[\frac{\int \frac{d\nu_o}{\nu_o} f_\nu(\nu_o) R(\nu_o)}{\int \frac{d\nu_o}{\nu_o} g_\nu^R(\nu_o) R(\nu_o)} \right] \tag{2.16}$$

where the integrals are over the observed frequencies ν_o. $g_\nu^R(\nu)$ is the spectral density of flux for the zero-magnitude or "standard" source that, in our case, we considered for AB magnitudes [115], a hypothetical constant source with $\mathrm{g_\nu^{AB}}(\nu) = 3631$ [Jy] (where 1 [Jy] = 10^{-26} [W m $^{-2}$ Hz $^{-1}$] = 10^{-23} [erg cm $^{-2}$ s $^{-1}$ Hz $^{-1}$]) at all frequencies ν. Because the detector is a photon counter, like a CCD, R(ν) is just the probability that a photon of frequency ν_o gets counted. The absolute magnitude M_Q is defined to be the apparent magnitude that the source would have if it were 10 [pc] away, at rest (i.e., not redshifted), and compact. It is related to the spectral density of the luminosity $\mathrm{L}_\nu(\nu)$ (energy per unit time per unit frequency) of the source by

$$M_Q = -2.5 \log_{10} \left[\frac{\int \frac{d\nu_e}{\nu_e} \frac{L_\nu(\nu_e)}{4\pi(10\ [pc])^2} Q(\nu_e)}{\int \frac{d\nu_e}{\nu_e} g_\nu^Q(\nu_e) Q(\nu_e)} \right] \tag{2.17}$$

where the integrals are over emitted (i.e., rest-frame) frequencies ν_e, D_L is the luminosity distance and Q(ν) is the equivalent of R(ν) but for the band-pass Q.

If the source is at redshift z, then its luminosity is related to its flux by

$$L_\nu(\nu_e) = \frac{4\pi D_L^2}{1+z} f_\nu(\nu_o), \tag{2.18}$$

$$\nu_e = [1+z]\nu_e. \tag{2.19}$$

K correction emitted-frame luminosity $L_\nu(\nu_e)$ is represented by,

$$K_{QR} = -2.5\ \log_{10}\left[[1+z]\frac{\int \frac{d\nu_o}{\nu_o} L_\nu([1+z]\nu_o) R(\nu_o) \int \frac{d\nu_e}{\nu_e} g_\nu^Q(\nu_e) Q(\nu_e)}{\int \frac{d\nu_o}{\nu_o} g_\nu^Q(\nu_o) Q(\nu_o) \int \frac{d\nu_e}{\nu_e} L_\nu(\nu_e) Q(\nu_e)}\right]. \tag{2.20}$$

All the last calculations were performed in frequency units. For get it in wavelength units, the spectral density of flux $f_\nu(\nu)$ per unit frequency should be replaced with the spectral density of flux $f_\lambda(\lambda)$ per unit wavelength using

$$\nu f_\nu(\nu) = \lambda f_\lambda(\lambda), \tag{2.21}$$

$$\lambda\nu = c \tag{2.22}$$

where c is the speed of light.

2.7 Surveys

2.7.1 Cosmic Assembly Near-IR Deep Extragalactic Legacy Survey

The CANDELS [8, 9] is designed to document the first third of galactic evolution from redshift = 8 to 1.5 via deep imaging of more than 250,000 galaxies with WFC3/IR and ACS. It will also find the first Type Ia SNe beyond redshift > 1.5 and establish their accuracy as standard candles for cosmology. Five premier multi-wavelength sky regions are selected; each has multi-wavelength data from Spitzer and other facilities and has extensive spectroscopy of the brighter galaxies. The use of five widely separated fields mitigates cosmic variance and yields complete samples of galaxies down to 10^9 solar masses out to redshift ~ 8.

Description

The CANDELS survey consists of a two-tier Deep+Wide survey designed. The CANDELS Deep portion covers ∼125 [arcmin^2] to ∼10-orbit depth within the GOODS-N and GOODS-S fields [116], including the E-CDFS [117] as well as the WFC3 ERS2 field [118]. The full area of the CANDELS survey covers a total lower Wide portion to ∼2-orbit depth around the Deep portions of ∼800 [arcmin^2], where the additional area includes the shallower Wide portion to ∼2-orbit depth around the Deep portions of GOODS, together with subsections of three additional fields, namely EGS [119], COSMOS [120, 121] and UKIDSS UDS [122, 123].

All five fields have extensive catalogs that can serve as astrometric and photometric reference standards as well as being combined with the catalogs from new HST data to obtain derived measurements of source properties as photometric redshifts, stellar masses and SFHs.

GOODS-N

The GOODS-N field is located near the northern Hubble Deep Field [124] and like its southern counterpart has been extensively observed by NASA's Great Observatories. The field is centered at α(J2000) = 12h 36m 55s and δ(J2000) = +62° 14m 15s. The GOODS region of the field has been imaged in the optical with Hubble/ACS in the B, V, i, and z bands as part of the GOODS Hubble Treasury Program.

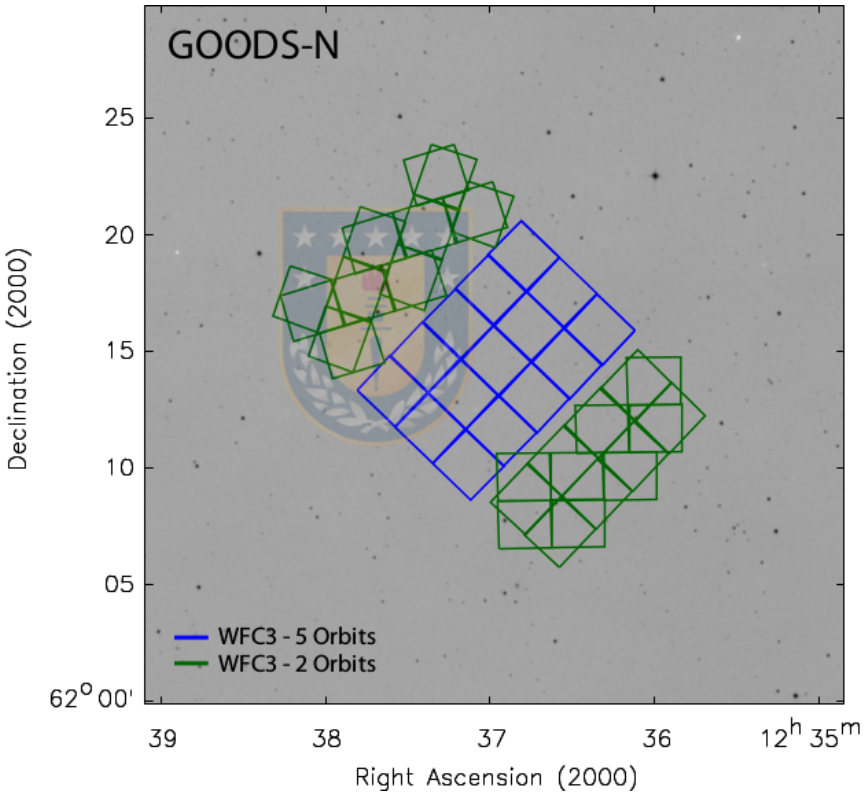

Figure 2.11: GOODS-N field. Source: [9].

Filters and Exposure Times

The GOODS-N field contains the Deep portions of the CANDELS survey, with a total depth of at least 4 orbits in both WFC3/IR F125W and F160W and 3 orbits in F105W, spread across 10 epochs. Each single-orbit pointing, for each epoch, contains four WFC3/IR exposures (two F125W and two F160W) and one WFC3/UVIS

(F350LP). In parallel, it also obtains five ACS/WFC exposures, where the primary requirement is to obtain at least 32,000 [s] depth in F814W. Then, next ACS/WFC priorities are ∼2500 [s] of F850LP, followed by ∼5000 [s] in F606W and finally, any remaining depth is placed back into F814W.

Since the GOODS-N field is in the CVZ, some portions of the orbit are too bright for observations using WFC3/IR, so WFC3/UVIS exposures are substituted using the F275W and F336W filters. In these cases, the ACS parallels retain their structure as described for the remainder of the Deep observations.

Mosaic Layout Design

For each of the five CANDELS fields, the goal is to cover a contiguous area with WFC3/IR (thus, the larger ACS/WFC parallel exposures overlap somewhat to create deeper pointing), and to overlap as much as possible the existing relevant ancillary data sets. For the GOODS-N and GOODS-S Deep regions, the layout consists of a smaller rectangular grid of 3×5 tiles ($\sim 6.'5 \times 10.'8$). An important feature of CANDELS is the fact that GOODS-N field is in the HST CVZ and thus, it uses the bright day side of the orbit to observe with WFC3/UVIS in the UV (F275W and F336W). This enables measurements of the Lyman continuum (LyC) escape fraction (f_{esc}) from galaxies at z ≈ 2.5, identification of ∼350 LBGs at z ≈ 2, and measurements of the SFR in low-luminosity dwarfs which may just be "turning on" at z ≈ 1 [125, 126]. There are ∼40-50 UV-luminous LBGs ($L_{UV} > 0.25L_*$) in this field at $2.38 < z < 2.55$ (half with spectroscopic redshifts), which is the optimal redshift for constraints with the F275W filter, many of which may be bright enough to detect if $f_{esc} > 0.5$ e.g. [127, 128]. The structure of the survey includes essential elements of two MCT programs that were submitted separately. The first program involved studying the full area of the GOODS-North and GOODS-South fields [116] to a uniform depth, including also ultraviolet (UV) imaging, and carrying out an extensive search for high-redshift SNe Ia. The other program, was aimed at studying half the GOODS-N and GOODS-S areas to a greater depth, together with wider and shallower imaging of the Extended Groth Strip EGS [119], COSMOS [120, 121], and the UKIDSS Ultra-Deep Survey UDS [122, 123].

2.7.2 Hubble Deep UV Legacy Survey

The HDUV is a legacy program using the Hubble Space Telescope to obtain deep UV images of the central parts of the two GOODS fields, which was approved in HST Cycle 22. It builds on existing WFC3/UVIS data to obtain deep images at 250-350 nm (in F275W and F336W). These unique UV imaging data provide a complete census of low-luminosity star-forming galaxies at z 0.5-2 and enable a wealth of research by the community. This includes measuring the physical properties of sub-L* galaxies, and characterizing resolved stellar populations to decipher the build-up of the Hubble sequence from sub-galactic clumps. It provides background-subtracted, drizzled F275W and F336W images of the complete HDUV survey data in addition to all the CANDELS F275W UV imaging in GOODS-N.

2.7.3 Sloan Digital Sky Survey

The SDSS [3, 129] searches to get spectroscopic and photometric data across π sr. The survey is conducted using a dedicated 2.5-m telescope at Apache Point Observatory. The photometry is obtained using drift-scanning with a unique CCD camera [130], allowing near-simultaneous photometry in five bands u, g, r, i, z, [131–133]. The resulting data are reduced in a dedicated photometric pipeline, PHOTO [134] and astrometrically calibrated [135].

Chapter 3

Extraction procedure and data manipulation

We present the methodology used in the thesis. This chapter includes data collection, selection criteria, data reduction and details about the tools used to get the physical parameters.

3.1 Specification

With HST spatial resolution, for the low z galaxies, the F160W image from CANDELS project can be used to trace the stellar mass distribution while the F275W image from the HDUV project is just the rest frame UV. We use images of GOODS-North field and catalog corresponding to this region. We use the equatorial coordinates, photometric and spectroscopic redshift (if it is available), stellar masses, magnitudes, fluxes of the second aperture from UV to IR bands and their respective errors.

Besides, we analyze current mosaics from ACS and WFC3/IR data with 30 [mas/pix]. The available filters are 15, 10 of WFC3 and 5 of ACS. For this thesis, we analyze the filters F275W, F125W, and F160W of WCF3 and all of ACS. The filters F098M, F105W, F110W, F127W, F139W, F140W, and F153W have not to image or is defective.

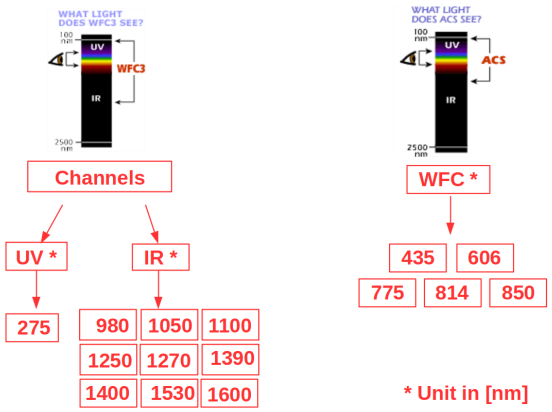

Figure 3.1: Bands of ACS and WFC3. Source: Made by the author.

3.2 Selection criteria

The initial catalog presents 35445 objects. In this section, z is spectroscopic redshift, specified as "z_spec".

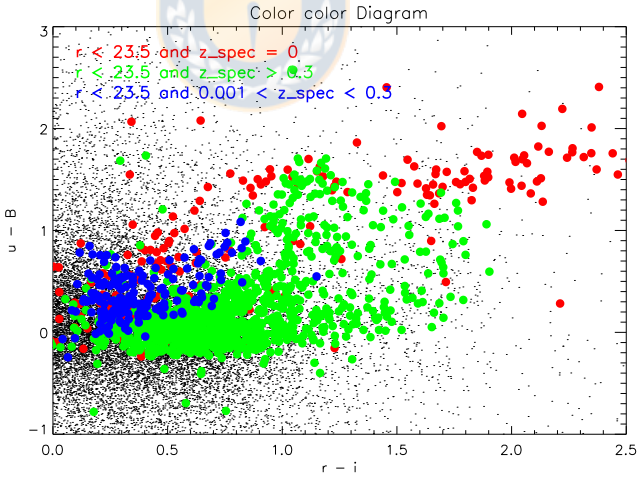

Figure 3.2: r - i vs. u - B color - color diagram. Source: Made by the author.

Figure 3.2 represents the color - color diagram with r-i color in the x-axis and u-B color in the y-axis. Red dots are galaxies with apparent magnitude $r < 23.5$ and $z = 0$, that mean z_{spec} was not measure, green dots are galaxies with $r < 23.5$ and $z > 0.3$ and blue dots are galaxies with $r < 23.5$ and $0.001 < z < 0.3$. Black dots complete the total of objects presents in the catalog.

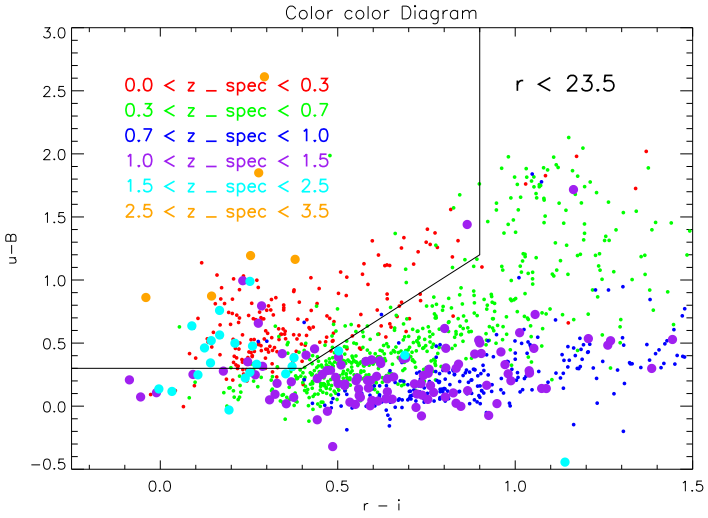

Figure 3.3: r-i vs. u-B color-color diagram. Source: Made by the author.

In Figure 3.3, our targets located in the red dots region and are contaminated by some of z > 1 sources. We plot r-i vs. r-[3.6] to divide the galaxies with z < 1 in Figure 3.4.

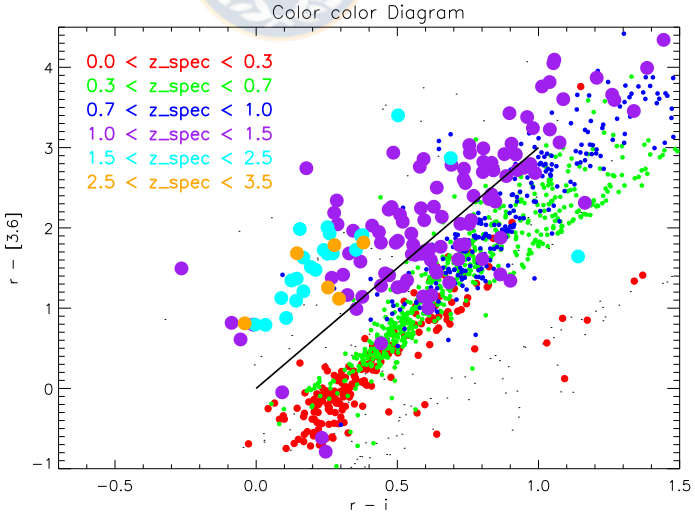

Figure 3.4: r-i vs. r-(3.6) color color diagram. Source: Made by the author.

Figure 3.4 has the same redshift color code as Figure 3.3. Galaxies with z >1 are redder in $r - [3.6]$ and we can select the sources below the thick line because they have mainly z < 1.

The sample of galaxies is defined by these criteria:

$$r < 24 \tag{3.1}$$

$$u - B > 0.3 \tag{3.2}$$

$$r - i < 0.9 \tag{3.3}$$

$$u - B > 1.8 \times (r - i) - 0.42 \tag{3.4}$$

$$r - [3.6] < 3 \times (r - i) \tag{3.5}$$

$$\text{class star} = 0 \tag{3.6}$$

and we define the target as faint when

$$\text{Abs } B > -18. \tag{3.7}$$

Given the selection criteria by the equations (3.1), (3.2), (3.3), (3.4), (3.5), (3.6) and (3.7), we can replot Figure 3.3. We see that most of contamination of high redshift sources were removed.

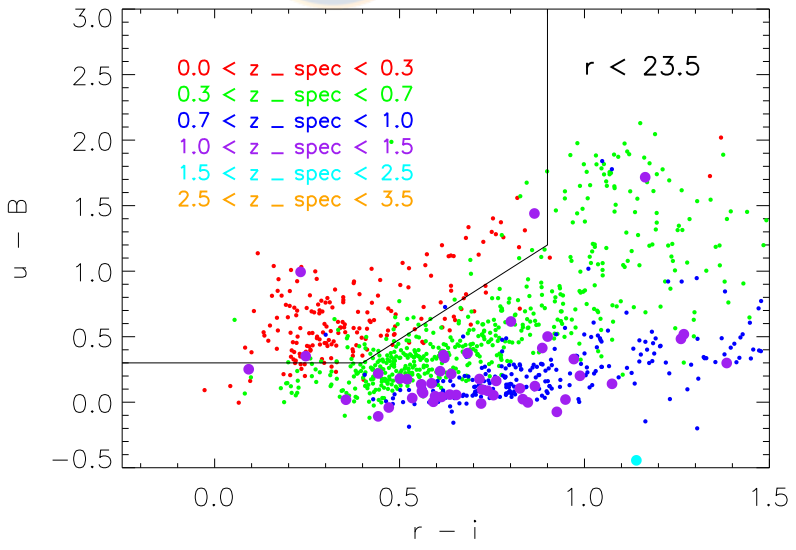

Figure 3.5: r-i vs. u-B color-color diagram. Source: Made by the author.

Red dots of Figure 3.5 show the data that finally we analyze.

To get the sample of galaxies of each band, we extract and align the stamp images of every source that agree the location of each object, using the catalog magnitude parameters in the different bands, from UV to IR. The scheme of the procedure is shown in Figure 3.6.

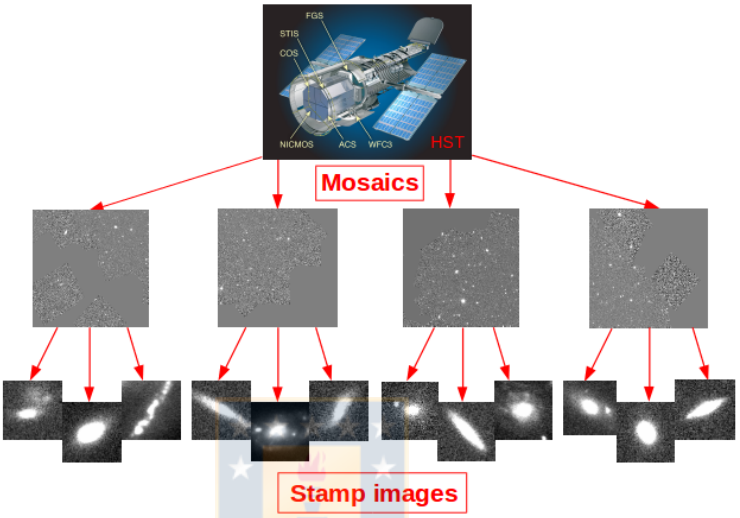

Figure 3.6: Cutting process scheme. Source: Made by the author.

Some of the low redshift spiral galaxies in the HST images show some bright clumps in the spiral arms, which may also be selected as one or several targets in the CANDELS catalog (mainly for the photometric redshift selected targets). We perform a visual check for the images to make sure the targets are reliable. Finally, we list the galaxies in table 3.1.

Band	Instrument/Camera [8]	Total galaxies
F275W	WFC3/UVIS	31
F435W	ACS/WFC	132
F606W	ACS/WFC	132
F775W	ACS/WFC	132
F814W	ACS/WFC	132
F850LP	ACS/WFC	132
F125W	WFC3/IR	132
F160W	WFC3/IR	132

Table 3.1: Images of the low redshift galaxies sample for each band. Source: Made by the author.

3.3 Calculating radius of the galaxies

The process for calculating the Petrosian radius of each galaxy is done computationally. The values of these radii are in units of pixel [px]. We convert the values to the physical unit of arcsecond [arcsec] and kiloparsec [kpc], respectively.

To get the radius [arcsec], we multiply the values of [px] by the pixel scale of the CCD of the instrument.

Thus,

$$\text{R [arcsec]} = \text{R [px]} \times \text{pixel scale} \tag{3.8}$$

where pixel scale is shown in table 3.2 and R [px] is the Petrosian radius at 20%, 50% or 90%.

Instrument/Camera	Pixel Scale [arcsec]
WFC3/UVIS	0.03
ACS/WFC	0.03
WFC3/IR	0.06

Table 3.2: Pixel scale for each Instrument. Source: [8].

To obtain R [kpc], we use the cosmological web calculator [136] to calculate the plate scale PS [kpc] and distance per arcsecond using the redshift values. Then, we multiply the Petrosian R [arcsec] by PS [kpc].

$$\text{R [kpc]} = \text{R [arcsec]} \times \text{PS [kpc/arcsec]}. \tag{3.9}$$

3.4 Calculating fluxes with Sextractor

For filter F275W, it is necessary to calculate the fluxes of 31 galaxies using Sextractor [137], which is a standard tool used to build a catalog of objects from an astronomical image.

In Sextractor, a complete analysis of an image is done in 6 steps:

- Estimation of the sky background
- Segmentation of the image or thresholding
- Separation of overlapping or deblending signals
- Filtering the detection
- Photometry
- Separation of stars and galaxies

In our case, we already have got stamp images, so only need to calculate the fluxes.

3.4.1 Detection

In Sextractor, source detection is part of a process called segmentation. An object is defined as a group of pixels selected by some detection process and for which it is believed that the flux contribution of an astronomical source is dominant over that of other objects. In this context, the segmentation process consists of separating objects from the bottom of the sky. Segmentation is achieved if it is found a group of connected pixels exceed some limit above the background, i.e., a detection. As we have stamp images, we have not problems related to crowded regions nor sources that are superimposed.

The parameters modified to calculate the fluxes are,

detect minarea	=	16
detect thresh	=	1.0
analysis thresh	=	5.0
filter name	=	gauss 4.0 7x7.conv
deblend nthresh	=	32
deblend mincont	=	0.005
phot apertures	=	$5, 10, 20, 30.$

The parameters modified according to the characteristics of the data are the following,

phot autoparams	=	$2.5, 3.5$	
mag zeropoint	=	24.1305	magnitude zero-point
gain	=	1.5	detector gain in e-/ADU
pixel scale	=	0.06	size of pixel in arcsec
seeing FWHM	=	0.07	stellar FWHM in arcsec.

3.5 Calculating parameters with FAST

To calculate stellar mass, SFR and SSFR, we use Fitting and Assessment of Synthetic Templates FAST [2], an IDL-based code that fits stellar population synthesis templates to broadband photometry and/or spectra. Depending on the input parameters, FAST outputs the best-fit z, age, dust content, star formation timescale τ, metallicity, stellar mass, SFR and their confidence intervals.

The input parameters required by FAST are,

1. SPS models: Bruzual & Charlot [138], Maraston [139], Conroy [140].
2. IMF: Kroupa [141], Chabrier [142], Salpeter [143].
3. Reddening law: Calzetti [144], mw [145], Kc [146].
4. Stellar population properties: age, star formation timescale τ, dust content AV, metallicity, redshift (the minimum and maximum value and the step size can be defined).

Furthermore, FAST read an input file with ID, spectroscopic redshifts, fluxes and their errors.

To determine the best-fit parameters, it calculates the χ^2 of every point of the model cube. In case spectroscopic or photometric redshift are provided, the redshift will be fixed to the closest value in the grid.

The confidence levels are calibrated using Monte Carlo simulations. The observed fluxes are modified according to their photometric errors and these modified fluxes are fitted as well. The 68% (95% or 99%) confidence intervals are defined by the χ^2 value in the original grid that encloses 68% (95% or 99%) of these simulations. Thus, the confidence intervals on all properties are the minimum and maximum values allowed by this χ^2 threshold.

3.5.1 The spectral energy distribution

The SED of a galaxy contains information regarding its SFH, dust content, and chemical abundance pattern. These properties provide clues to the physical processes governing the formation and evolution of galaxies from high redshift to the present. However, the process of translating observed SEDs into physical properties is difficult, because it requires

1. An accurate understanding of all phases of stellar evolution.

2. A well-calibrated stellar spectral library for converting stellar evolution calculations into measurable fluxes.

3. An initial mass function (IMF), specifying the weight given to each stellar mass.

4. Detailed knowledge of the star–dust geometry in conjunction with an appropriate extinction curve, i.e., knowledge of the physical conditions of the interstellar medium (ISM).

Each of these requirements depends on chemical composition, further compounding the problem. The combination of these ingredients in order to predict the spectrum of a galaxy is known as stellar population synthesis (SPS), e.g. [138, 139, 147–164].

3.5.2 Population synthesis

The stars cannot be resolved for the majority of galaxies, so we depend on models developed to analyze stellar populations by the study of the integrated light of galaxies, which holds information about the age and metallicity distributions of their stellar populations and SFHs. These models are called stellar population synthesis on galaxies.

Two main types of approaches have been developed:

- **Empirical population synthesis** ([165–168])
  In the empirical population synthesis approach, also known as "stellar population synthesis with a database", the observed spectrum of a galaxy is reproduced by a combination of spectra of individual stars or star clusters with different ages and metallicities from a library. The results following this approach do not consider the stellar evolution and do not allow one to predict the past and future spectral appearance of galaxies.

- **Evolutionary Population Synthesis** ([139, 148, 152, 153, 156, 169–172])
  The EPS approach uses the knowledge of stellar evolution to model the spectrophotometric properties of stellar populations, and has enjoyed more widespread use. In this approach, the main adjustable parameters are the stellar evolution tracks, stellar spectral library, IMF, SFH, grids of ages and metallicities. EPS represents a real physical model but is restricted by the lack of comprehensive stellar spectral library, accurate IMF and SFH, and poor understanding of some advanced phases of stellar evolution, such as the blue stragglers (BSs), the horizontal branch (HB) stars, and the thermally pulsating asymptotic giant branch (TP-AGB) stars.

Stellar Population Models

The construction of models for simple and composite stellar populations is conceptually straightforward. However, exist certain constraints that make the creation of such models rather difficult in practice (incomplete isochrone tables and empirical stellar libraries, poorly calibrated physics and others).

In figure 3.7, it is shown an overview of the stellar population synthesis technique. The upper panels highlight the necessary ingredients for constructing simple stellar populations (SSPs): an IMF, isochrones (for a range of ages and metallicities) and stellar spectra (spanning a range of T_{eff}, L_{bol}, and metallicity). The middle panels highlight the ingredients necessary for constructing composite stellar populations (CSPs): star formation histories and chemical evolution, SSPs, and a model for dust attenuation and emission. Bottom row shows the final CSPs both before and after a dust model is applied.

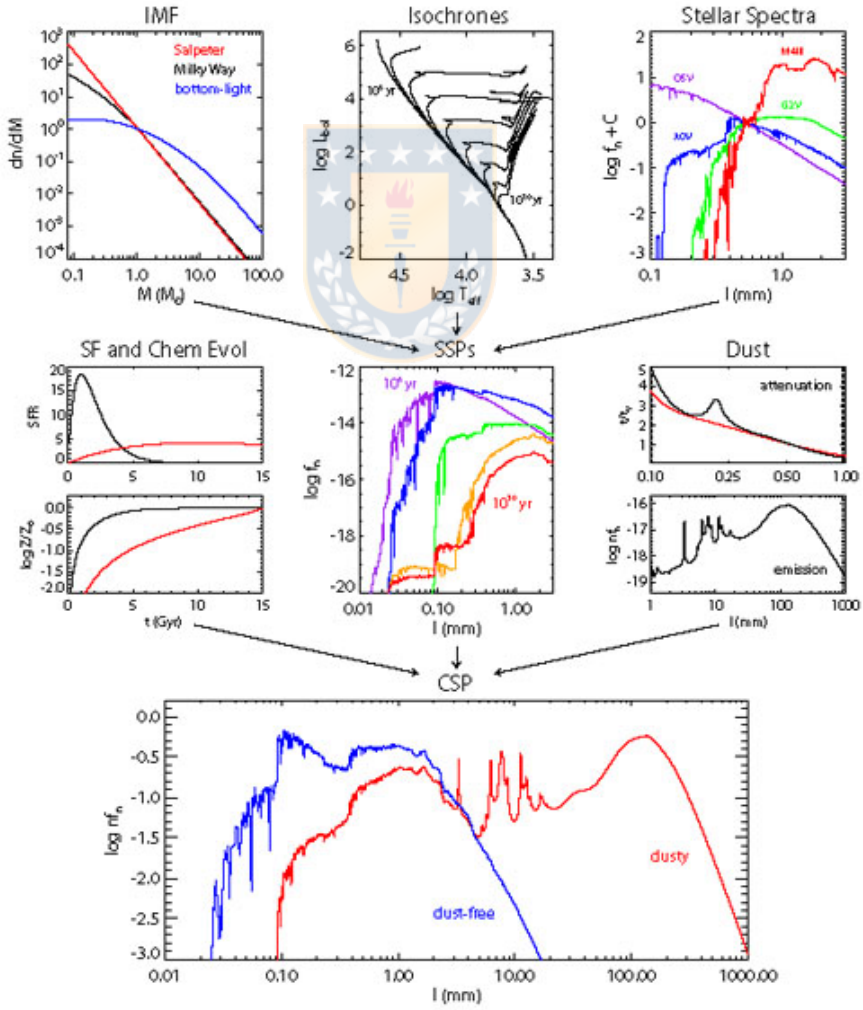

Figure 3.7: Overview of the stellar population synthesis. Source: [173].

Simple Stellar Population

The first step of any Stellar Population Synthesis model is the Simple Stellar Population (SSP) that describes the evolution in time of the SED of a single stellar population at a single metallicity and abundance pattern. Therefore, an SSP requires three basic inputs: stellar evolution theory in the form of isochrones, stellar spectral libraries and an IMF, each of which may in principle be a function of metallicity and/or elemental abundance pattern.

Stellar Evolution and Isochrones

An isochrone specifies the location in the Hertzsprung-Russell (HR) diagram of stars with a common age and metallicity. Isochrones are constructed from stellar evolution calculations for stars from the hydrogen burning limit (≈ 0.1 $M_\odot$) to the maximum stellar mass (≈ 100 $M_\odot$). The construction of isochrones is straightforward for stellar evolution tracks that are infinitely well-sampled in mass and time. In practice, evolutionary tracks are discretely sampled and this can lead to issues in isochrone construction for fast evolutionary phases. Modern sets of isochrones have constructed specifically to ensure that the models are relatively immune to these effects [174].

Initial Mass Function

The IMF is defined as a probability distribution function (PDF) for the mass at which a star enters the main sequence (begins hydrogen fusion).

$$\int_{M_L}^{M_U} \mathrm{dm}\ \mathrm{m}N(\mathrm{m}) = 1M_\odot,$$

N(m) dm specifies the fraction of stars in the mass interval of width dm around m, where the distribution is normalized.

Typically, in the integration limits one put $M_L \sim 0.1$ $M_\odot$ because less massive stars do not ignite their hydrogen (and are thus brown dwarfs), and $M_U \sim 100$ $M_\odot$, because more massive stars have not been observed, because of their very short lifetime.

The properties and evolution of a star are closely related to its mass, so the IMF is an important diagnostic tool for studying large quantities of stars. For example, the initial mass of a star is the primary factor determining its color, luminosity and lifetime and is relatively invariant from one group of stars to another, though some observations suggest that the IMF is different in different environments.

The IMF is often stated in terms of a series of power laws, where N(m)dm (sometimes also represented as $\xi(\mathrm{m})\Delta\mathrm{m}$), the number of stars with masses in the range m to m+dm within a specified volume of space, is proportional to $\mathrm{m}^{-\alpha}$, where α is a dimensionless exponent. The IMF can be inferred from the present day stellar luminosity function by using the stellar mass-luminosity relation together with a model of how the star formation rate varies with time. Commonly used forms of the IMF are the Kroupa (2001) broken power law and the Chabrier (2003) log-normal, though also we can find Salpeter (1955) and Miller-Scalo (1979).

- **Salpeter** [143]

  The IMF of stars more massive than our sun was first quantified by Edwin Salpeter in 1955. His work favored an exponent of $\alpha = 2.35$. This form of the IMF is called the Salpeter function or a Salpeter IMF. It shows that the number of stars in each mass range decreases rapidly with increasing mass. The Salpeter Initial Mass Function is

  $$\xi(\mathrm{m})\Delta\mathrm{m} = \xi_0 \left(\frac{\mathrm{m}}{M_\odot}\right)^{-2.35} \left(\frac{\Delta\mathrm{m}}{M_\odot}\right),$$

  where $\mathrm{M}_\odot$ is the solar mass, and ξ_0 is a constant relating to the local stellar density.

- **Miller-Scalo** [175]

  Later, Glenn E. Miller and John M. Scalo suggested that the IMF approached $\alpha = 1$ below one solar mass. This IMF is a parametrization of the IMF by a log-normal distribution of the form

  $$\xi[\log(m)] = A_0 + A_1 \log(m) + A_2[\log(m)]^2.$$

- **Kroupa** [176]

  Pavel Kroupa kept $\alpha = 2.3$ above half a solar mass, but introduced $\alpha = 1.3$ between 0.08 - 0.5 $M_\odot$ and $\alpha = 0.3$ below 0.08 $M_\odot$.

$$\xi(m) = m^{-\alpha}, \quad \alpha = \begin{cases} 0.3, & \text{for } 0.01 \leqslant m/M_\odot < 0.08, \\ 1.3, & \text{for } 0.08 \leqslant m/M_\odot < 0.50, \\ 2.3, & \text{for } 0.50 \leqslant m/M_\odot. \end{cases} \tag{3.10}$$

- **Chabrier** [142]

  Chabrier IMF is a combination of log-normal distribution (for low mass stars with masses less than 1 $M_\odot$) and a power-law distribution (for larger masses). The difference between the IMF and the system IMF is to merge resolved objects into multiple systems to compute the magnitude of systems instead of individual stars.

  The next equations represent Chabrier IMFs

$$\xi(\log\ m) = A\ \left[-\frac{(\log\ m - \log\ m_c)^2}{2\sigma^2} \right]. \tag{3.11}$$

  For simple objects:

	A	m_c	σ
m $\leqslant$ 1.0 $M_\odot$	0.158	0.079	0.69

Table 3.3: Disk IMF for simple objects for equation (3.11). Source: [142].

For the various components of the galaxy:

	A	m_c	σ
m $\leqslant$ 1.0 $M_\odot$	0.158	0.079	0.69
m $\leqslant$ 0.9 $M_\odot$		0.33	0.34
m $\leqslant$ 0.7 $M_\odot$	3.6×10^{-4}	0.22	0.33

Table 3.4: IMFs for the various components of the galaxy for equation (3.11). Source: [142].

$$\xi(\log\ m) = A\ ^{-x}. \tag{3.12}$$

For simple objects:

	A	x
m > 1.0 $M_\odot$	4.43 × 10^{-2}	1.3

Table 3.5: Disk IMF for simple objects for equation (3.12). Source: [142].

For the various components of the galaxy:

	A	x
m > 1.0 $M_\odot$	4.4 × 10^{-2}	1.3
m > 0.9 $M_\odot$		1.3
m > 0.7 $M_\odot$	7.1 × 10^{-5}	1.3

Table 3.6: IMFs for the various components of the galaxy for equation (3.12). Source: [142].

In this case, we get stellar mass, SFR and SSFR using the following parameters:

Parameters of Stellar Population Library	
AB ZP	23.90
Library	Bruzual & Charlot (2003)
SFH	Exponentially declining SFH: SFR $\sim$ exp(-t/τ)
Stellar IMF	Chabrier
Dust law	Calzetti (2000) dust attenuation law
Parameters of the grid	
Metallicity	0.05
log(τ/yr)	6.5 - 11.0, in steps of 0.1
log(age/yr)	6.5 - 11.0, in steps of 0.1
A_V	0.0 - 4.0, in steps of 0.1
z	0.01 - 0.3, in steps of 0.01
Parameters of Cosmology	
H_0	70.0
Ω_M	0.3
Ω_Λ	0.7

Table 3.7: Input parameters used in FAST. Source: Made by the author.

3.5.3 Star formation rate

To calculate this parameter, we use the equation (3.13) from [1]

$$\log\left(\dot{\mathrm{M}}_{*}\right)[\mathrm{M}_{\odot}\mathrm{yr}^{-1}] = \log(\mathrm{L}_{x}) - \log(\mathrm{C}_{x}) \tag{3.13}$$

where log C_x is a logarithmic calibration constant SFR equal to 43.35 and $L_x = \nu L_\nu$ the luminosity in [ergs s $^{-1}$].

We have to take into account that there is a difference between the flux that the galaxy emits and the flux that we observe. To correct this difference we use the correction K

$$m_R = M_Q + DM + K_{QR} \tag{3.14}$$

where the source has an apparent magnitude R observed and an absolute magnitude Q emitted. To calculate the K correction, it is necessary to know the apparent magnitude in the UV band and three transmission curves corresponding to NUV of GALEX, UVIS1 of HST and a template model. In this case, we used [140]. After calculating the correction K, we calculate the absolute magnitude in UV, the flux in frequency units, the luminosity in frequency units and finally calculate the SFR.

3.5.4 Specific star formation rate

To calculate Specific Star Formation Rate,

$$\text{SSFR } [1/\text{yr}] = \frac{\text{SFR}[M_{\odot}yr^{-1}]}{\mathrm{M}_{*}[M_{\odot}]}. \tag{3.15}$$

with SFR calculated from the previous section.

Chapter 4

Analysis

In this chapter the analysis of the sample is presented. We show the stamp images of all galaxies. Afterward, the relations between spectroscopic and photometric redshift, besides other parameters as size, SFR and SSFR related to stellar mass.

4.1 Stamp images

One of the most important aspect is identify the galaxies within the CANDELS's catalog due to the difficulty to distinguish between stars and different kind of galaxies with a computational rutine. From the total catalog, 132 galaxies are identified in the following filters: F435W, F606W, F775W, F814W, F850LP, F125W and F160W. Only 31 present star formation (F275W).

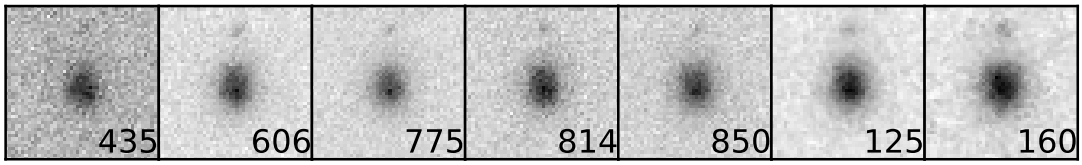

Figure 4.1: Galaxy 2.

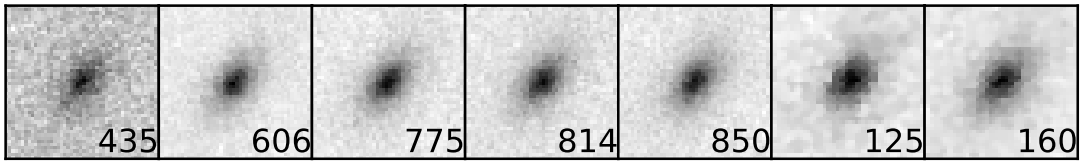

Figure 4.2: Galaxy 3.

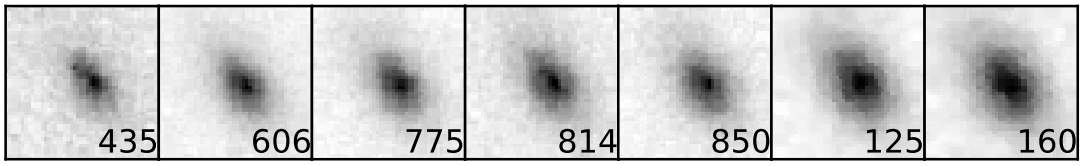

Figure 4.3: Galaxy 4.

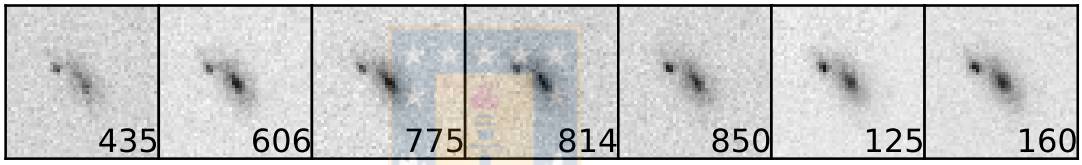

Figure 4.4: Galaxy 5.

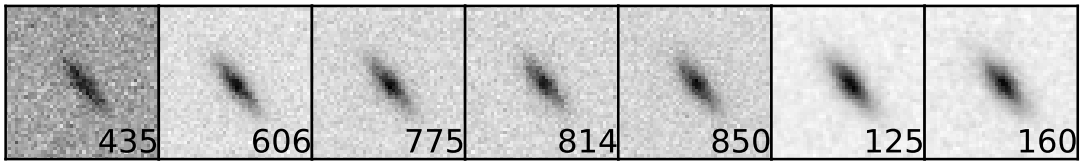

Figure 4.5: Galaxy 7.

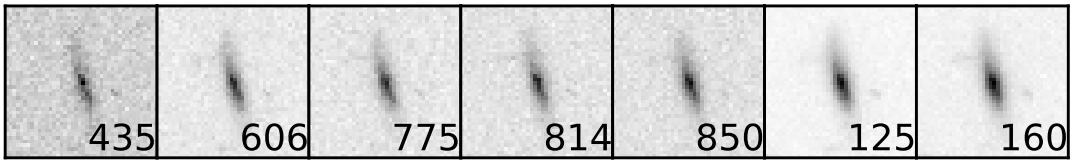

Figure 4.6: Galaxy 8.

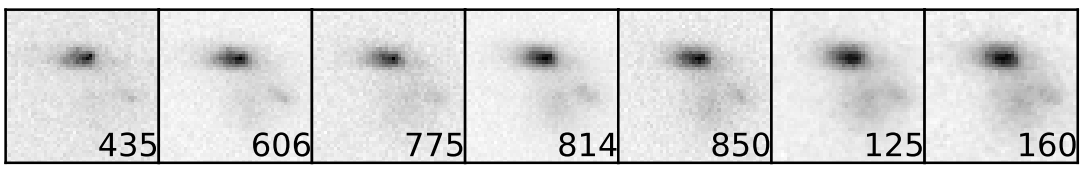

Figure 4.7: Galaxy 10.

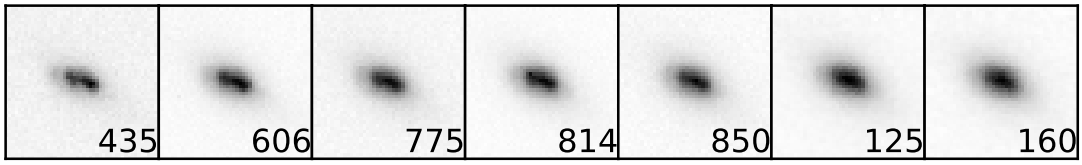

Figure 4.8: Galaxy 11.

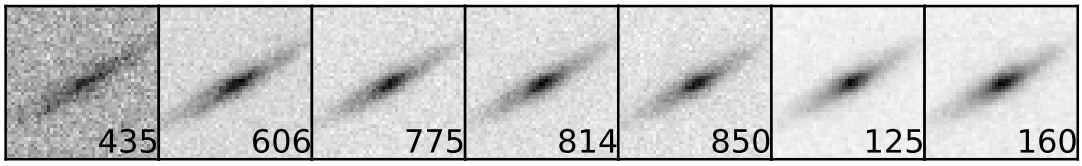

Figure 4.9: Galaxy 15.

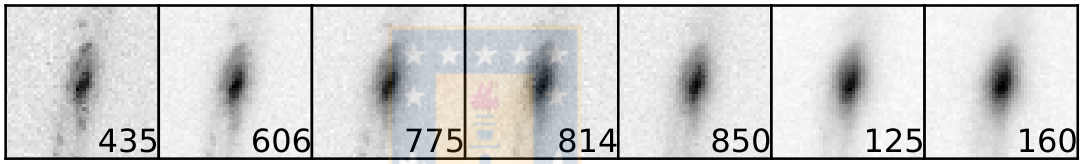

Figure 4.10: Galaxy 16.

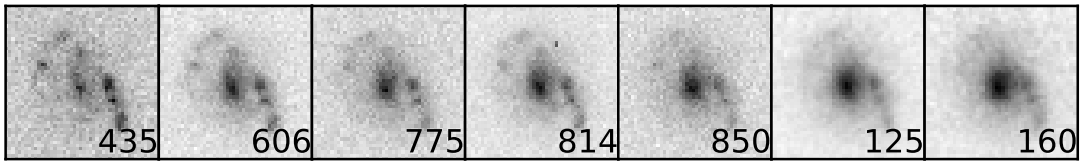

Figure 4.11: Galaxy 17.

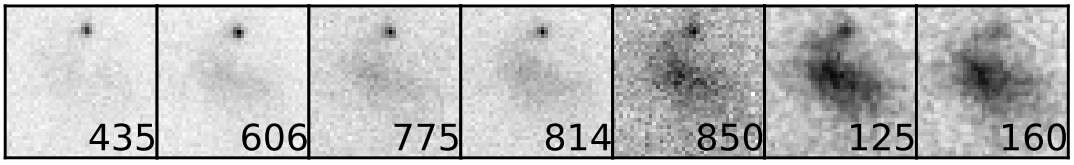

Figure 4.12: Galaxy 18.

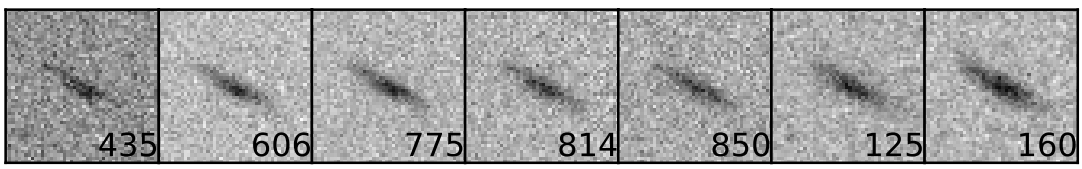

Figure 4.13: Galaxy 19.

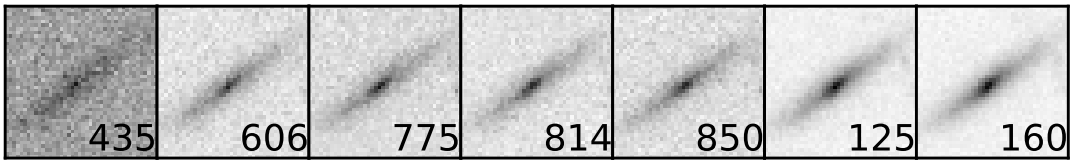

Figure 4.14: Galaxy 20.

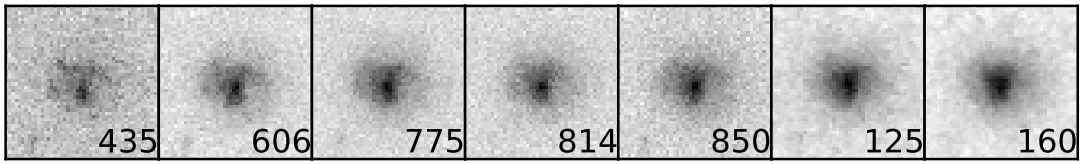

Figure 4.15: Galaxy 21.

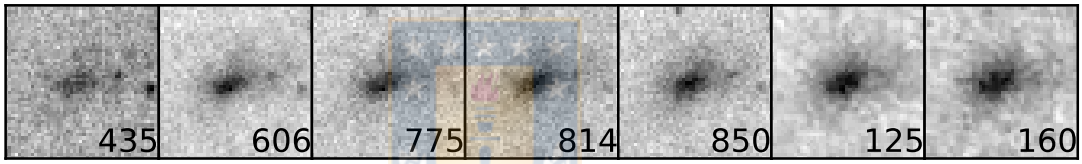

Figure 4.16: Galaxy 23.

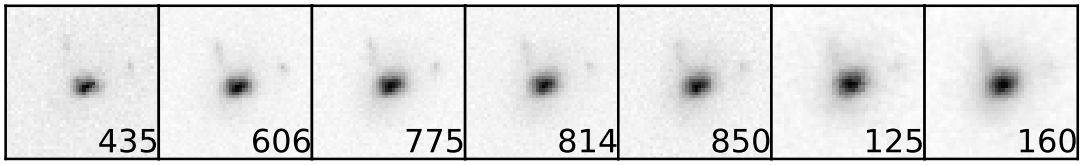

Figure 4.17: Galaxy 24.

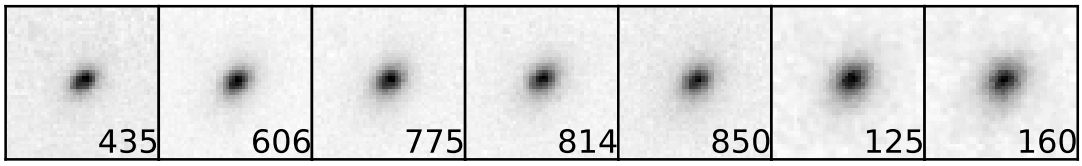

Figure 4.18: Galaxy 26.

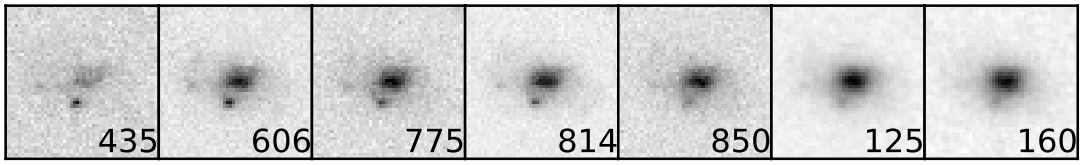

Figure 4.19: Galaxy 28.

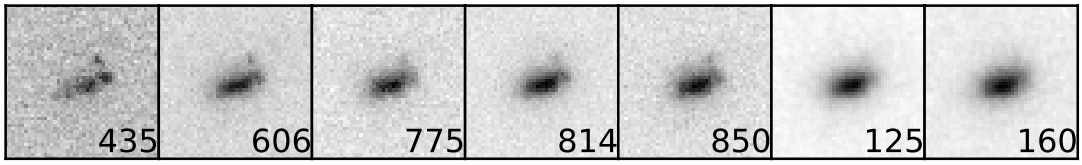

Figure 4.20: Galaxy 29.

Figure 4.21: Galaxy 30.

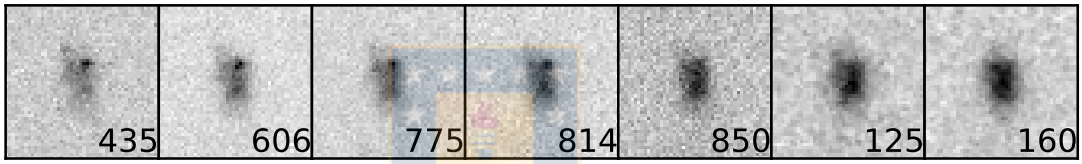

Figure 4.22: Galaxy 31.

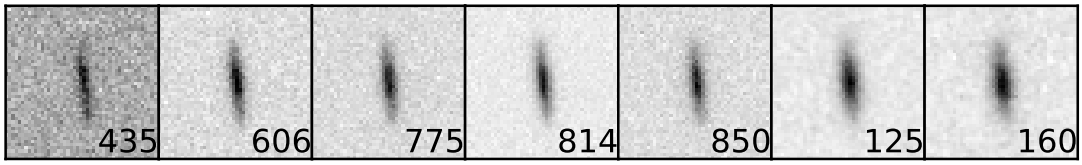

Figure 4.23: Galaxy 33.

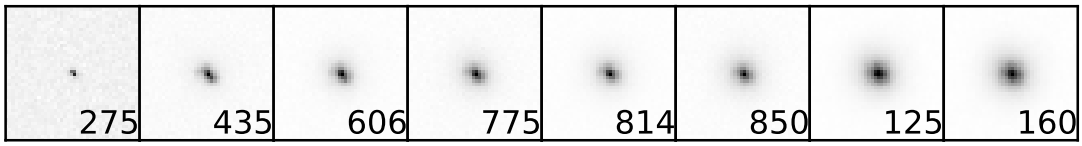

Figure 4.24: Galaxy 34.

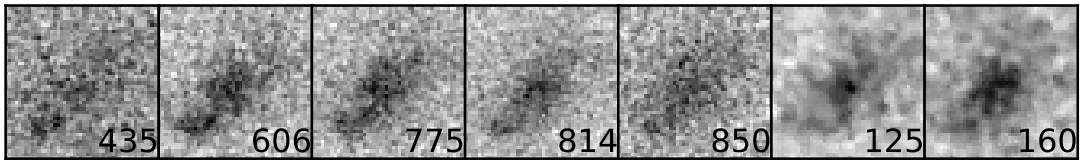

Figure 4.25: Galaxy 36.

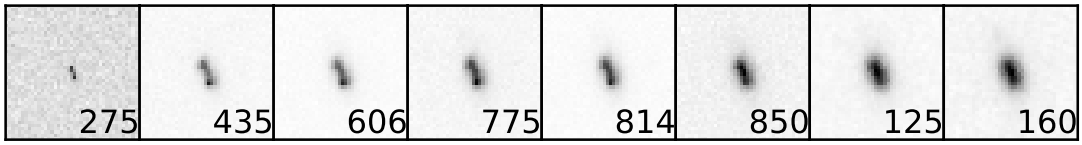

Figure 4.26: Galaxy 37.

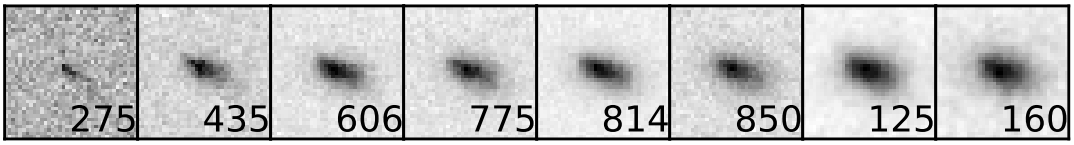

Figure 4.27: Galaxy 38.

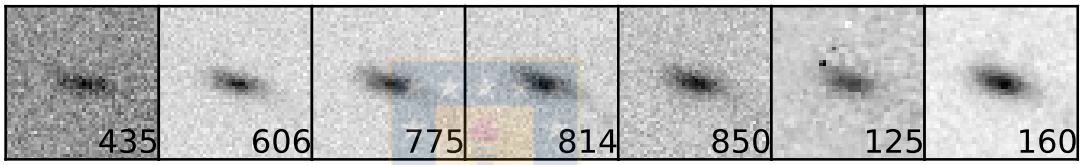

Figure 4.28: Galaxy 39.

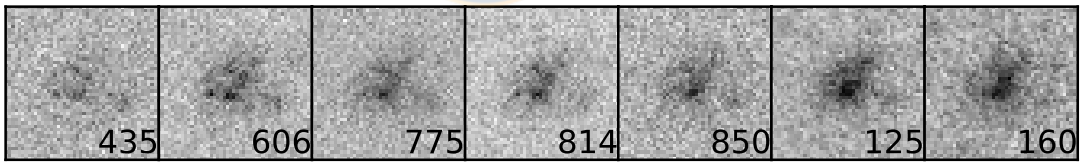

Figure 4.29: Galaxy 40.

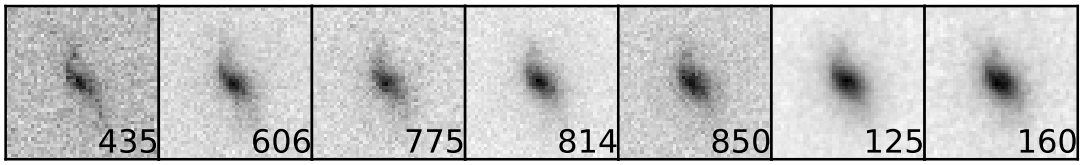

Figure 4.30: Galaxy 42.

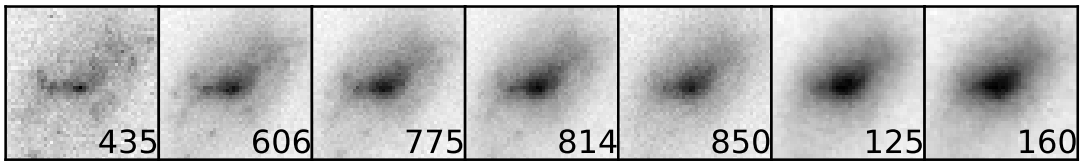

Figure 4.31: Galaxy 46.

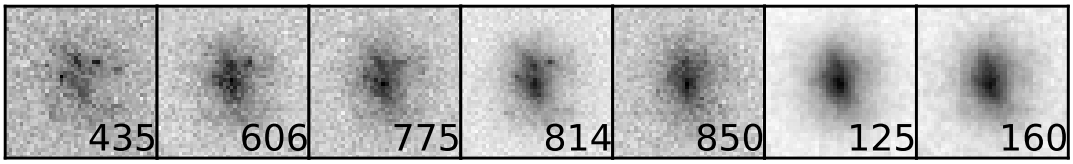

Figure 4.32: Galaxy 47.

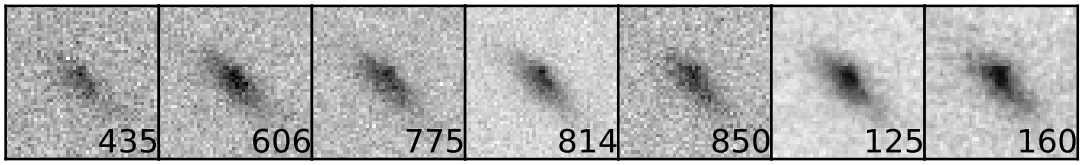

Figure 4.33: Galaxy 50.

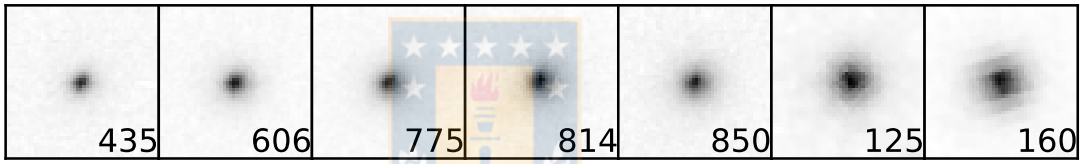

Figure 4.34: Galaxy 51.

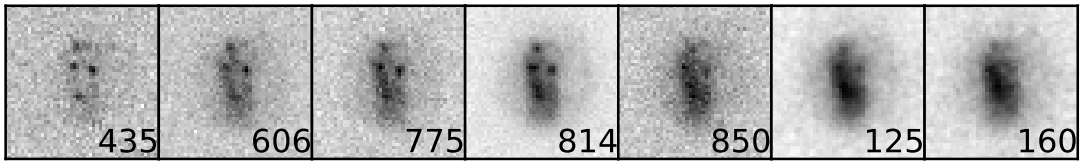

Figure 4.35: Galaxy 52.

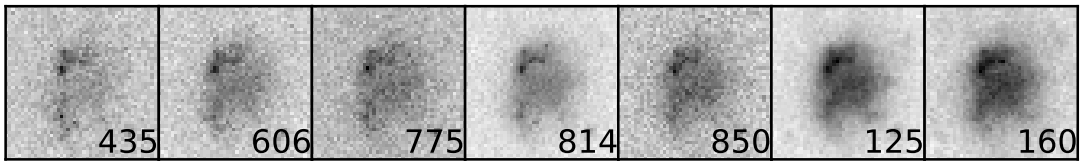

Figure 4.36: Galaxy 53.

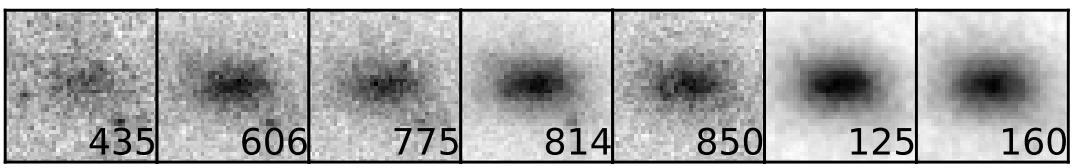

Figure 4.37: Galaxy 54.

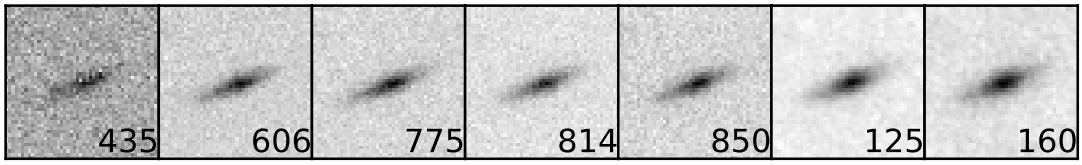

Figure 4.38: Galaxy 55.

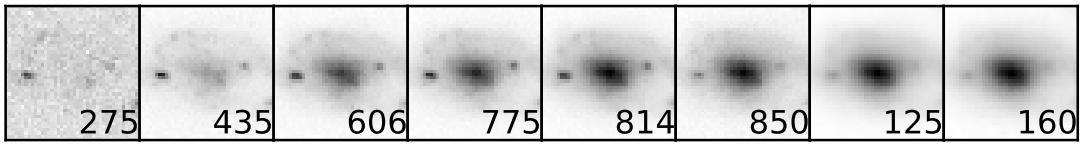

Figure 4.39: Galaxy 56.

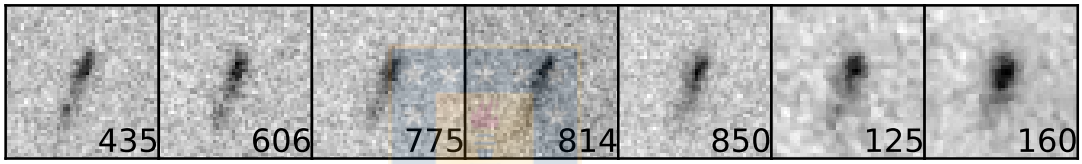

Figure 4.40: Galaxy 58.

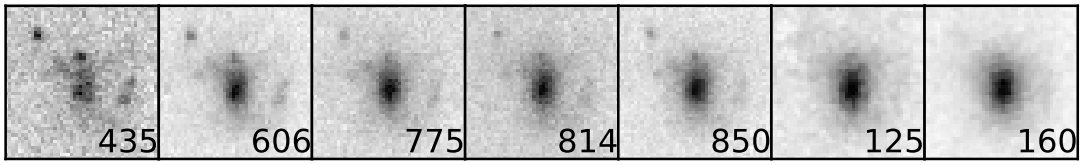

Figure 4.41: Galaxy 59.

Figure 4.42: Galaxy 61.

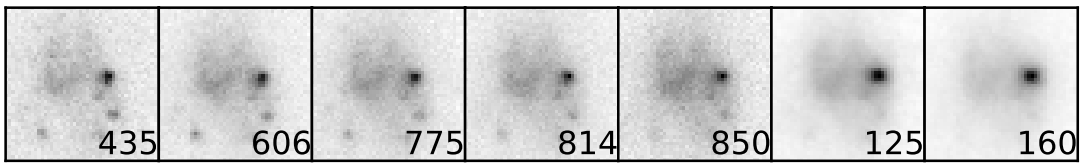

Figure 4.43: Galaxy 62.

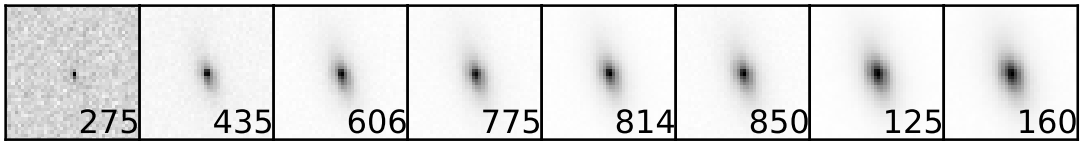

Figure 4.44: Galaxy 63.

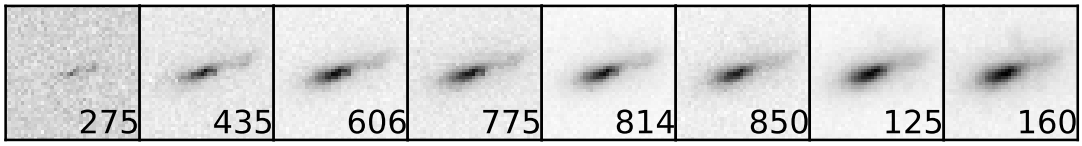

Figure 4.45: Galaxy 65.

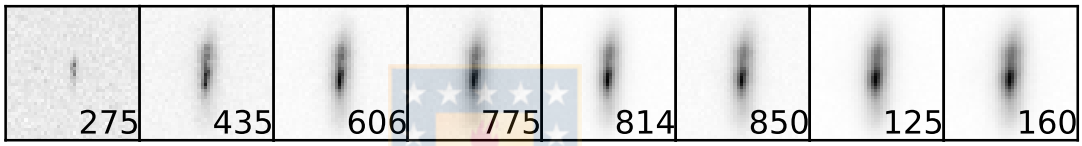

Figure 4.46: Galaxy 66.

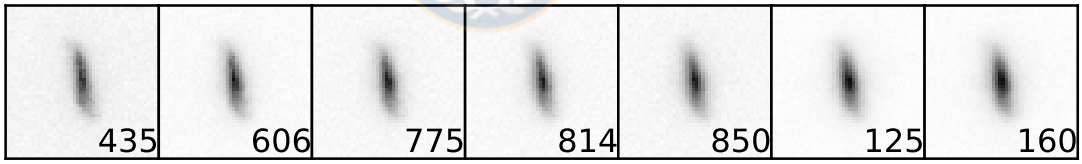

Figure 4.47: Galaxy 67.

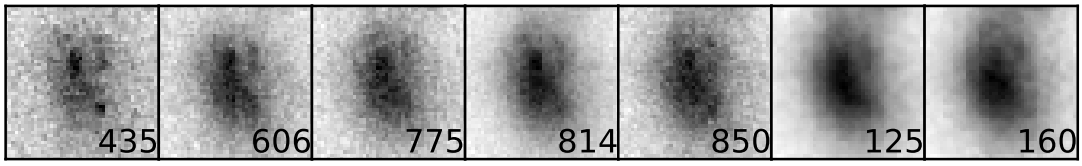

Figure 4.48: Galaxy 68.

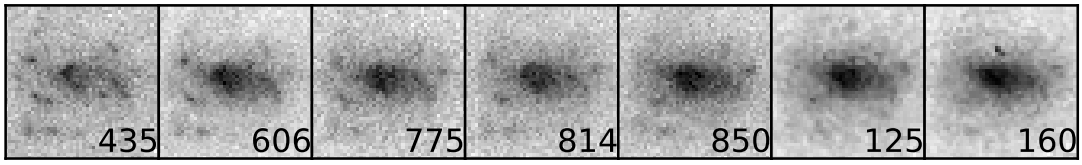

Figure 4.49: Galaxy 69.

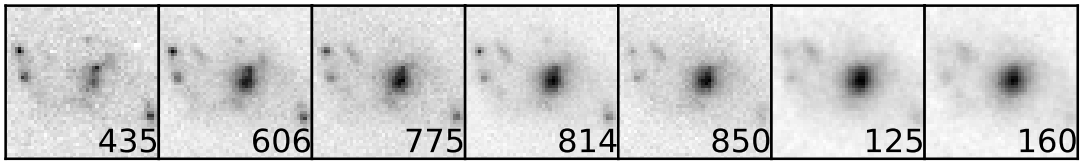

Figure 4.50: Galaxy 70.

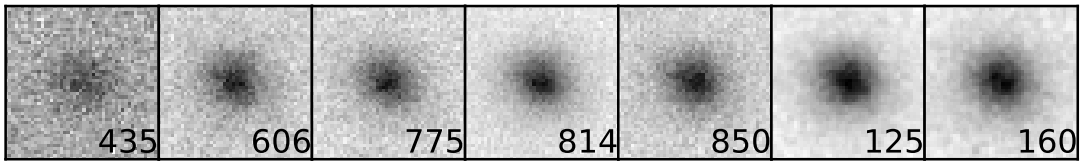

Figure 4.51: Galaxy 74.

Figure 4.52: Galaxy 76.

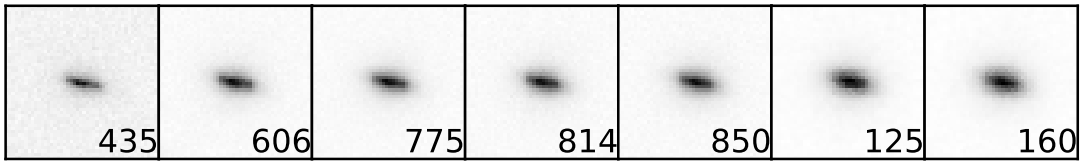

Figure 4.53: Galaxy 77.

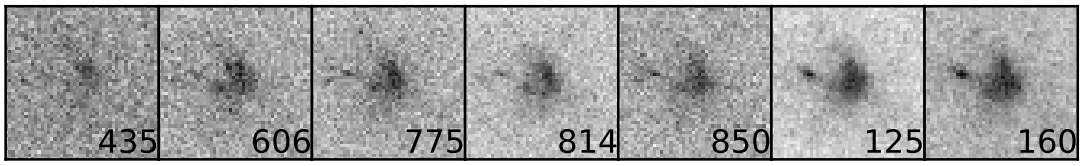

Figure 4.54: Galaxy 79.

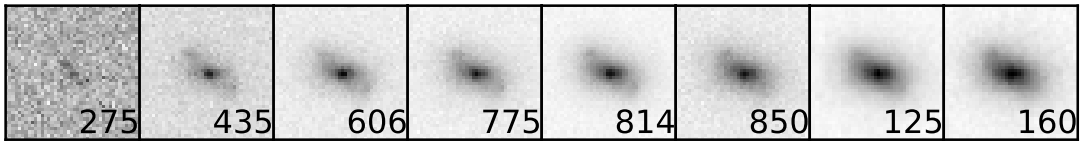

Figure 4.55: Galaxy 80.

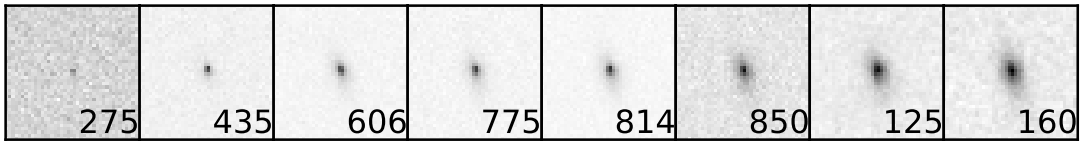

Figure 4.56: Galaxy 81.

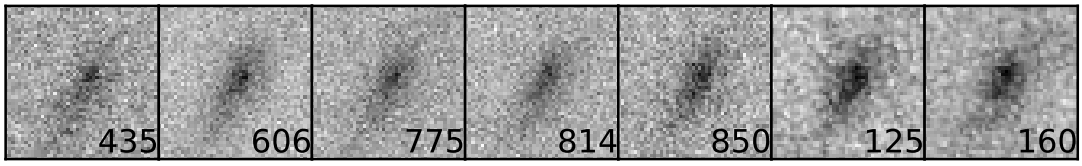

Figure 4.57: Galaxy 82.

Figure 4.58: Galaxy 87.

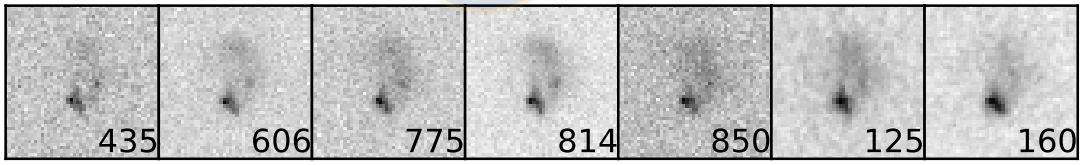

Figure 4.59: Galaxy 89.

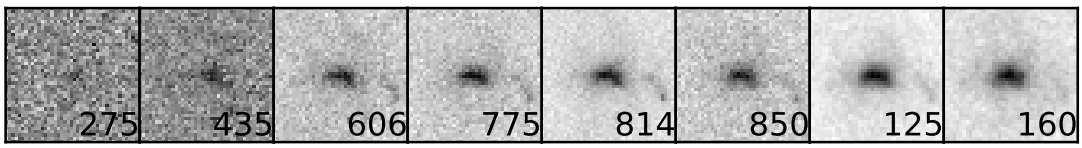

Figure 4.60: Galaxy 90.

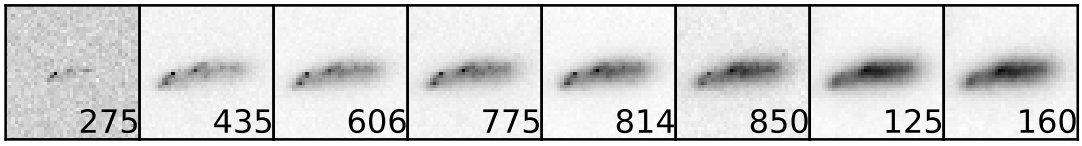

Figure 4.61: Galaxy 91.

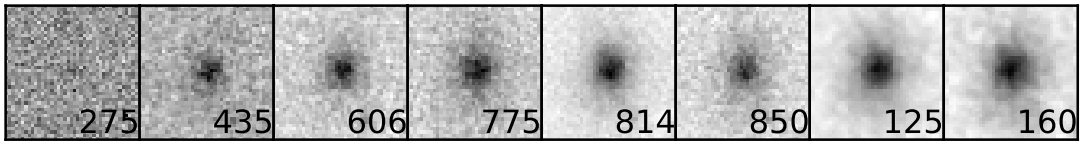

Figure 4.62: Galaxy 92.

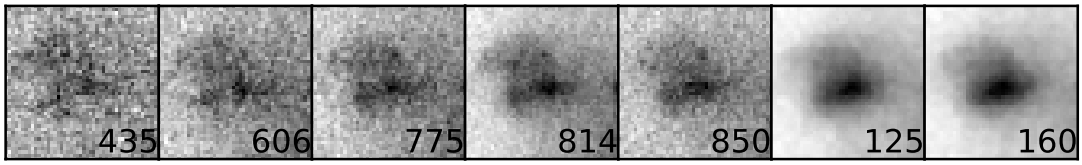

Figure 4.63: Galaxy 93.

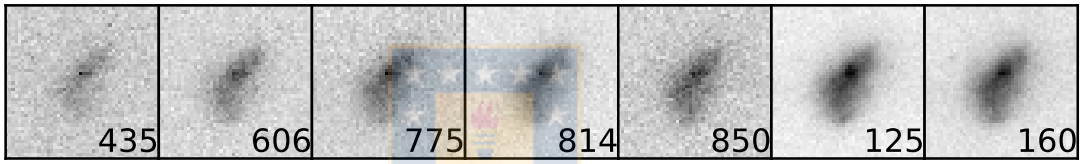

Figure 4.64: Galaxy 94.

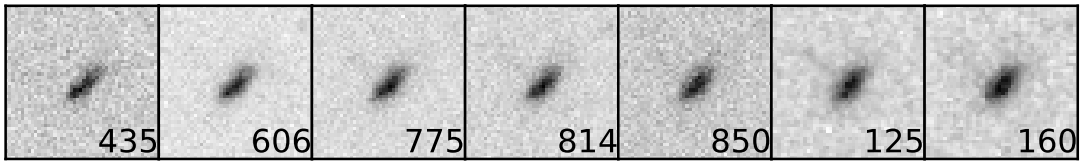

Figure 4.65: Galaxy 95.

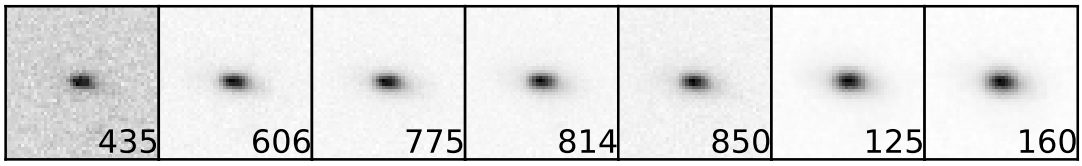

Figure 4.66: Galaxy 96.

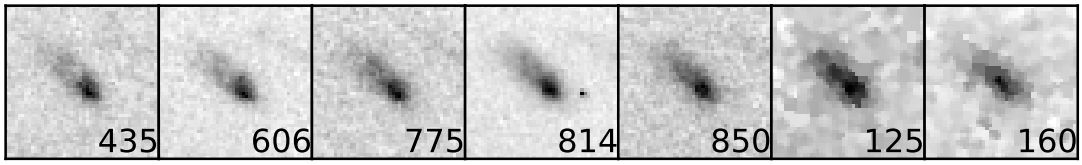

Figure 4.67: Galaxy 99.

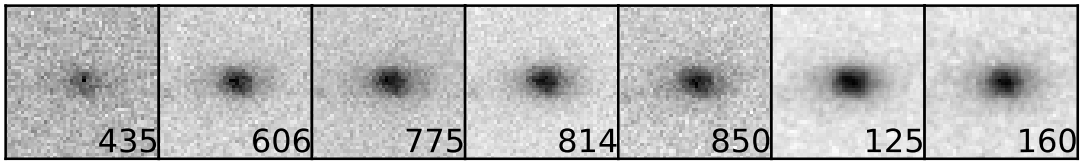

Figure 4.68: Galaxy 101.

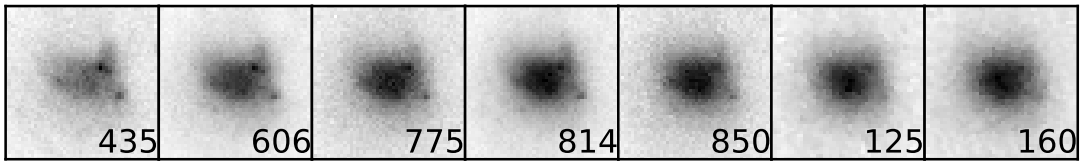

Figure 4.69: Galaxy 103.

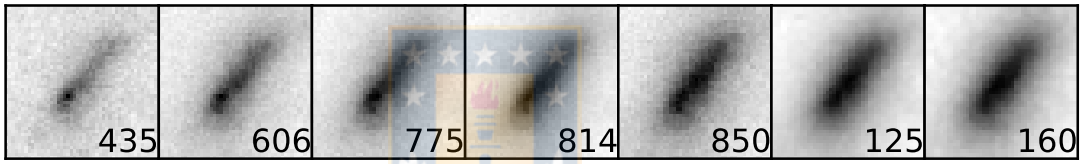

Figure 4.70: Galaxy 104.

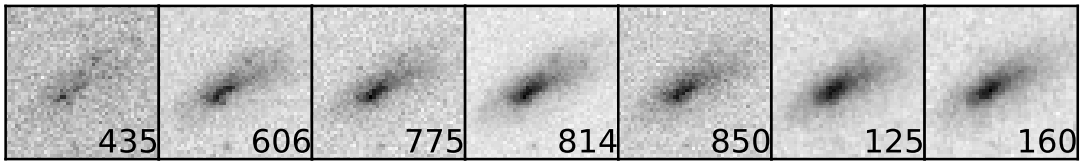

Figure 4.71: Galaxy 108.

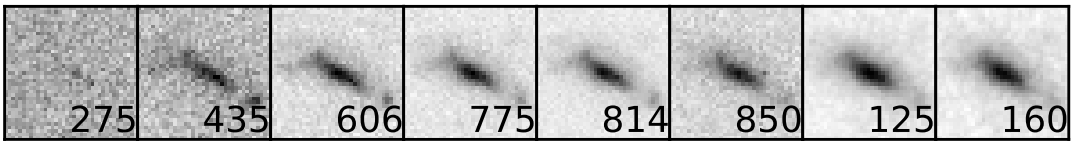

Figure 4.72: Galaxy 111.

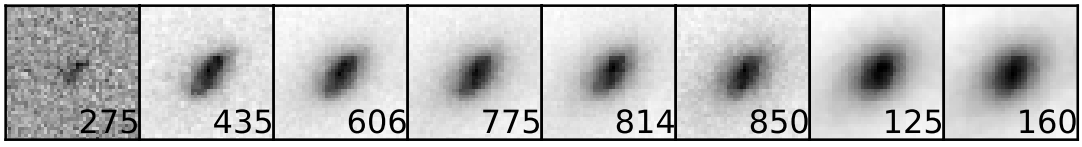

Figure 4.73: Galaxy 112.

Figure 4.74: Galaxy 113.

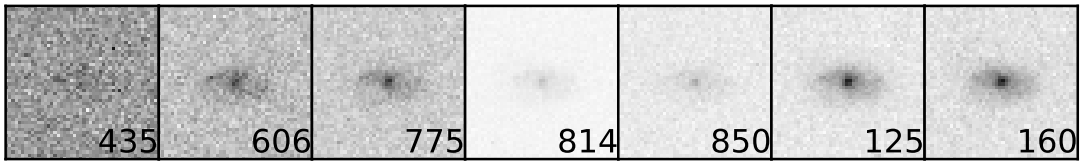

Figure 4.75: Galaxy 114.

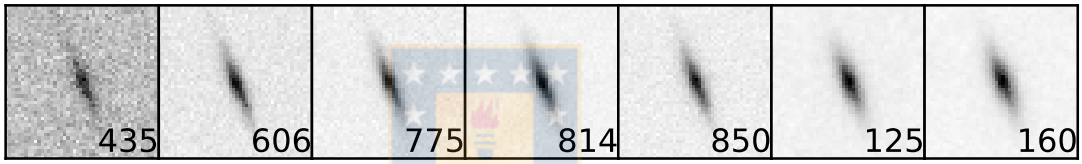

Figure 4.76: Galaxy 115.

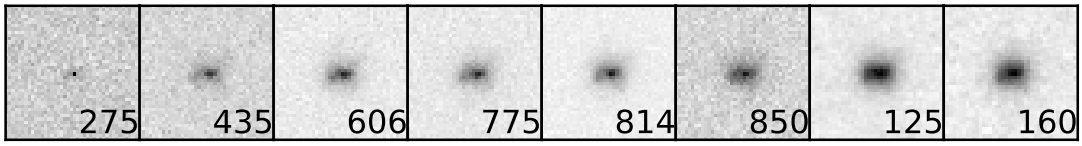

Figure 4.77: Galaxy 118.

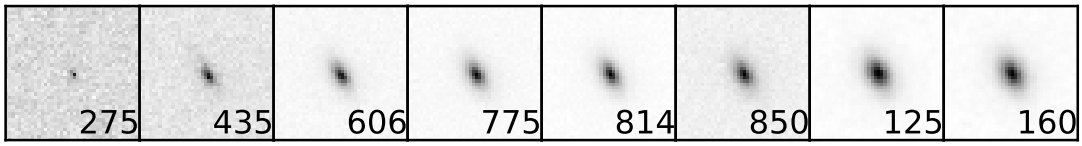

Figure 4.78: Galaxy 119.

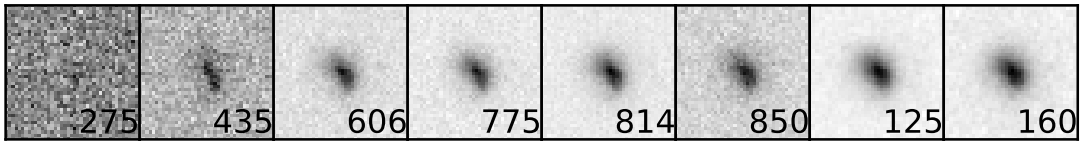

Figure 4.79: Galaxy 122.

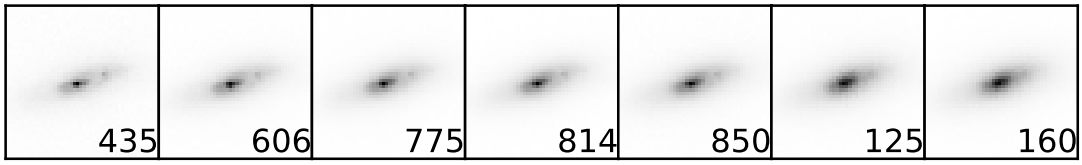

Figure 4.80: Galaxy 123.

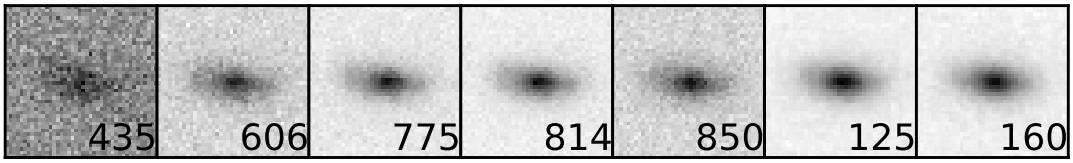

Figure 4.81: Galaxy 124.

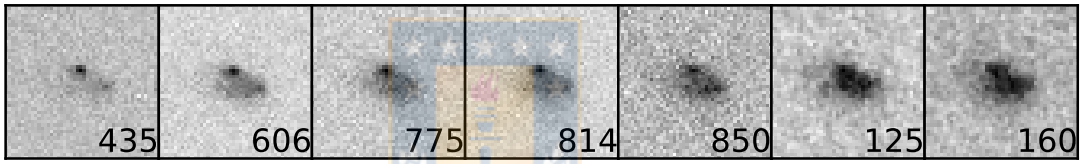

Figure 4.82: Galaxy 125.

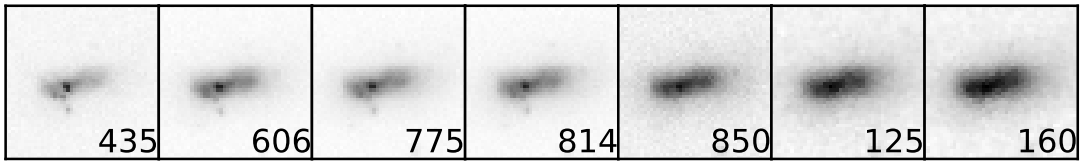

Figure 4.83: Galaxy 126.

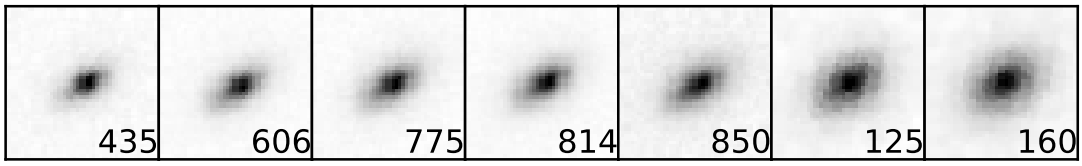

Figure 4.84: Galaxy 128.

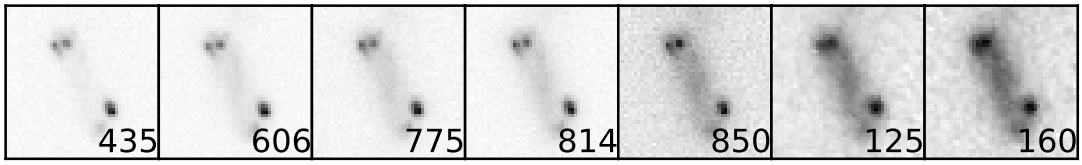

Figure 4.85: Galaxy 129.

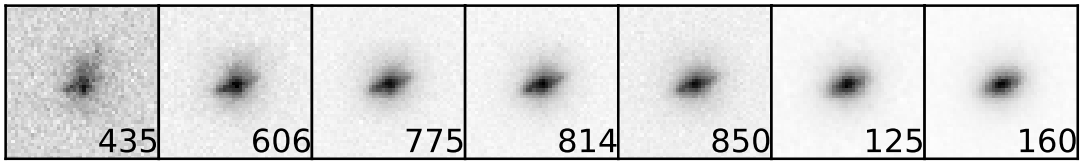

Figure 4.86: Galaxy 130.

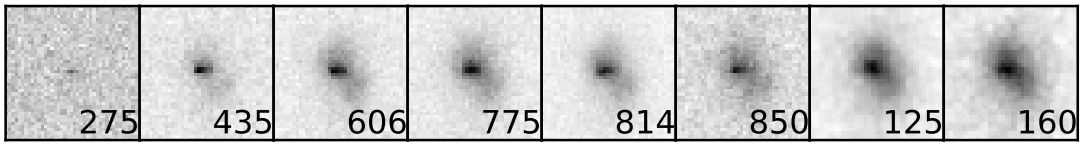

Figure 4.87: Galaxy 132.

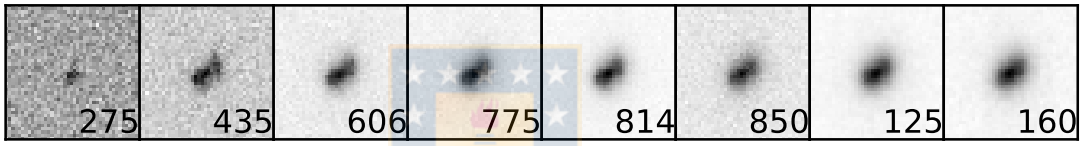

Figure 4.88: Galaxy 133.

Figure 4.89: Galaxy 135.

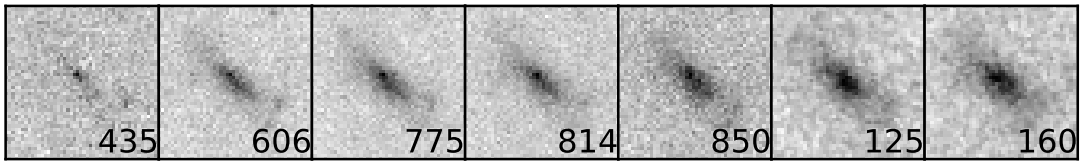

Figure 4.90: Galaxy 136.

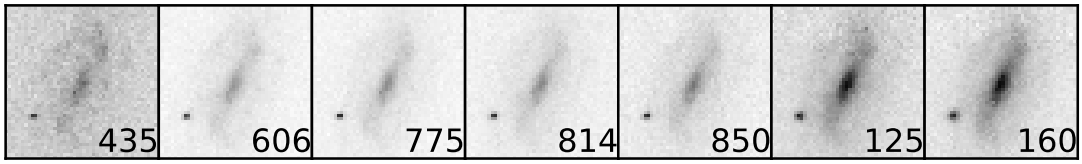

Figure 4.91: Galaxy 137.

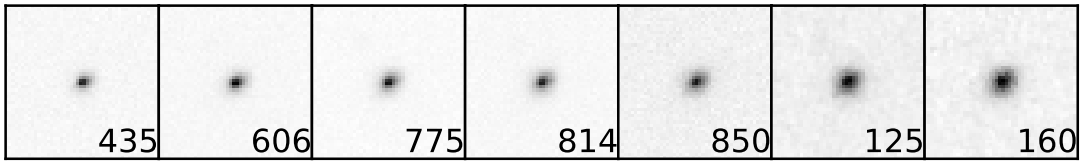

Figure 4.92: Galaxy 138.

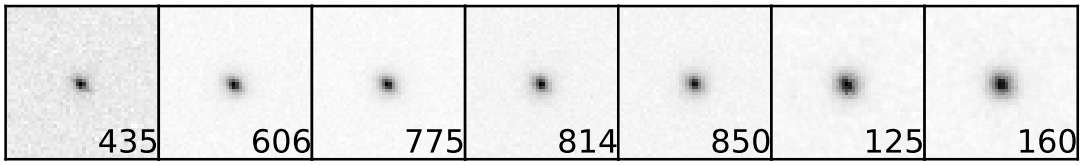

Figure 4.93: Galaxy 139.

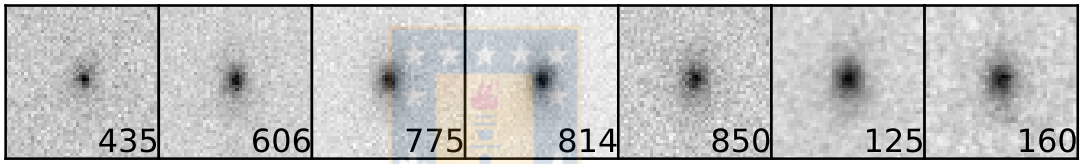

Figure 4.94: Galaxy 140.

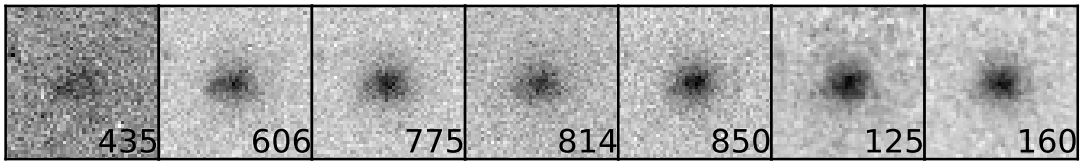

Figure 4.95: Galaxy 141.

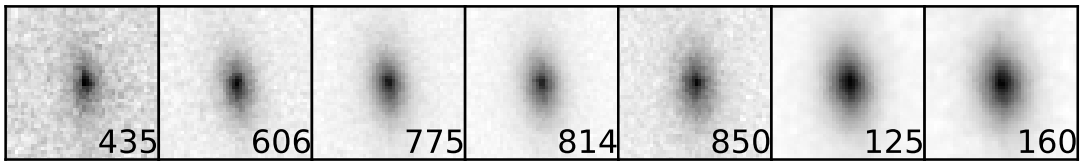

Figure 4.96: Galaxy 142.

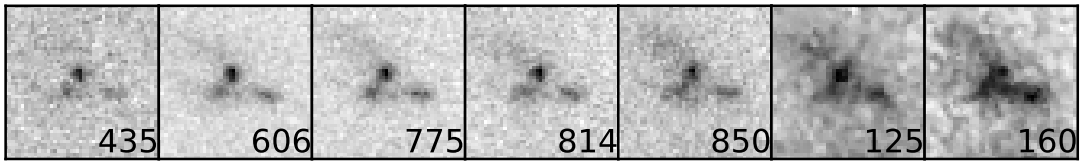

Figure 4.97: Galaxy 144.

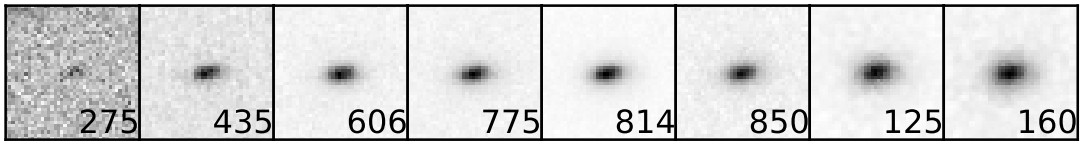

Figure 4.98: Galaxy 145.

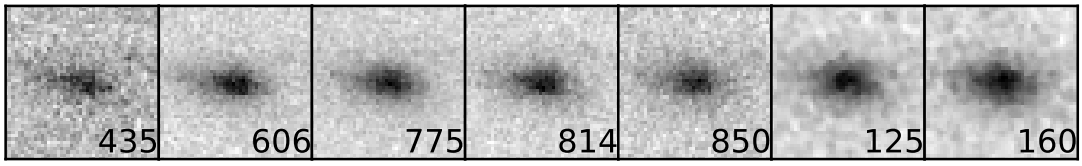

Figure 4.99: Galaxy 146.

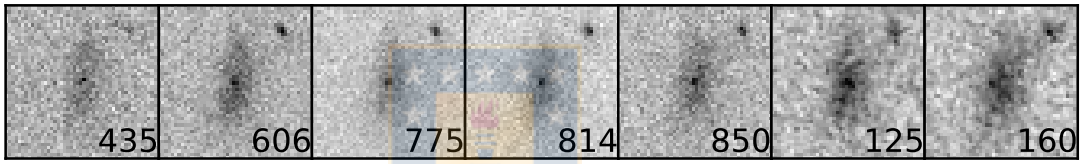

Figure 4.100: Galaxy 147.

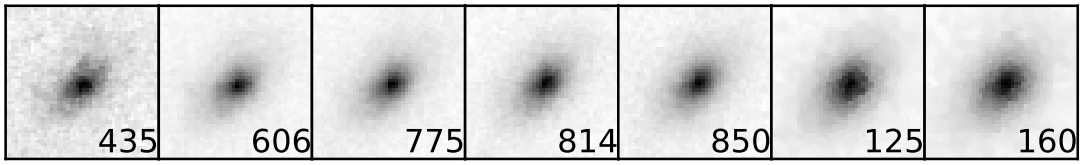

Figure 4.101: Galaxy 149.

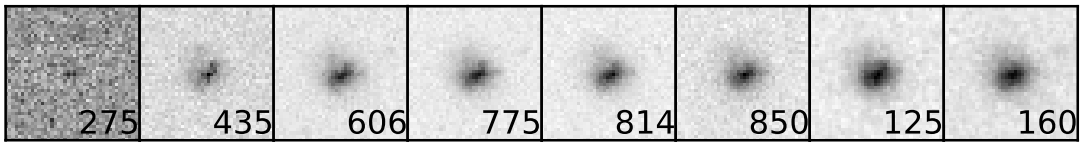

Figure 4.102: Galaxy 150.

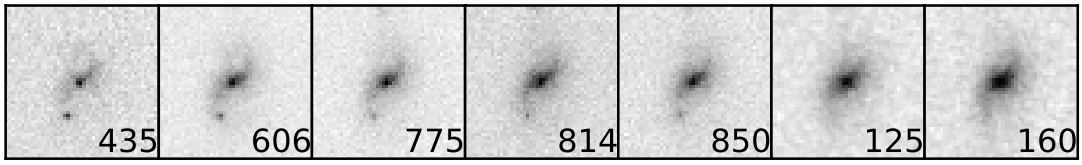

Figure 4.103: Galaxy 151.

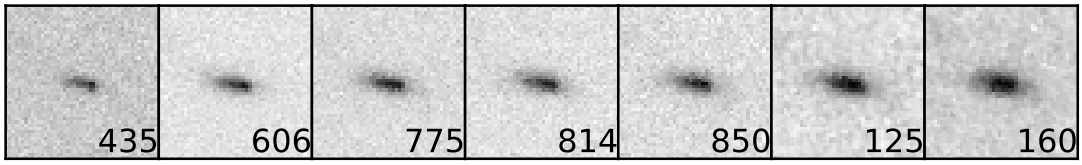

Figure 4.104: Galaxy 152.

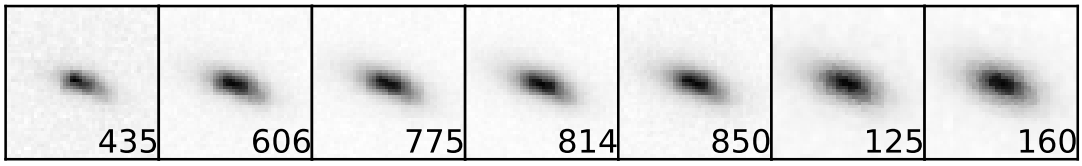

Figure 4.105: Galaxy 153.

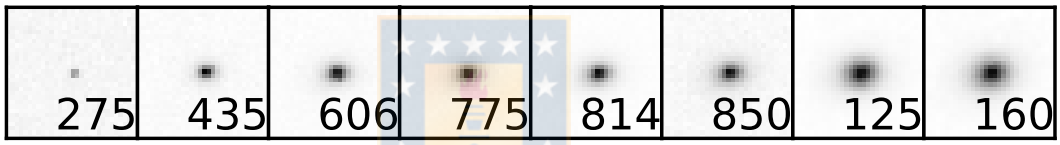

Figure 4.106: Galaxy 154.

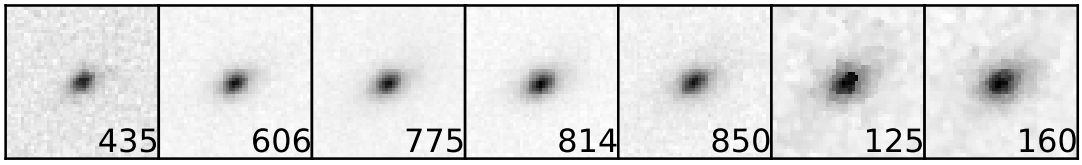

Figure 4.107: Galaxy 155.

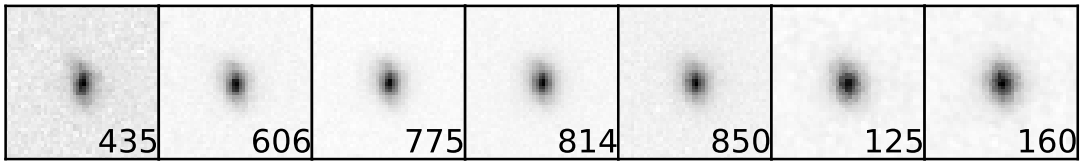

Figure 4.108: Galaxy 158.

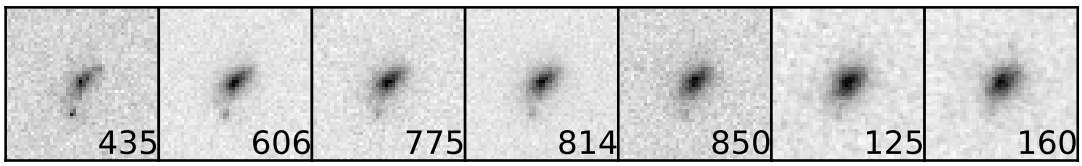

Figure 4.109: Galaxy 159.

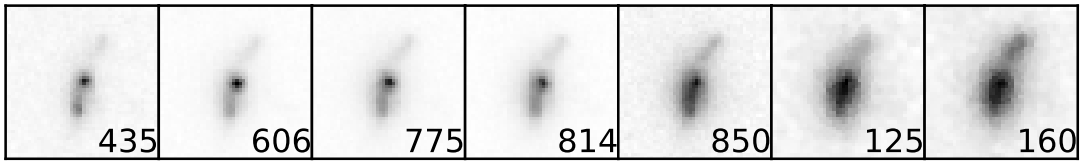

Figure 4.110: Galaxy 160.

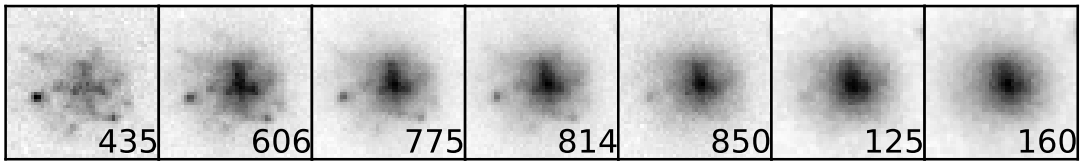

Figure 4.111: Galaxy 161.

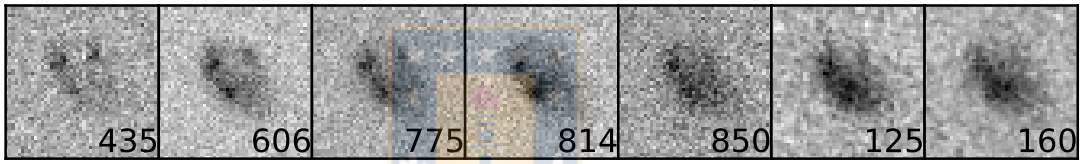

Figure 4.112: Galaxy 162.

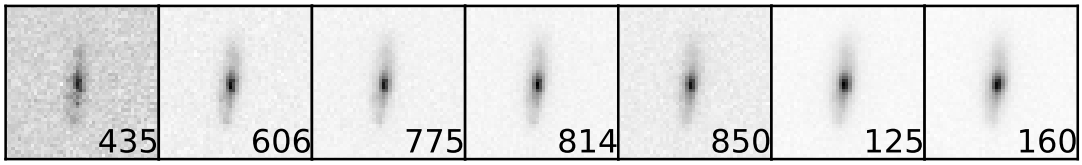

Figure 4.113: Galaxy 163.

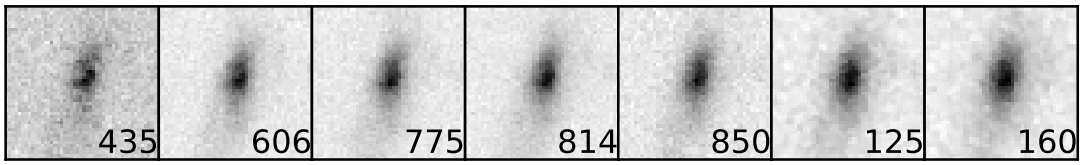

Figure 4.114: Galaxy 164.

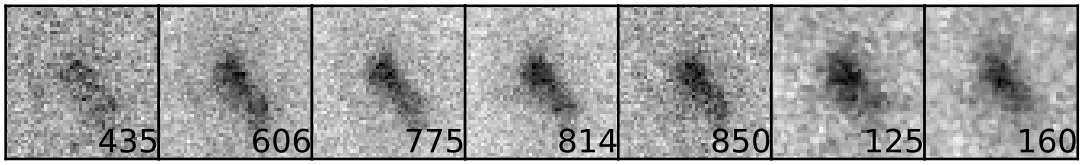

Figure 4.115: Galaxy 166.

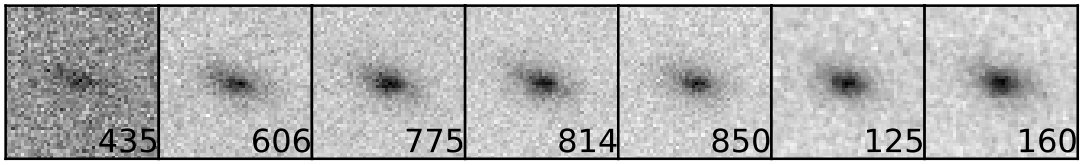

Figure 4.116: Galaxy 167.

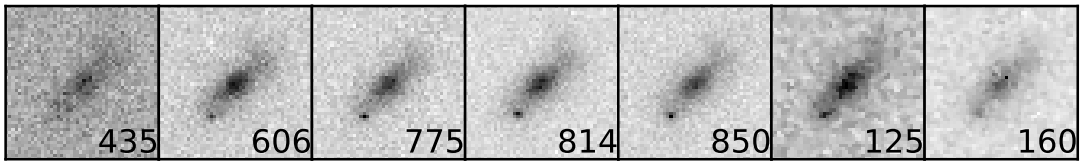

Figure 4.117: Galaxy 168.

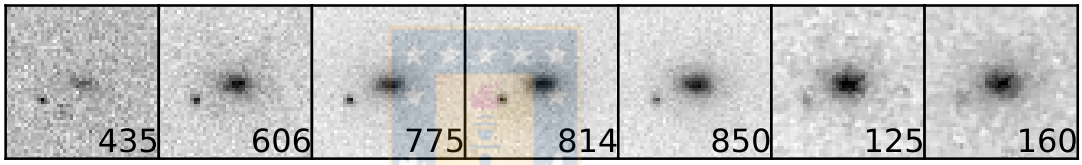

Figure 4.118: Galaxy 169.

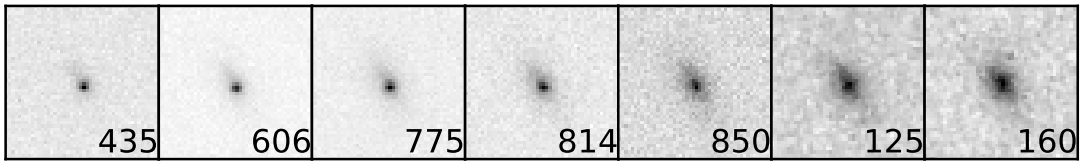

Figure 4.119: Galaxy 171.

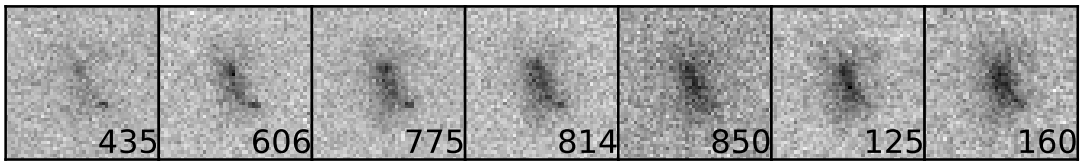

Figure 4.120: Galaxy 172.

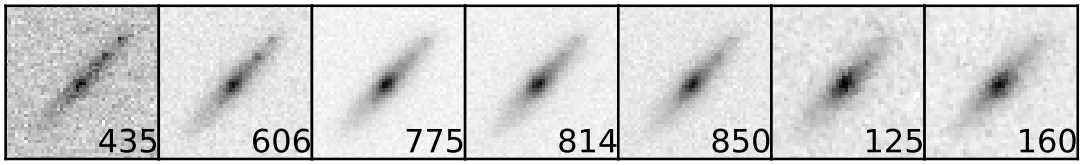

Figure 4.121: Galaxy 173.

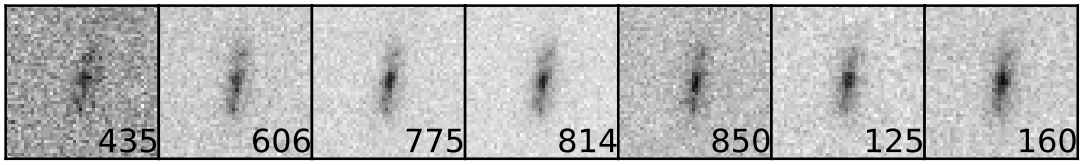

Figure 4.122: Galaxy 174.

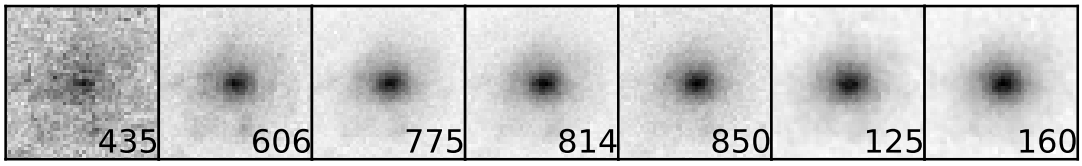

Figure 4.123: Galaxy 176.

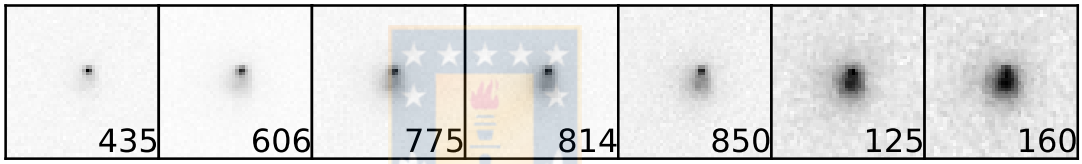

Figure 4.124: Galaxy 177.

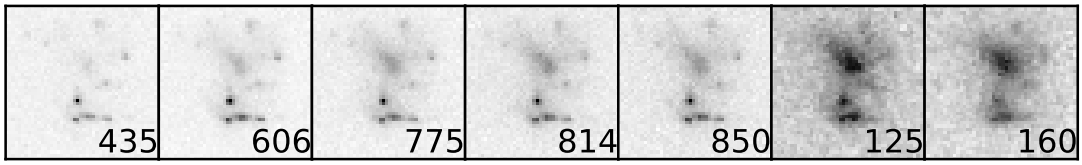

Figure 4.125: Galaxy 178.

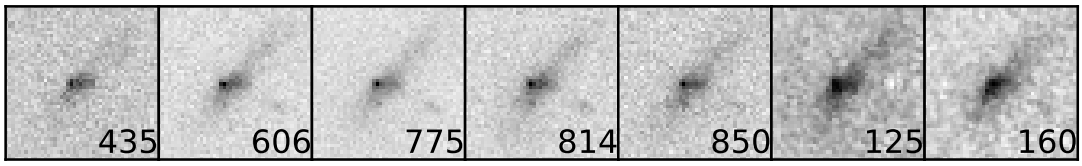

Figure 4.126: Galaxy 179.

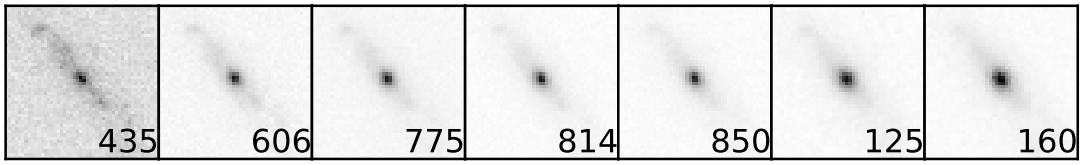

Figure 4.127: Galaxy 180.

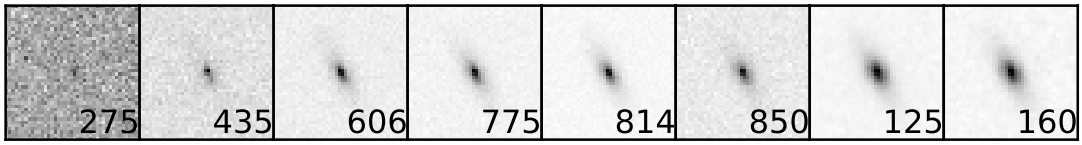

Figure 4.128: Galaxy 181.

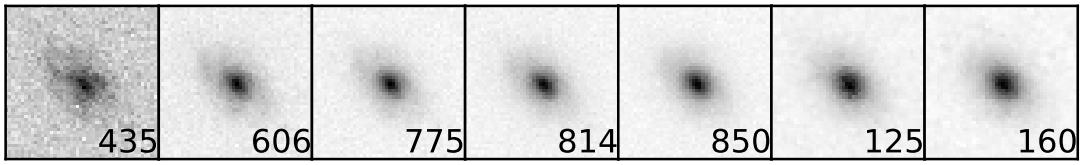

Figure 4.129: Galaxy 184.

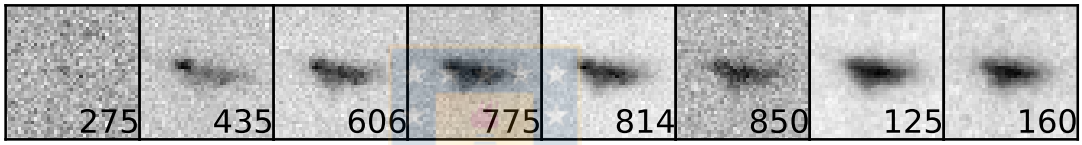

Figure 4.130: Galaxy 187.

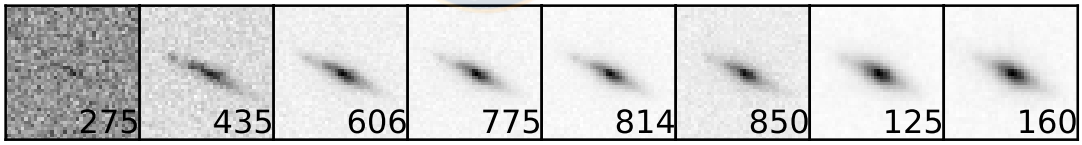

Figure 4.131: Galaxy 188.

Figure 4.132: Galaxy 189.

Figures from 4.1 to 4.132 have been made by the author.

4.2 Spectroscopic and photometric redshift

The redshift is an important parameter to calculate the stellar mass of the galaxies. From the catalog, the photometric and spectroscopic redshift can be obtained. Most of the galaxies have available the photometric redshift, but is less accurate than the spectroscopic one. Therefore, it is necessary to realize spectroscopic observations that require large observation time.

We compare both spectroscopic and photometric redshift in Figure 4.133.

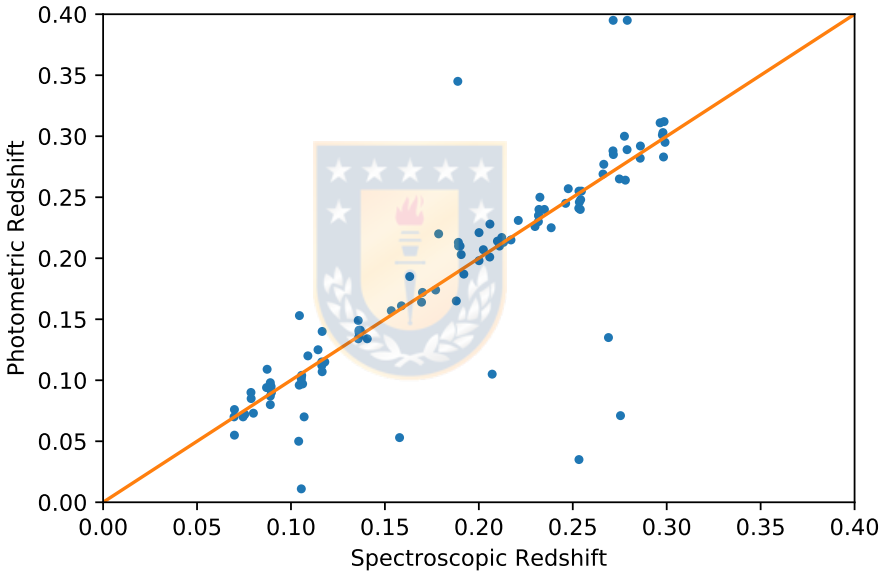

Figure 4.133: Comparison of spectroscopic and photometric redshift for the galaxies from GOODS-N. Source: Made by the author.

Figures 4.134 and 4.135 show both redshifts distribution. Both histogram present 104 galaxies with spectroscopic redshift and 28 galaxies with photometric redshift, respectively. For the calculations, is considered spectroscopic redshift if it is available, and photometric redshift if it is not.

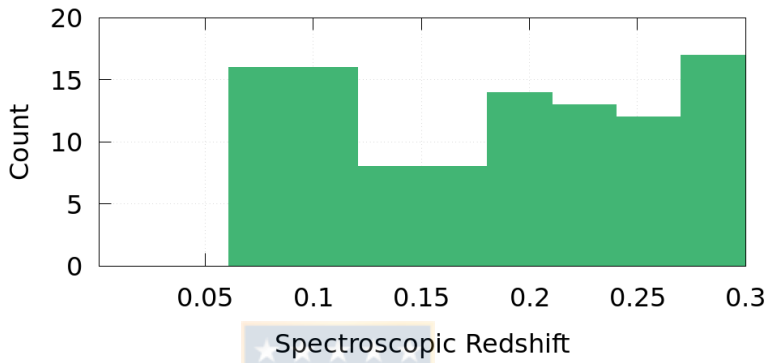

Figure 4.134: Spectroscopic redshift distribution. Source: Made by the author.

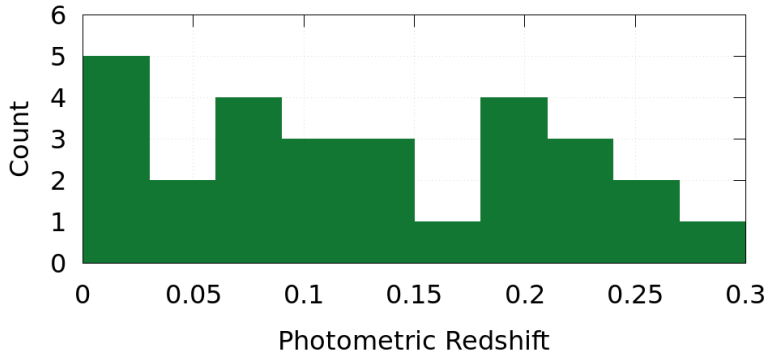

Figure 4.135: Photometric redshift distribution. Source: Made by the author.

4.3 Stellar mass and redshift

Figure 4.136 shows the relation between stellar mass and redshift for the low redshift galaxies sample in the GOODS-North field, using spectroscopic redshift (spec-z) and photometric redshift (phot-z).

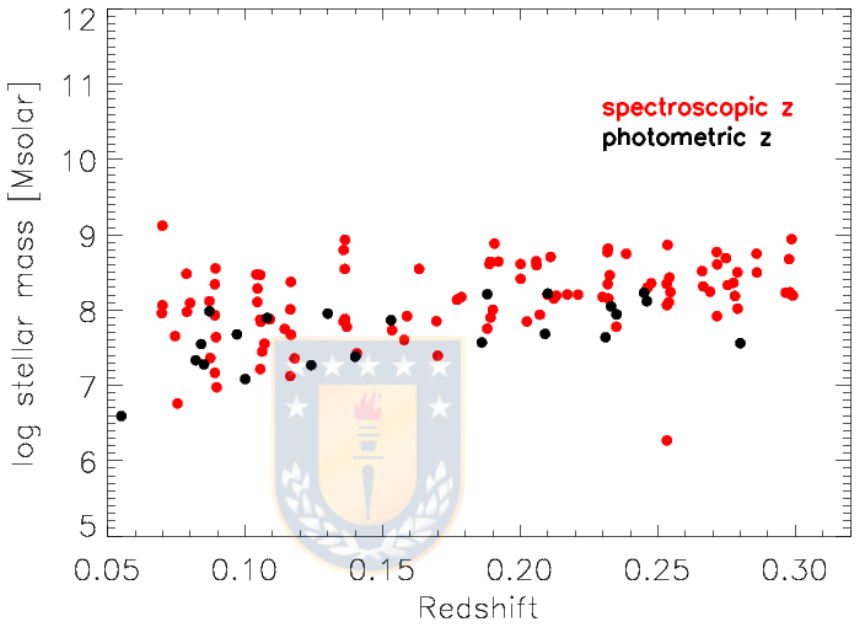

Figure 4.136: The spec-z and phot-z distribution of the low redshift galaxy sample. Source: Made by the author.

4.4 Stellar mass and size

In this section, we present the results referent to mass and size, with stellar mass from CANDELS's catalog. Histogram of stellar mass is shown in Figure 4.137, where the stellar masses are between 5 $M_\odot$ and 9.5 $M_\odot$.

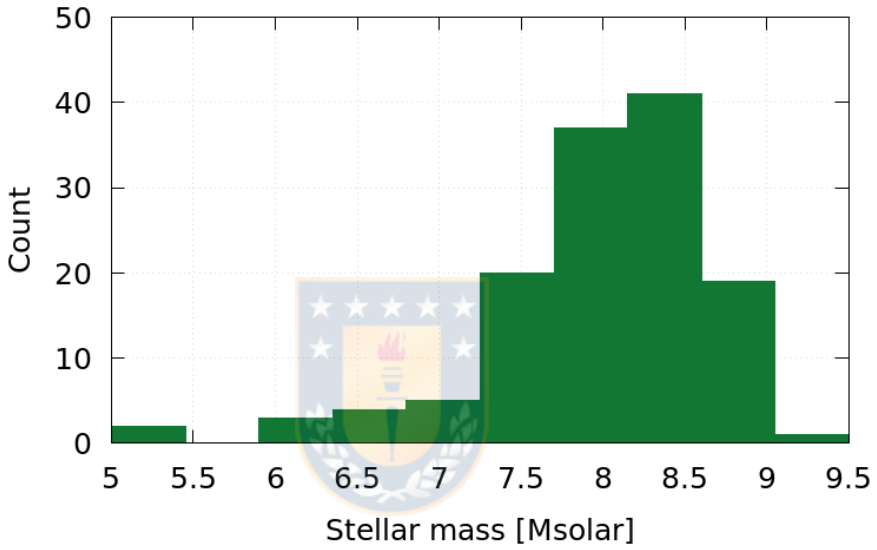

Figure 4.137: Histogram of stellar mass. Source: Made by the author.

Using spectroscopic and photometric redshift, we calculate r_{50} [arcsec] and r_{90} [arcsec] for convert it to [kpc]. The results for R_{50} and R_{90} are shown in Figures 4.138 and 4.140 as a function of the stellar mass of galaxies. Figures 4.139 and 4.141 show a comparison with SDSS [3] and [4]. We define the radii encircling half (R_{50}) and 90 percent light (R_{90}) in a circular aperture.

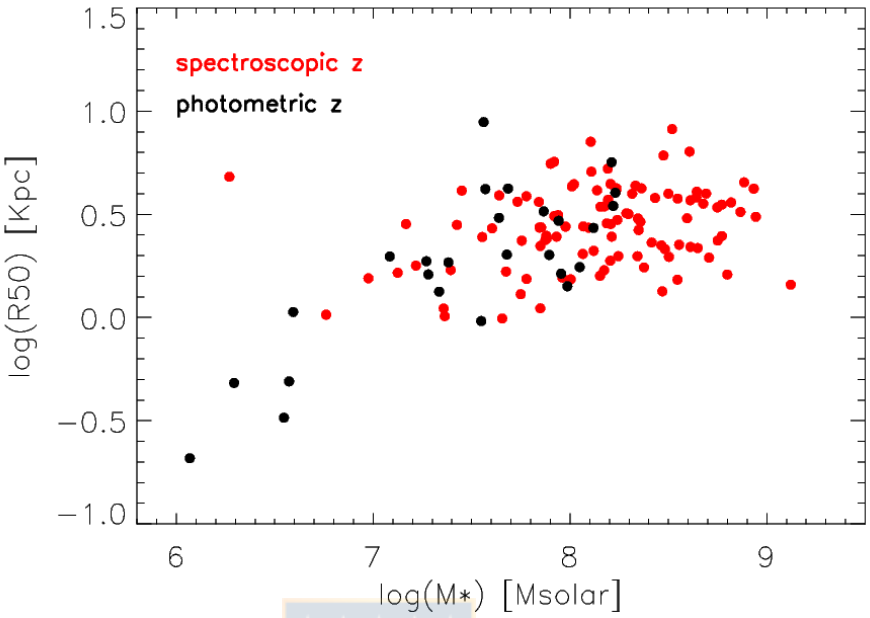

Figure 4.138: Petrosian radius (R_{50}) as a function of the stellar mass for spectroscopic and photometric redshifts. Source: Made by the author.

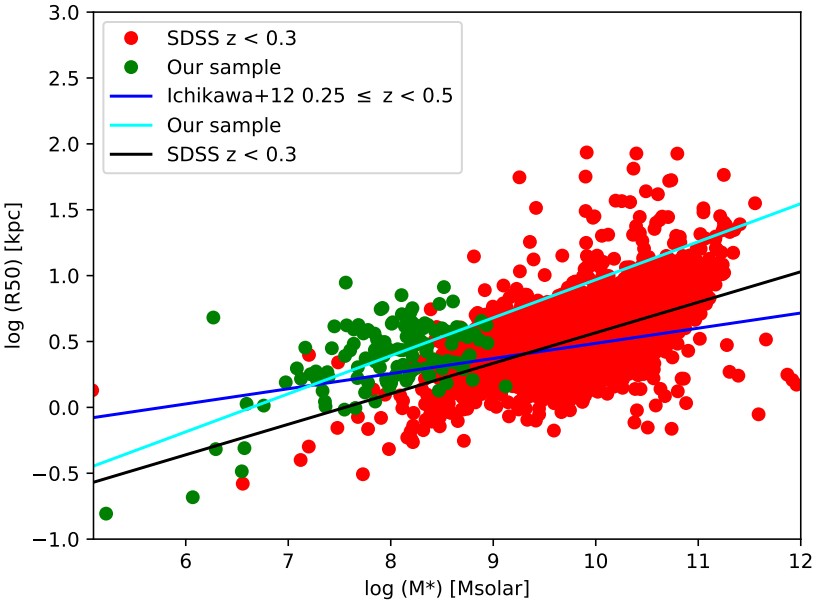

Figure 4.139: Comparison between Petrosian radius (R_{50}) of the galaxies and SDSS [3], as a function of the stellar mass with slope from [4]. Source: Made by the author.

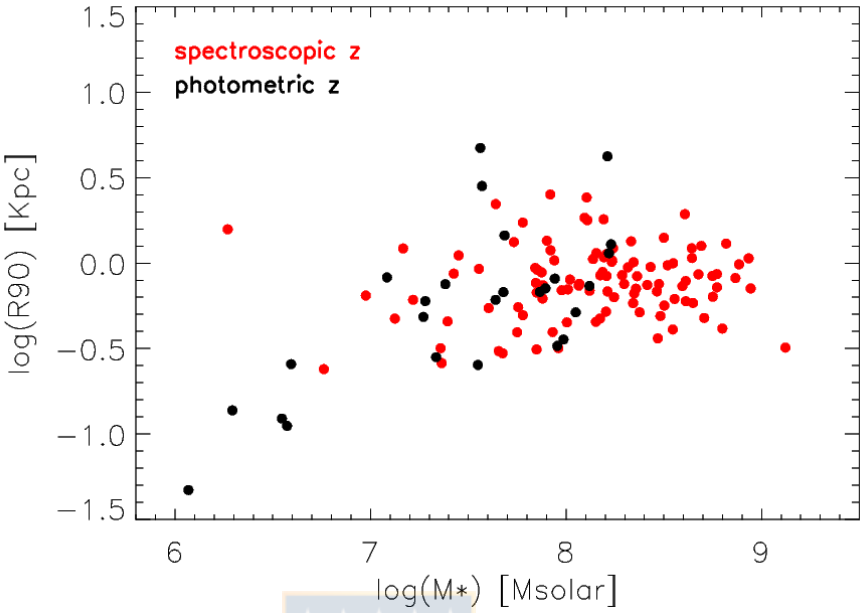

Figure 4.140: Petrosian radius (R_{90}), as a function of the stellar mass for spectroscopic and photometric redshifts. Source: Made by the author.

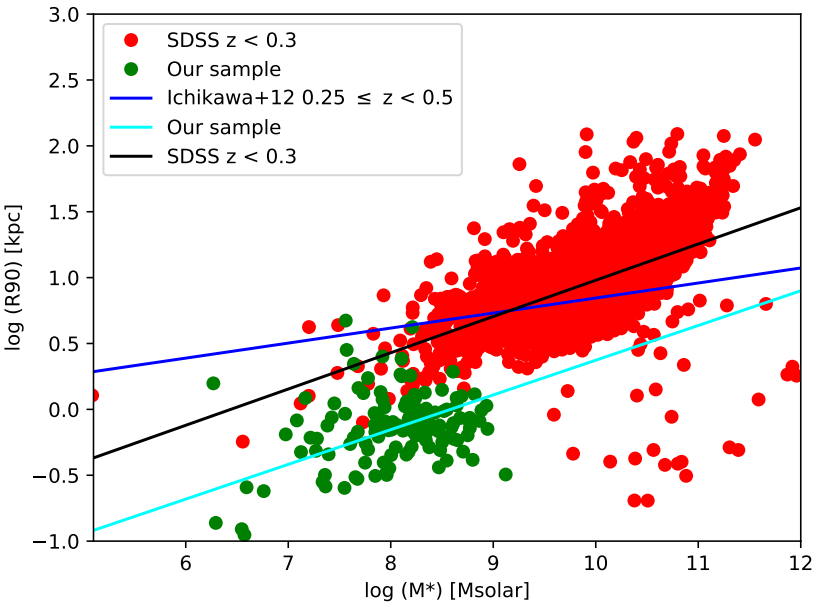

Figure 4.141: Comparison between Petrosian radius (R_{90}) of the galaxies and SDSS [3], as a function of the stellar mass with slope from [4]. Source: Made by the author.

To get the fit of [4], we use linear regression of size-stellar mass relation,

$$\log R = a_r(\log M_* - M) + \log R_r^M, \tag{4.1}$$

where r is 50 for 50% light radius and 90 for 90% light radius. R_r^M is the radius at $M_* = 10^M$ $M_\odot$. For star-forming galaxies, M is 10. In our case, the scatter for R_{50} and R_{90} are 1.504 and 0.658, respectively. The size-mass relation from [4] have a universal slope ($\alpha \sim 0.1 - 0.2$) and the scatter for $R_{50} = 0.133$, while that for $R_{90} = 0.170$.

The slopes and offsets of the regression lines are shown in table 4.1.

Sample	m_{50}	b	m_{90}	b
This work	0.28861326	-1.91755702	0.2635576	-2.26256
SDSS z $<$ 0.3 [3]	0.23152212	-1.74911533	0.27516814	-1.77183271
Ichikawa 0.25 $<$ z $<$ 0.5 [4]	0.115	-0.664	0.114	-0.295

Table 4.1: Linear fit of radius and stellar mass. m_{50} and m_{90} corresponding to the best fit slopes and b is the position coefficient. Source: Made by the author.

4.5 Stellar mass and SFR

In this section, Figure 4.142 shows SFR and stellar mass of 31 star-forming galaxies from our catalog and 5,000 galaxies at z $<$ 0.3 and stellar mass $>$ 10^6 $M_\odot$ from SDSS. Stellar mass is present in GOODS-N catalog and SFR is calculated from [1].

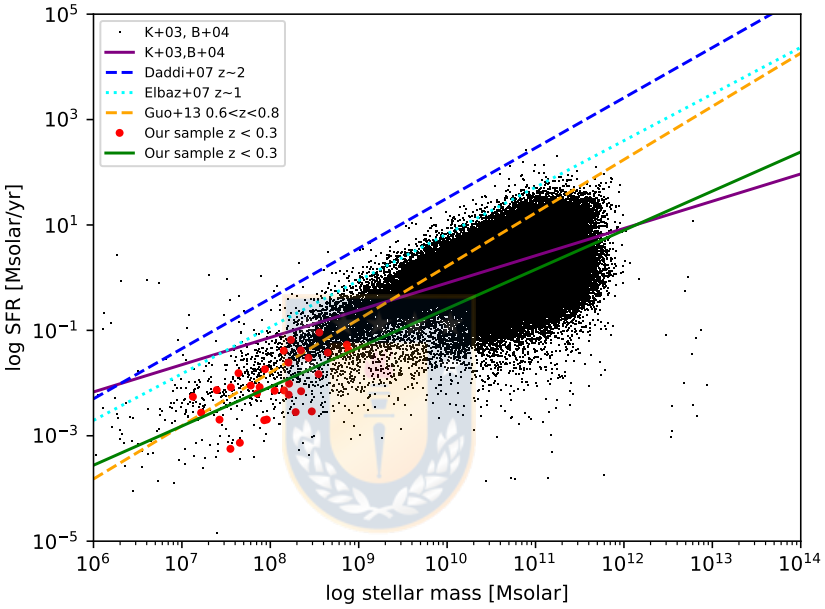

Figure 4.142: Relation between SFR and stellar mass and comparison with [5–7]. Source: Made by the author.

Figure 4.143 shows SFR and stellar mass of 31 star-forming galaxies from the catalog and 5,000 galaxies at z $<$ 0.3 from SDSS. Now, Stellar mass and SFR is calculated using FAST [2]. The input parameters used are shown in Table 3.7.

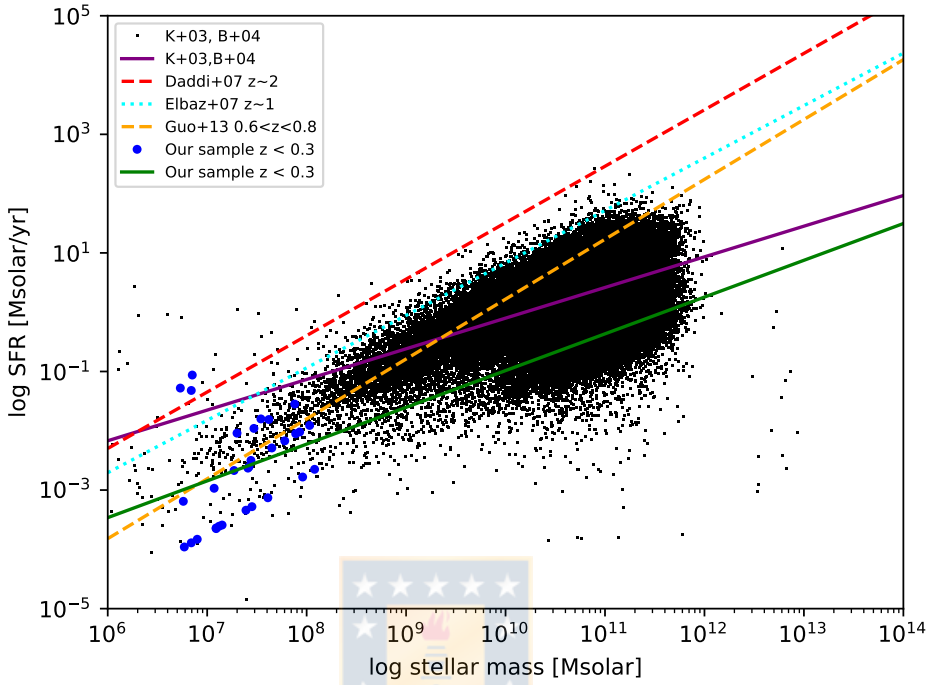

Figure 4.143: Relation between SFR and stellar mass using FAST and comparison with [5–7]. Source: Made by the author.

The slopes and offsets of the regression lines are shown in table 4.2.

Sample	m	b
Figure 4.142	0.74302093	-8.01713569
Figure 4.143	0.62009778	-7.1860299
Sample K+03 [177], B+04 [29]	0.51702293	-5.27058306
Sample Daddi+07 [5]	0.952	-8.0108
Sample Elbaz+07 [6]	0.884615384	-8.0154
Sample Guo+13 [7]	1.01	-9.88

Table 4.2: Linear fit of SFR to stellar mass of Figure 4.142. Source: Made by the author.

The scatter in SFR using the definition of [1] is $\sigma \sim 0.5$, while that using FAST is $\sigma \sim 0.8$. In [6], they have found a tight correlation between the SFR and stellar

mass of blue star-forming galaxies in GOODS at z = 0.8 - 1.2 fitted by,

$$\mathrm{SFR}^{z\sim1}_{\mathrm{GOODS}}[M_{\odot}yr^{-1}] = 7.2[-3.6, +7.2] \times [M_{\star}/10^{10}M_{\odot}]^{0.9}. \tag{4.2}$$

where $M_{\star}$ is stellar mass range $M_{\star} \sim 5 \times 10^{10} - 5 \times 10^{11}$ $\mathrm{M}_{\odot}$.

In other works as [6,34], have shown that star formation and stellar mass define a tight correlation (0.2 dex scatter) in galaxies at z $\sim$ 1 , with rough proportionality (logarithmic slope of 0.9). Similar proportionality is also seen at z = 0 in data from the SDSS [6], although with a lower normalization showing the overall down in cosmic SFR density with time.

For example, [5] has found that a relatively tight stellar mass-SFR relation is already in place at z = 2, for star-forming galaxies detected at 24 μm. The typical star-forming galaxy at z = 2 is forming stars more rapidly by factors of 3.7 and 27 with respect to an object with similar mass at z = 1 and 0.

For the SFG sample of [7] at 0.6 < z < 0.8, the cosmic SFR density decreases about 50% from z = 0.8 to z = 0.6. The fitting of SFR as a function of the stellar mass is given by

$$\log\big(\mathrm{SFR}/\mathrm{M}_{\odot}yr^{-1}\big) = \alpha \log(\mathrm{M}/\mathrm{M}_{\odot}) + \beta \tag{4.3}$$

with $\alpha = 1.01$ and $\beta = -9.88$.

4.6 Stellar mass and SSFR

In this section, Figure 4.144 shows SSFR and stellar mass of 31 star-forming galaxies and 5,000 galaxies at z $<$ 0.3 from SDSS. Stellar mass is in GOODS-N catalog and SSFR is calculated using SFR from [1].

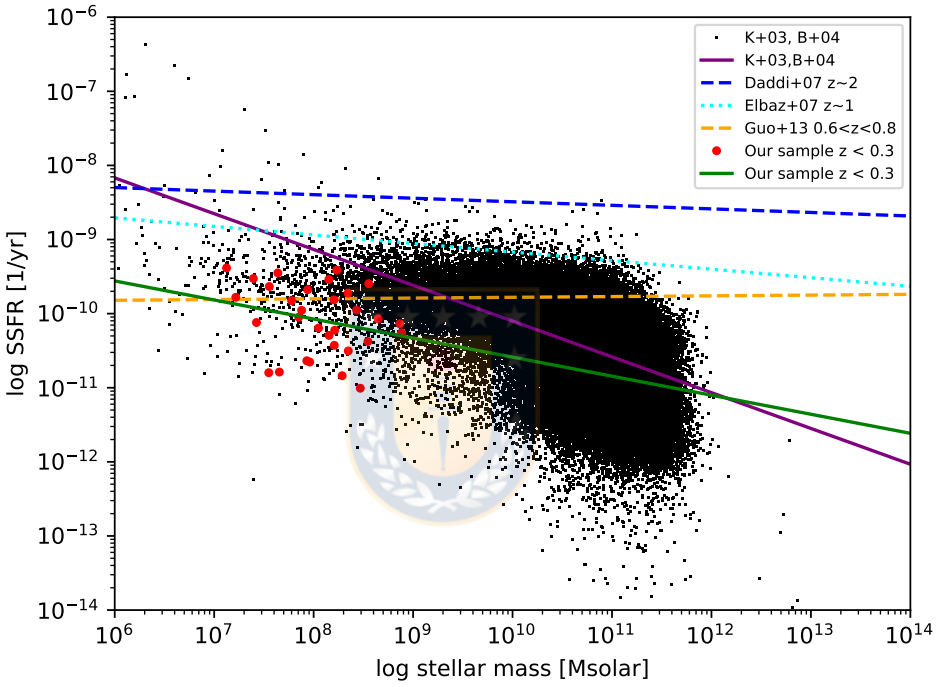

Figure 4.144: Relation between SSFR and stellar mass. Source: Made by the author.

[6] shows that the SSFR is slowly decreasing with stellar mass for z $\sim$ 1 galaxies, SSFR $\sim$ M $_{\star}^{-0.1}$.
[5] finds that at fixed stellar masses, the model galaxies are forming stars at about $\frac{1}{4}$ of the observed rate for galaxies with M $\sim 10^{11}$M$_{\odot}$. The correlation is also substantially tilted, with decreasing specific SFR at larger masses.

Figure 4.145 shows SSFR and stellar mass of 31 star-forming galaxies and 5,000 galaxies at z $<$ 0.3 from SDSS. Now, Stellar mass and SFR is calculated using FAST [2]. The input parameters used are shown in Table 4.3.

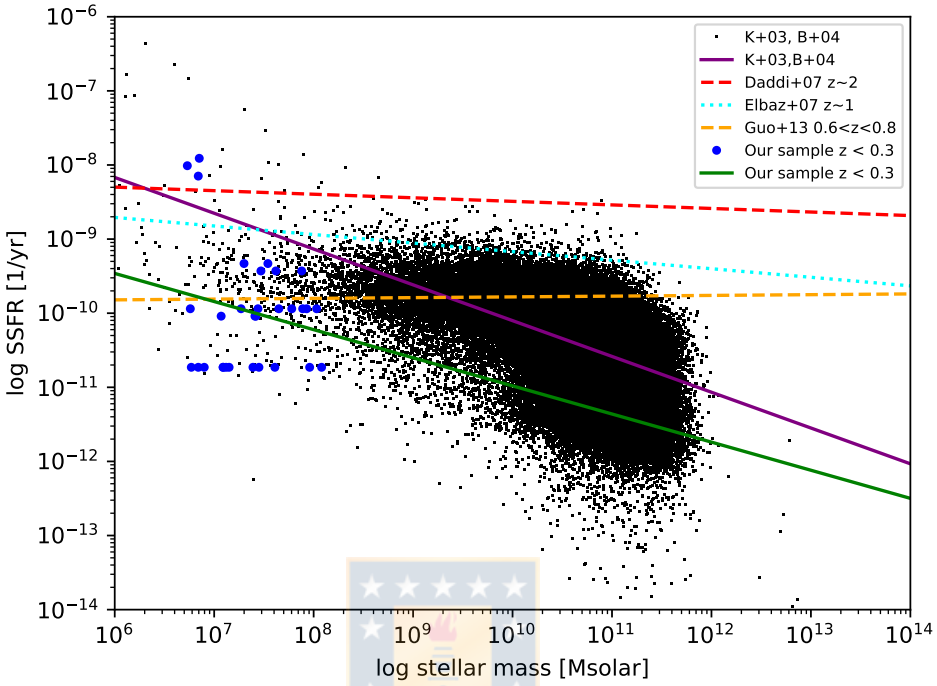

Figure 4.145: Relation between SSFR and stellar mass using FAST. Source: Made by the author.

The slopes and offsets of the regression lines are shown in the table 4.3.

Sample	m	b
Figure 4.144	-0.25697907	-8.01713569
Figure 4.145	-0.37941267	-7.1867324
Sample K+03 [177], B+04 [29]	-0.48297707	-5.27058306
Sample Daddi+07 [5]	-0.048	-8.0108
Sample Elbaz+07 [6]	-0.11538462	-8.0154
Sample Guo+13 [7]	0.01	-9.88

Table 4.3: Linear fit of SSFR to stellar mass of Figures 4.144 and 4.145. Source: Made by the author.

The scatter in SSFR using the definition of [1] is $\sigma \sim 0.4$, while that using FAST is $\sigma \sim 0.8$. In [7], the slope of SFR as a function of the stellar mass equal to the unity suggests a constant SSFR for SFGs over the entire mass ranges examined ($10^{9.5}$ - 10^{10} $M_{\odot}$, 10^{10} - $10^{10.5}$ $M_{\odot}$, $10^{10.5}$ - 10^{11} $M_{\odot}$, 10^{11} - $10^{11.5}$ $M_{\odot}$).

Chapter 5

Conclusion

In this work, it is analyzed different parameters of low redshift galaxies sample between 10^6 and 10^9 $M_\odot$ using images got with Hubble Space Telescope, from CANDELS GOODS-North field. The HST UV data shows a very compact UV morphology in some low mass galaxies, indicating a small range of the star formation. In this sample, it can identify 32 star - forming galaxies. The mass - size relation of the dwarf galaxies has slopes $m_{50} = 0.2886$ and $m_{90} = 0.2635$, and present the same magnitude order of SDSS and [4], although our definition of half-light radius is different from that of [4].

The mass - SFR relation has a slope m $\sim$ 0.7 and a scatter $\sigma \sim 0.5$. The mass - SSFR relation has a slope m $\sim$ -0.2 and a scatter $\sigma \sim 0.4$. In [6], the SSFR decreases with stellar mass while it increases with galaxy density within a limited stellar mass range ($M\star \sim 5 \times 10^{10}$ - 5×10^{11} $M\odot$).

For example, [7] is shown a slope of unity for the mass-SFR relation and it means that SFGs of different stellar masses have a nearly constant SSFR in the population average sense.

Two methods are using to calculate SFR y SSFR, moreover of stellar mass that we know from the CANDELS's catalog. The first way is using the method developed by [1], and the second way is using the software FAST. it is important to calculate with two or more different methods for comparing the results and to evaluate if are consistent. The calculation with FAST, it has been used the library from [171], Chabrier [142] IMF and other parameters indicated in 3.7.

In this research is analyzed a sample of dwarf galaxies to fulfill the gap the bottom tail of low mass galaxies, therefore we search to compare our research with works that uses similar methods and strategies for analyzing massive galaxies. With this analysis, we find relations that it can extrapolate the known properties of massive galaxies to is possible to the lower limit of the main sequence of star formation.

In the table 4.2, we see the resulting slopes after our calculations. The slopes of this work are ∼0.74 and ∼0.62, while the slope of sample of [29, 177] is ∼0.52, and the slopes of [5–7] are ∼0.95, ∼0.88 and ∼1.01, respectively. To the exception of the last slope, all present the same magnitude order. It means dwarf galaxies present a low star formation rate in comparison with massive galaxies.

The discrepancies of this research concerning the other works can be because the strategies or methods of calculation are different.

In future research, we hope to calculate three model-independent parameters, used as a robust classification system, since revealing its major ongoing and past formation modes. These parameters quantitatively measure the concentration (C), asymmetry (A), and clumpiness (S) of a galaxy's stellar light distribution.

To refine the models and values of stellar masses, SFR and SSFR it is important to obtain spectroscopic redshift and metallicity. Recently, we have shown that metallicity of local galaxies is tightly related with stellar mass and SFR [178]. As the fraction of the heaviest elements that helium increases as a function of cosmic time, the metallicity of a star is related to the moment it formed, which allows deducing its age or the area of the galaxy where it was born. These parameters are obtained directly from the spectrum of each galaxy, therefore it is necessary to perform a spectroscopic observation of these objects.

Appendix A

Catalog of galaxies at z $<$ 0.3

We present the catalog of our sample. The first column is a label for each galaxy. 104 galaxies have spectroscopic z (z spec) with their flag. The others present the best median of photometric z (z phot). In the tables A.1, A.2, A.3, A.4 and A.5 equatorial coordinates and z are detailed. In A.6, A.7, A.8 and A.9 are specified the UV images. In A.10, A.11, A.12 and A.13 are shown the stellar masses data and size plotted in 4.138,4.139, 4.140 and 4.141. Finally, in the tables A.14 and A.15 are presented the stellar mass data and SFR plotted in 4.142 and 4.143, and the stellar mass data and SSFR plotted in 4.144 and 4.145, respectively.

A.1 Equatorial coordinates and redshift

The equatorial coordinates, spectroscopic z and photometric z are detailed.

Table A.1: Equatorial coordinates and z part I

Galaxy	RA [deg]	DEC [deg]	z spec	z spec flag	z phot
2	189.16891	62.111804	0.000000	0.000	0.108000
3	189.19627	62.113372	0.000000	0.000	0.130000
4	189.14366	62.113594	0.1144000	2.000	0.125000
5	189.18500	62.115890	0.1164000	2.000	0.112000
7	189.12232	62.130832	0.2476000	2.000	0.257000
8	189.10846	62.130790	0.2001000	2.000	0.221000
10	189.25414	62.136683	0.000000	0.000	0.188000
11	189.24781	62.137401	0.1166000	2.000	0.140000

Table A.2: Equatorial coordinates and z part II

Galaxy	Ra [deg]	Dec [deg]	z spec	z spec flag	z phot
15	189.04104	62.140515	0.2385000	2.000	0.225000
16	189.18064	62.138707	0.08700000	1.000	0.094000
17	189.23948	62.143891	0.17700000	1.000	0.174000
18	189.06227	62.144775	0.1534000	1.000	0.157000
19	189.14027	62.148289	0.000000	0.000	0.209000
20	189.10831	62.148121	0.1920000	2.000	0.187000
21	189.14097	62.150297	0.2099000	2.000	0.214000
23	189.17328	62.150869	0.2754000	1.000	0.071000
24	189.14629	62.151444	0.2001000	1.000	0.198000
26	189.16243	62.153279	0.08730000	2.000	0.109000
28	189.21809	62.158857	0.2299000	1.000	0.226000
29	189.20827	62.159875	0.2860000	1.000	0.292000
30	189.21299	62.160729	0.2058000	1.000	0.201000
31	189.10913	62.163782	0.08960000	1.000	0.090000
33	189.16384	62.164588	0.000000	0.000	0.246000
34	189.21521	62.165152	0.1362000	1.000	0.141000
36	189.09325	62.167383	0.000000	0.000	0.231000
37	189.16608	62.167173	0.1369000	2.000	0.141000
38	189.31320	62.168396	0.2024000	2.000	0.207000
39	189.08724	62.170703	0.000000	0.000	0.235000
40	189.11119	62.172157	0.2540000	1.000	0.240000
42	189.19532	62.172268	0.1695000	2.000	0.164000
46	189.13529	62.177065	0.1363000	2.000	0.136000
47	189.30939	62.180542	0.1363000	1.000	0.140000
50	189.16138	62.183113	0.000000	0.000	0.055000
51	189.05031	62.187146	0.1358000	1.000	0.134000
52	189.32391	62.190905	0.2131000	1.000	0.213000
53	189.21608	62.190400	0.08940000	2.000	0.095000
54	189.27329	62.191455	0.1363000	1.000	0.139000
55	189.13113	62.193600	0.2533000	2.000	0.255000
56	189.17356	62.192184	0.08920000	1.000	0.094000
58	189.04591	62.194241	0.000000	0.000	0.013000
59	189.05098	62.195813	0.2748000	1.000	0.265000
61	189.02923	62.197044	0.1057000	1.000	0.104000
62	189.13803	62.192688	0.08000000	1.000	0.073000
63	189.32620	62.197407	0.1055000	2.000	0.101000
65	189.35814	62.201834	0.08900000	1.000	0.087000
66	189.33161	62.201335	0.06970000	1.000	0.070000

Table A.3: Equatorial coordinates and z part III

Galaxy	Ra [deg]	Dec [deg]	z spec	z spec flag	z phot
67	188.94834	62.201915	0.07870000	1.000	0.090000
68	189.34266	62.203519	0.1055000	2.000	0.011000
69	189.02920	62.204486	0.07880000	1.000	0.085000
70	189.37398	62.209942	0.1588000	2.000	0.161000
74	189.31627	62.211709	0.000000	0.000	0.097000
76	189.25928	62.212006	0.1070000	1.000	0.070000
77	189.02656	62.214747	0.1358000	1.000	0.149000
79	189.21417	62.216837	0.08900000	1.000	0.098000
80	189.27385	62.217589	0.1090000	1.000	0.120000
81	189.06522	62.218126	0.1700000	1.000	0.172000
82	188.99909	62.218144	0.000000	0.000	0.100000
87	189.09044	62.220473	0.2665000	2.000	0.277000
89	189.43150	62.222083	0.000000	0.000	0.186000
90	189.36006	62.222767	0.2991000	2.000	0.295000
91	189.42599	62.223736	0.1045000	2.000	0.153000
92	189.29898	62.224781	0.000000	0.000	0.015000
93	189.39083	62.227673	0.000000	0.000	0.210000
94	189.39951	62.227520	0.1044000	2.000	0.096000
95	189.00945	62.231191	0.000000	0.000	0.140000
96	189.05311	62.232334	0.2859000	1.000	0.282000
99	189.47135	62.235842	0.000000	0.000	0.048000
101	189.11426	62.236525	0.1055000	1.000	0.103000
103	189.47207	62.236531	0.06990000	1.000	0.055000
104	189.24746	62.234660	0.08900000	1.000	0.080000
108	189.44472	62.239042	0.2716000	2.000	0.285000
111	189.14613	62.241565	0.2965000	1.000	0.311000
112	189.03814	62.241135	0.07450000	1.000	0.070000
113	189.09569	62.241971	0.1906000	1.000	0.203000
114	189.23995	62.243862	0.2661000	1.000	0.269000
115	189.44348	62.243837	0.2986000	2.000	0.312000
118	189.24123	62.252002	0.1164000	1.000	0.115000
119	189.10083	62.254030	0.2210000	1.000	0.231000
122	189.11502	62.256681	0.2071000	2.000	0.105000
123	189.42621	62.255104	0.06990000	1.000	0.076000
124	189.20706	62.259516	0.2542000	2.000	0.248000
125	189.40563	62.259754	0.2349000	2.000	0.240000
126	189.45716	62.259131	0.1632000	1.000	0.185000
128	189.41219	62.261406	0.1900000	1.000	0.210000

Table A.4: Equatorial coordinates and z part IV

Galaxy	Ra [deg]	Dec [deg]	z spec	z spec flag	z phot
129	189.41293	62.261775	0.1892000	1.000	0.210000
130	189.48138	62.263028	0.1888000	2.000	0.345000
132	189.35107	62.266069	0.000000	0.000	0.124000
133	189.12664	62.266291	0.2318000	1.000	0.235000
135	189.37497	62.266568	0.2171000	1.000	0.215000
136	189.45727	62.268382	0.000000	0.000	0.085000
137	189.51536	62.265747	0.1041000	1.000	0.050000
138	189.45164	62.276385	0.1180000	1.000	0.115000
139	189.51875	62.277098	0.2789000	2.000	0.289000
140	189.06699	62.277804	0.000000	0.000	0.030000
141	189.51873	62.279567	0.000000	0.000	0.245000
142	189.25179	62.279169	0.000000	0.000	0.084000
144	189.53326	62.280375	0.000000	0.000	0.020000
145	189.07836	62.283334	0.000000	0.000	0.233000
146	189.34876	62.285826	0.000000	0.000	0.005000
147	189.45112	62.285047	0.2533000	3.000	0.035000
149	189.50980	62.287007	0.2325000	2.000	0.250000
150	189.34336	62.288386	0.2320000	1.000	0.240000
151	189.50749	62.288013	0.2775000	2.000	0.300000
152	189.51810	62.290223	0.2780000	1.000	0.264000
153	189.35974	62.290493	0.2714000	1.000	0.288000
154	189.21445	62.292543	0.2122000	1.000	0.217000
155	189.36036	62.293388	0.2690000	2.000	0.135000
158	189.49710	62.298075	0.1786000	2.000	0.220000
159	189.40280	62.300645	0.1880000	1.000	0.165000
160	189.34122	62.301733	0.1166000	1.000	0.107000
161	189.48779	62.301396	0.1891000	1.000	0.213000
162	189.41554	62.302794	0.2715000	2.000	0.395000
163	189.28677	62.304999	0.2319000	1.000	0.235000
164	189.38391	62.307745	0.2462000	1.000	0.245000
166	189.40403	62.313490	0.2790000	2.000	0.395000
167	189.36643	62.304394	0.000000	0.000	0.082000
168	189.27891	62.371171	0.000000	0.000	0.153000
169	189.35448	62.368112	0.000000	0.000	0.087000
171	189.31297	62.364011	0.07540000	1.000	0.072000
172	189.29745	62.361801	0.1062000	2.000	0.097000
173	189.26733	62.356710	0.2977000	2.000	0.301000
174	189.26478	62.339516	0.2980000	1.000	0.303000

Table A.5: Equatorial coordinates and z part V

Galaxy	Ra [deg]	Dec [deg]	z spec	z spec flag	z phot
176	189.32672	62.346331	0.2317000	1.000	0.230000
177	189.33804	62.338803	0.2546000	1.000	0.255000
178	189.30676	62.334519	0.000000	0.000	0.280000
179	189.31470	62.330229	0.1578000	2.000	0.053000
180	189.34047	62.334810	0.2110000	1.000	0.210000
181	189.17104	62.315358	0.2983000	1.000	0.283000
184	189.39224	62.320116	0.2059000	2.000	0.228000
187	189.21460	62.313228	0.1406000	2.000	0.134000
188	189.21093	62.317699	0.2532000	2.000	0.241000
189	189.23455	62.314765	0.2535000	1.000	0.246000

A.2 UV morphology

Here is specifying the results of UV images. The second column indicates if the camera of telescope captured UV image and the third column if this image has star formation traces.

Table A.6: UV Morphology part I

Galaxy	UV image	Star formation
2	NO	NO
3	NO	NO
4	NO	NO
5	NO	NO
7	NO	NO
8	NO	NO
10	YES	NO
11	YES	NO
15	NO	NO
16	NO	NO
17	YES	NO
18	NO	NO
19	NO	NO
20	NO	NO
21	NO	NO
23	YES	NO
24	NO	NO
26	YES	NO
28	YES	NO
29	YES	NO
30	YES	YES
31	NO	NO
33	YES	NO
34	YES	YES
36	NO	NO
37	YES	YES
38	YES	YES
39	NO	NO
40	NO	NO
42	YES	NO
46	YES	NO

Table A.7: UV Morphology part II

Galaxy	UV image	Star formation
47	YES	NO
50	YES	NO
51	NO	NO
52	YES	NO
53	YES	NO
54	YES	NO
55	YES	NO
56	YES	YES
58	NO	NO
59	NO	NO
61	NO	NO
62	YES	NO
63	YES	YES
65	YES	YES
66	YES	YES
67	NO	NO
68	YES	NO
69	NO	NO
70	YES	NO
74	YES	NO
76	YES	YES
77	NO	NO
79	YES	NO
80	YES	YES
81	YES	YES
82	NO	NO
87	YES	YES
89	YES	NO
90	YES	YES
91	YES	YES
92	YES	YES
93	YES	NO
94	YES	NO
95	YES	NO
96	YES	NO
99	NO	NO
101	YES	NO

Table A.8: UV Morphology part III

Galaxy	UV image	Star formation
103	NO	NO
104	YES	NO
108	YES	NO
111	YES	YES
112	YES	YES
113	YES	YES
114	YES	NO
115	YES	NO
118	YES	YES
119	YES	YES
122	YES	YES
123	YES	NO
124	YES	NO
125	YES	NO
126	NO	NO
128	YES	NO
129	YES	NO
130	NO	NO
132	YES	YES
133	YES	YES
135	YES	YES
136	NO	NO
137	NO	NO
138	NO	NO
139	NO	NO
140	YES	NO
141	NO	NO
142	YES	NO
144	NO	NO
145	YES	YES
146	YES	NO
147	NO	NO
149	NO	NO
150	YES	YES
151	NO	NO
152	NO	NO
153	YES	NO
154	YES	YES

Table A.9: UV Morphology part IV

Galaxy	UV image	Star formation
155	YES	NO
158	NO	NO
159	NO	NO
160	NO	NO
161	NO	NO
162	NO	NO
163	YES	NO
164	NO	NO
166	NO	NO
167	NO	NO
168	NO	NO
169	NO	NO
171	NO	NO
172	NO	NO
173	NO	NO
174	NO	NO
176	NO	NO
177	NO	NO
178	NO	NO
179	NO	NO
180	NO	NO
181	YES	YES
184	NO	NO
187	YES	YES
188	YES	YES
189	YES	YES

A.3 Mass and size relation

We present the measurements of stellar mass and the results of Petrosian Radius at 20%, 50% and 90% light concentration.

Table A.10: Petrosian radius and stellar mass part I

Galaxy	log Stellar mass [$M_\odot$]	log R_{20} [kpc]	log R_{50} [kpc]	log R_{90} [kpc]
2	7.894229	3.80058	2.01099	0.711942
3	7.955050	2.88680	1.63119	0.327717
4	7.749600	1.97671	1.29717	0.393780
5	8.009650	6.88680	4.31651	0.702228
7	8.357400	6.22229	2.90941	0.708513
8	8.611769	10.4586	3.69956	0.785584
10	8.211399	7.67778	5.65772	4.21156
11	8.376049	3.55965	1.74902	0.515437
15	8.748697	9.44366	3.41769	0.841246
16	8.120200	4.62062	2.10499	0.689244
17	8.137750	7.30999	4.13315	1.05685
18	7.732999	5.60353	3.64033	1.32866
19	7.684999	9.39042	4.21697	1.45187
20	8.643900	15.7789	4.07005	1.07021
21	8.205694	7.53512	4.43817	1.12595
23	8.332499	8.36584	4.35214	1.34007
24	8.414957	6.41536	2.30827	0.745254
26	7.363591	1.92139	1.01581	0.260028
28	8.175000	6.65786	3.45414	0.848770
29	8.500205	7.10915	3.98159	1.40642
30	8.648805	4.59358	2.17003	0.584436
31	6.975663	2.62448	1.54880	0.645753
33	8.119400	6.23746	2.71798	0.735598
34	8.545786	3.53843	1.52491	0.408887
36	7.638891	5.60113	3.04017	0.609782
37	7.778800	2.69602	1.53759	0.495703
38	7.849750	4.11973	2.22201	0.672889
39	7.942219	5.66598	2.94143	0.811141
40	8.105000	11.6535	7.10823	2.42043
42	7.853250	5.85128	2.73327	0.912778
46	8.933692	6.78410	4.21026	1.06618

Table A.11: Petrosian radius and stellar mass part II

Galaxy	log Stellar mass [$M_\odot$]	log R_{20} [kpc]	log R_{50} [kpc]	log R_{90} [kpc]
47	7.841949	5.63513	3.63163	0.937046
50	6.593497	2.08156	1.06342	0.256217
51	7.849000	1.99076	1.10726	0.312543
52	8.192149	8.20079	5.26187	1.80477
53	7.639999	6.59347	3.90391	2.21455
54	7.881899	3.94655	2.41820	0.741933
55	8.067305	6.49256	2.76316	0.757290
56	8.554600	4.94647	2.25181	0.617248
58	5.222999	0.280612	0.156109	0.0387823
59	8.691349	8.01458	3.98546	1.26058
61	7.844999	5.17891	2.72776	0.766109
62	8.094838	4.08077	2.72204	1.84152
63	8.469139	3.58573	1.33940	0.362850
65	7.931250	5.32329	2.46603	0.395086
66	7.960499	3.61954	1.56073	0.318043
67	8.482223	4.45040	2.14410	0.490528
68	7.875000	3.71644	2.37482	0.883049
69	7.977350	4.31238	2.75743	0.693875
70	7.919999	7.40816	3.09866	1.18909
74	7.679073	3.54086	2.01712	0.676674
76	7.554149	4.28087	2.45499	0.925534
77	8.799149	3.19931	1.61525	0.414054
79	7.166450	7.15921	2.83866	1.21845
80	7.879349	4.43442	2.48747	0.620732
81	7.393835	3.66328	1.69900	0.456060
82	7.083999	4.12582	1.97661	0.824818
87	8.315849	9.14181	3.98050	0.944250
89	7.569827	6.45165	4.19196	2.82581
90	8.193703	11.5358	3.72519	1.08278
91	8.286699	6.01529	3.19970	0.850630
92	6.068416	0.395380	0.207941	0.0470040
93	8.219328	6.96782	3.47322	1.14350
94	8.108549	7.75967	5.09363	1.78352
95	7.382200	4.75647	1.85035	0.753198
96	8.750360	5.27032	2.35991	0.635604
99	6.572650	1.00311	0.490482	0.111510
101	7.217299	3.66843	1.78513	0.609893

Table A.12: Petrosian radius and stellar mass part III

Galaxy	log Stellar mass [$M_\odot$]	log R_{20} [kpc]	log R_{50} [kpc]	log R_{90} [kpc]
103	8.064999	3.21408	2.03414	0.737987
104	8.342650	3.04304	1.98106	0.583075
108	8.607760	12.2191	6.36684	1.93319
111	8.233549	8.65344	4.09442	1.01742
112	7.655450	1.75880	0.988855	0.305672
113	8.884600	11.4987	4.51825	0.983633
114	8.518652	14.8385	8.18274	0.971082
115	8.943828	6.73726	3.07601	0.710803
118	7.124450	2.95045	1.64734	0.473956
119	8.204449	3.56800	1.88386	0.520485
122	7.939899	5.61446	3.13416	1.03693
123	9.121499	4.47881	1.44233	0.320312
124	8.432100	7.59048	3.79539	0.948902
125	7.778249	6.41555	3.86910	1.72795
126	8.547034	6.75827	3.76983	0.998065
128	8.003849	2.71217	1.53092	0.449946
129	7.901500	7.41817	5.56177	1.35253
130	8.612000	4.59362	2.19766	0.598505
132	7.269999	3.28602	1.87361	0.484562
133	8.345299	5.52593	3.01889	1.01303
135	8.207257	5.93727	2.83899	0.840127
136	7.280000	4.71564	1.61700	0.599487
137	8.474999	10.8239	6.09700	0.754695
138	7.358050	2.01809	1.10550	0.317975
139	8.502603	3.88460	1.96830	0.564636
140	6.293191	1.18292	0.481785	0.137477
141	8.230200	8.56221	4.02302	1.28851
142	7.548788	1.77976	0.961428	0.253570
144	6.546606	0.494974	0.326902	0.123194
145	8.049149	3.38601	1.75548	0.515059
146	5.205000	0.157637	0.0816669	0.0235634
147	6.269374	9.11708	4.80684	1.57597
149	8.464351	3.98764	2.23657	0.683197
150	8.154600	5.88948	3.44365	1.14490
151	8.362955	8.42559	4.22256	0.838557
152	8.186924	6.07283	2.85935	0.887493
153	8.771649	4.78132	2.48267	0.721585
154	8.152629	3.18543	1.59202	0.453493

Table A.13: Petrosian radius and stellar mass part IV

Galaxy	log Stellar mass [$M_\odot$]	log R_{20} [kpc]	log R_{50} [kpc]	log R_{90} [kpc]
155	8.245300	4.07596	1.98136	0.631547
158	8.173550	3.05824	1.69381	0.474307
159	7.754999	4.53330	2.35707	0.552235
160	7.674999	2.80874	1.66946	0.296883
161	8.642580	6.22713	3.82429	1.22057
162	7.919400	8.89495	5.68341	2.52084
163	8.818600	11.1586	3.60966	1.30139
164	8.296950	7.47646	3.17488	0.755432
166	8.019999	8.61322	4.42355	0.801320
167	7.334917	2.90058	1.33367	0.281621
168	7.866050	5.52725	3.26905	0.678887
169	7.986506	3.24187	1.41709	0.357150
171	6.760849	2.18206	1.03140	0.239687
172	7.450000	6.74598	4.12089	1.10921
173	8.676850	9.05700	3.56185	0.859520
174	8.235862	11.8894	4.22842	1.03360
176	8.771240	7.07947	3.52222	0.862083
177	8.240096	6.94593	2.97242	1.21891
178	7.561146	12.5375	8.84868	4.72034
179	7.604000	5.82257	2.70520	0.545696
180	8.706358	6.75291	1.94959	0.477566
181	8.211949	5.67538	2.46528	0.682742
184	8.594725	6.00065	3.02585	0.732933
187	7.425279	4.77493	2.81123	0.868124
188	8.348530	6.05582	2.65367	0.664097
189	8.866099	7.03785	3.24823	0.817321

A.4 Stellar mass, SFR and SSFR

We present the measurements of stellar mass and the results of SFR and SSFR.

Table A.14: Results of stellar mass, SFR and SSFR calculated using [1].

Galaxy	log Stellar mass [$M_\odot$]	log SFR [$M_\odot$/yr]	log SSFR [1/yr]
30	8.648805	-1.421892	-10.070697
34	8.545786	-1.830843	-10.376629
37	7.778800	-2.046498	-9.825298
38	7.849750	-2.198421	-10.048171
56	7.639999	-1.810745	-9.450745
63	8.554600	-1.040976	-9.595576
65	8.469139	-2.537644	-11.006784
66	7.931250	-2.704891	-10.636141
76	7.960499	-2.692412	-10.652912
80	7.554149	-2.079903	-9.634053
81	7.879349	-2.076275	-9.955625
87	7.393835	-2.132148	-9.525983
90	8.286699	-2.550811	-10.837511
91	7.217299	-2.562565	-9.779865
92	8.233549	-1.180398	-9.413948
111	7.655450	-3.132976	-10.788426
112	8.884600	-1.374464	-10.259064
113	7.124450	-2.259294	-9.383744
118	8.204449	-1.610005	-9.814455
119	7.939899	-1.737104	-9.677004
122	8.432100	-1.520505	-9.952605
132	8.345299	-1.378672	-9.723972
133	8.207257	-2.220550	-10.427807
135	7.548788	-3.248344	-10.797132
145	8.049149	-2.145639	-10.194788
150	8.154600	-2.138985	-10.293585
154	8.152629	-1.386877	-9.539506
181	8.211949	-2.011810	-10.223760
187	7.425279	-2.694363	-10.119642
188	8.348530	-2.154694	-10.503224
189	8.866099	-1.271201	-10.137301

Table A.15: Stellar mass, SFR and SSFR calculated with FAST [2].

Galaxy	log Stellar mass [$M_\odot$]	log SFR [$M_\odot$/yr]	log SSFR [1/yr]
30	7.89	-2.05	-9.94
34	8.03	-1.91	-9.94
37	7.54	-1.80	-9.33
38	7.09	-3.64	-10.73
56	7.96	-2.78	-10.73
63	8.08	-2.65	-10.73
65	7.30	-2.04	-9.33
66	7.93	-2.02	-9.94
76	6.90	-3.83	-10.73
80	7.27	-2.67	-9.94
81	6.85	-1.06	-7.91
87	7.12	-3.61	-10.73
90	6.84	-3.89	-10.73
91	7.45	-3.28	-10.73
92	6.76	-3.19	-9.94
111	7.07	-2.97	-10.04
112	7.44	-2.50	-9.94
113	7.61	-3.13	-10.73
118	6.84	-1.32	-8.15
119	7.65	-2.29	-9.94
122	7.09	-3.65	-10.73
132	6.73	-1.28	-8.01
133	7.39	-3.34	-10.73
135	7.41	-2.63	-10.04
145	7.47	-1.96	-9.43
150	7.15	-3.59	-10.73
154	7.78	-2.17	-9.94
181	7.42	-2.61	-10.04
187	6.77	-3.96	-10.73
188	7.62	-1.81	-9.43
189	7.88	-1.55	-9.43

Bibliography

[1] R. C. Kennicutt y N. J. Evans, Annual Review of Astronomy and Astrophysics **50**, 1 (sep 2012).

[2] M. Kriek, P. G. van Dokkum, I. Labbé, M. Franx, G. D. Illingworth, D. Marchesini y R. F. Quadri, The Astrophysical Journal **700**, 1 (jul 2009).

[3] D. G. York, J. Adelman, J. E. Anderson, Jr., S. F. Anderson, J. Annis, N. A. Bahcall, J. A. Bakken, R. Barkhouser, S. Bastian, E. Berman, W. N. Boroski, S. Bracker, C. Briegel, J. W. Briggs, J. Brinkmann, R. Brunner, S. Burles, L. Carey, M. A. Carr, F. J. Castander, B. Chen, P. L. Colestock, A. J. Connolly, J. H. Crocker, I. Csabai, P. C. Czarapata, J. E. Davis, M. Doi, T. Dombeck, D. Eisenstein, N. Ellman, B. R. Elms, M. L. Evans, X. Fan, G. R. Federwitz, L. Fiscelli, S. Friedman, J. A. Frieman, M. Fukugita, B. Gillespie, J. E. Gunn, V. K. Gurbani, E. de Haas, M. Haldeman, F. H. Harris, J. Hayes, T. M. Heckman, G. S. Hennessy, R. B. Hindsley, S. Holm, D. J. Holmgren, C.-h. Huang, C. Hull, D. Husby, S.-I. Ichikawa, T. Ichikawa, Ž. Ivezić, S. Kent, R. S. J. Kim, E. Kinney, M. Klaene, A. N. Kleinman, S. Kleinman, G. R. Knapp, J. Korienek, R. G. Kron, P. Z. Kunszt, D. Q. Lamb, B. Lee, R. F. Leger, S. Limmongkol, C. Lindenmeyer, D. C. Long, C. Loomis, J. Loveday, R. Lucinio, R. H. Lupton, B. MacKinnon, E. J. Mannery, P. M. Mantsch, B. Margon, P. McGehee, T. A. McKay, A. Meiksin, A. Merelli, D. G. Monet, J. A. Munn, V. K. Narayanan, T. Nash, E. Neilsen, R. Neswold, H. J. Newberg, R. C. Nichol, T. Nicinski, M. Nonino, N. Okada, S. Okamura, J. P. Ostriker, R. Owen, A. G. Pauls, J. Peoples, R. L. Peterson, D. Petravick, J. R. Pier, A. Pope, R. Pordes, A. Prosapio, R. Rechenmacher, T. R. Quinn, G. T.

Richards, M. W. Richmond, C. H. Rivetta, C. M. Rockosi, K. Ruthmansdorfer, D. Sandford, D. J. Schlegel, D. P. Schneider, M. Sekiguchi, G. Sergey, K. Shimasaku, W. A. Siegmund, S. Smee, J. A. Smith, S. Snedden, R. Stone, C. Stoughton, M. A. Strauss, C. Stubbs, M. SubbaRao, A. S. Szalay, I. Szapudi, G. P. Szokoly, A. R. Thakar, C. Tremonti, D. L. Tucker, A. Uomoto, D. Vanden Berk, M. S. Vogeley, P. Waddell, S.-i. Wang, M. Watanabe, D. H. Weinberg, B. Yanny y N. Yasuda, The Astronomical Journal **120**, 3 (sep 2000).

[4] T. Ichikawa, M. Kajisawa y M. Akhlaghi, Monthly Notices of the Royal Astronomical Society **422**, 2 (2012).

[5] E. Daddi, M. Dickinson, G. Morrison, R. Chary, A. Cimatti, D. Elbaz, D. Frayer, A. Renzini, A. Pope, D. M. Alexander, F. E. Bauer y M. Giavalisco, ApJ **670**, 156 (2007).

[6] D. Elbaz, E. Daddi, D. L. Borgne, M. Dickinson, D. M. Alexander, R.-R. Chary, J.-L. Starck, W. N. Brandt, M. Kitzbichler, E. MacDonald, M. Nonino, P. Popesso, D. Stern y E. Vanzella, Astronomy & Astrophysics **468**, 1 (mar 2007).

[7] Y. Guo, H. C. Ferguson, M. Giavalisco, G. Barro, S. P. Willner, M. L. N. Ashby, T. Dahlen, J. L. Donley, S. M. Faber, A. Fontana, A. Galametz, A. Grazian, K.-H. Huang, D. D. Kocevski, A. M. Koekemoer, D. C. Koo, E. J. McGrath, M. Peth, M. Salvato, S. Wuyts, M. Castellano, A. R. Cooray, M. E. Dickinson, J. S. Dunlop, G. G. Fazio, J. P. Gardner, E. Gawiser, N. A. Grogin, N. P. Hathi, L.-T. Hsu, K.-S. Lee, R. A. Lucas, B. Mobasher, K. Nandra, J. A. Newman y A. van der Wel, The Astrophysical Journal Supplement Series **207**, 2 (2013).

[8] A. M. Koekemoer, S. M. Faber, H. C. Ferguson, N. A. Grogin, D. D. Kocevski, D. C. Koo, K. Lai, J. M. Lotz, R. A. Lucas, E. J. McGrath, S. Ogaz, A. Rajan, A. G. Riess, S. A. Rodney, L. Strolger, S. Casertano, M. Castellano, T. Dahlen, M. Dickinson, T. Dolch, A. Fontana, M. Giavalisco, A. Grazian,

Y. Guo, N. P. Hathi, K.-H. Huang, A. van der Wel, H.-J. Yan, V. Acquaviva, D. M. Alexander, O. Almaini, M. L. N. Ashby, M. Barden, E. F. Bell, F. Bournaud, T. M. Brown, K. I. Caputi, P. Cassata, P. J. Challis, R.-R. Chary, E. Cheung, M. Cirasuolo, C. J. Conselice, A. R. Cooray, D. J. Croton, E. Daddi, R. Davé, D. F. de Mello, L. de Ravel, A. Dekel, J. L. Donley, J. S. Dunlop, A. A. Dutton, D. Elbaz, G. G. Fazio, A. V. Filippenko, S. L. Finkelstein, C. Frazer, J. P. Gardner, P. M. Garnavich, E. Gawiser, R. Gruetzbauch, W. G. Hartley, B. Häussler, J. Herrington, P. F. Hopkins, J.-S. Huang, S. W. Jha, A. Johnson, J. S. Kartaltepe, A. A. Khostovan, R. P. Kirshner, C. Lani, K.-S. Lee, W. Li, P. Madau, P. J. McCarthy, D. H. McIntosh, R. J. McLure, C. McPartland, B. Mobasher, H. Moreira, A. Mortlock, L. A. Moustakas, M. Mozena, K. Nandra, J. A. Newman, J. L. Nielsen, S. Niemi, K. G. Noeske, C. J. Papovich, L. Pentericci, A. Pope, J. R. Primack, S. Ravindranath, N. A. Reddy, A. Renzini, H.-W. Rix, A. R. Robaina, D. J. Rosario, P. Rosati, S. Salimbeni, C. Scarlata, B. Siana, L. Simard, J. Smidt, D. Snyder, R. S. Somerville, H. Spinrad, A. N. Straughn, O. Telford, H. I. Teplitz, J. R. Trump, C. Vargas, C. Villforth, C. R. Wagner, P. Wandro, R. H. Wechsler, B. J. Weiner, T. Wiklind, V. Wild, G. Wilson, S. Wuyts y M. S. Yun, The Astrophysical Journal Supplement Series **197**, 2 (2011).

[9] N. A. Grogin, D. D. Kocevski, S. M. Faber, H. C. Ferguson, A. M. Koekemoer, A. G. Riess, V. Acquaviva, D. M. Alexander, O. Almaini, M. L. N. Ashby, M. Barden, E. F. Bell, F. Bournaud, T. M. Brown, K. I. Caputi, S. Casertano, P. Cassata, M. Castellano, P. Challis, R.-R. R. Chary, E. Cheung, M. Cirasuolo, C. J. Conselice, A. R. Cooray, D. J. Croton, E. Daddi, T. Dahlen, R. Davé, D. F. De Mello, A. Dekel, M. Dickinson, T. Dolch, J. L. Donley, J. S. Dunlop, A. A. Dutton, D. Elbaz, G. G. Fazio, A. V. Filippenko, S. L. Finkelstein, A. Fontana, J. P. Gardner, P. M. Garnavich, E. Gawiser, M. Giavalisco, A. Grazian, Y. Guo, N. P. Hathi, B. Häussler, P. F. Hopkins, J.-S. S. Huang, K.-H. H. Huang, S. W. Jha, J. S. Kartaltepe, R. P. Kirshner, D. C. Koo, K. Lai, K.-S. S. Lee, W. Li, J. M. Lotz, R. A. Lucas, P. Madau, P. J. McCarthy,

E. J. McGrath, D. H. McIntosh, R. J. McLure, B. Mobasher, L. A. Moustakas, M. Mozena, K. Nandra, J. A. Newman, S.-M. M. Niemi, K. G. Noeske, C. J. Papovich, L. Pentericci, A. Pope, J. R. Primack, A. Rajan, S. Ravindranath, N. A. Reddy, A. Renzini, H.-W. W. Rix, A. R. Robaina, S. A. Rodney, D. J. Rosario, P. Rosati, S. Salimbeni, C. Scarlata, B. Siana, L. Simard, J. Smidt, R. S. Somerville, H. Spinrad, A. N. Straughn, L.-G. G. Strolger, O. Telford, H. I. Teplitz, J. R. Trump, A. van der Wel, C. Villforth, R. H. Wechsler, B. J. Weiner, T. Wiklind, V. Wild, G. Wilson, S. Wuyts, H.-J. J. Yan y M. S. Yun, The Astrophysical Journal Supplement Series **197**, 2 (dec 2011).

[10] R. G. Abraham, N. R. Tanvir, B. X. Santiago, R. S. Ellis, K. Glazebrook y S. v. d. Bergh, Monthly Notices of the Royal Astronomical Society **279**, 3 (apr 1996).

[11] C. J. Conselice, Astronomical Society of the Pacific **109**, 1251 (1997).

[12] M. Takamiya, Publications of the Astronomical Society of the Pacific **111**, 760 (jun 1999).

[13] M. A. Bershady, A. Jangren y C. J. Conselice, The Astronomical Journal **119**, 6 (jun 2000).

[14] C. J. Conselice, M. A. Bershady y A. Jangren, The Astrophysical Journal **1**, 529 (2000).

[15] MICHAEL R. CORBIN, ANDREA URBAN, ELIZABETH STOBIE, RODGER I. THOMPSON y G. SCHNEIDER, The Astrophysical Journal **551**, 23 (2001).

[16] C. J. Conselice **147**, 1 (2003).

[17] S. P. Driver, A. Fernández-Soto, W. J. Couch, S. C. Odewahn, R. A. Windhorst, S. Phillipps, K. Lanzetta y A. Yahil, The Astrophysical Journal **496**, 2 (apr 1998).

[18] S. van den Bergh, Cambridge Astrophysics Series **35** (2000).

[19] J. M. Lotz, B. W. Miller y H. C. Ferguson, The Astrophysical Journal **613**, 1 (2004).

[20] P. Cassata, A. Cimatti, A. Franceschini, E. Daddi, E. Pignatelli, G. Fasano, G. Rodighiero, L. Pozzetti, M. Mignoli y A. Renzini, Monthly Notices of the Royal Astronomical Society **357**, 3 (2005).

[21] C. J. Conselice, J. A. Blackburne y C. Papovich, The Astrophysical Journal **620**, 2 (2005).

[22] C. J. Conselice, S. Rajgor y R. Myers, Monthly Notices of the Royal Astronomical Society **386**, 2 (2008).

[23] P. Cassata, M. Giavalisco, Y. Guo, H. Ferguson, A. M. Koekemoer, A. Renzini, A. Fontana, S. Salimbeni, M. Dickinson, S. Casertano, C. J. Conselice, N. Grogin, J. M. Lotz, C. Papovich, R. A. Lucas, A. Straughn, J. P. Gardner y L. Moustakas, The Astrophysical Journal **714**, 1 (may 2010).

[24] R. A. Overzier, T. M. Heckman, D. Schiminovich, A. Basu-Zych, T. Gonçalves, D. C. Martin y R. M. Rich, The Astrophysical Journal **710**, 2 (feb 2010).

[25] E. Cameron, Astronomical society of Australia págs. 128–139 (dec 2010).

[26] C. J. Conselice, A. F. L. Bluck, F. Buitrago, A. E. Bauer, R. Grützbauch, R. J. Bouwens, S. Bevan, A. Mortlock, M. Dickinson, E. Daddi, H. Yan, D. Scott, S. C. Chapman, R.-R. Chary, H. C. Ferguson, M. Giavalisco, N. Grogin, G. Illingworth, S. Jogee, A. M. Koekemoer, R. A. Lucas, B. Mobasher, L. Moustakas, C. Papovich, S. Ravindranath, B. Siana, H. Teplitz, I. Trujillo, M. Urry y T. Weinzirl, Monthly Notices of the Royal Astronomical Society **413**, 1 (may 2011).

[27] S. Shen, H. J. Mo, S. D. M. White, M. R. Blanton, G. Kauffmann, W. Voges, J. Brinkmann y I. Csabai, Mon. Not. R. Astron. Soc **343**, 978 (2003).

[28] M. Bernardi, N. Roche, F. Shankar y R. K. Sheth, Monthly Notices of the Royal Astronomical Society: Letters **412**, 1 (2011).

[29] J. Brinchmann, S. Charlot, S. D. M. White, C. Tremonti, G. Kauffmann, T. Heckman y J. Brinkmann, Monthly Notices of the Royal Astronomical Society **351**, 4 (2004).

[30] S. Salim, R. M. Rich, S. Charlot, J. Brinchmann, B. D. Johnson, D. Schiminovich, M. Seibert, R. Mallery, T. M. Heckman, K. Forster, P. G. Friedman, D. C. Martin, P. Morrissey, S. G. Neff, T. Small, T. K. Wyder, L. Bianchi, J. Donas, Y. Lee, B. F. Madore, B. Milliard, A. S. Szalay, B. Y. Welsh y S. K. Yi, The Astrophysical Journal Supplement Series **173**, 2 (2007).

[31] L. A. M. Tasca, O. Le Fèvre, N. P. Hathi, D. Schaerer, O. Ilbert, G. Zamorani, B. C. Lemaux, P. Cassata, B. Garilli, V. Le Brun, D. Maccagni, L. Pentericci, R. Thomas, E. Vanzella, E. Zucca, R. Amorin, S. Bardelli, L. P. Cassarà, M. Castellano, A. Cimatti, O. Cucciati, A. Durkalec, A. Fontana, M. Giavalisco, A. Grazian, S. Paltani, B. Ribeiro, M. Scodeggio, V. Sommariva, M. Talia, L. Tresse y P. W. Wang, A&A J. Dunlop C. López-Sanjuan J. Pforr 1 **5814**, 20 (2015).

[32] D. Elbaz, M. Dickinson, H. S. Hwang, T. Díaz-Santos, G. Magdis, B. Magnelli, D. Le Borgne, F. Galliano, M. Pannella, P. Chanial, L. Armus, V. Charmandaris, E. Daddi, H. Aussel, P. Popesso, J. Kartaltepe, B. Altieri, I. Valtchanov, D. Coia, H. Dannerbauer, K. Dasyra, R. Leiton, J. Mazzarella, D. M. Alexander, V. Buat, D. Burgarella, R.-R. Chary, R. Gilli, R. J. Ivison, S. Juneau, E. Le Floc'h, D. Lutz, G. E. Morrison, J. R. Mullaney, E. Murphy, A. Pope, D. Scott, M. Brodwin, D. Calzetti, C. Cesarsky, S. Charlot, H. Dole, P. Eisenhardt, H. C. Ferguson, N. Förster Schreiber, D. Frayer, M. Giavalisco, M. Huynh, A. M. Koekemoer, C. Papovich, N. Reddy, C. Surace, H. Teplitz, M. S. Yun y G. Wilson, Astronomy & Astrophysics **533**, A119 (2011).

[33] J. M. Gabor, R. Davé, K. Finlator y B. D. Oppenheimer, Monthly Notices of the Royal Astronomical Society **407**, 2 (sep 2010).

[34] K. G. Noeske, B. J. Weiner, S. M. Faber, C. Papovich, D. C. Koo, R. S. Somerville, K. Bundy, C. J. Conselice, J. A. Newman, D. Schiminovich, E. L. Floc'h, A. L. Coil, G. H. Rieke, J. M. Lotz, J. R. Primack, P. Barmby, M. C. Cooper, M. Davis, R. S. Ellis, G. G. Fazio, P. Guhathakurta, J. Huang, S. A. Kassin, D. C. Martin, A. C. Phillips, R. M. Rich, T. A. Small, C. N. A. Willmer y G. Wilson **10**, 1 (2007).

[35] N. Drory y M. Alvarez págs. 41–53 (mar 2008).

[36] M. Kajisawa, T. Ichikawa, T. Yoshikawa, T. Yamada, M. Onodera, M. Akiyama y I. Tanaka, Publications of the Astronomical Society of Japan **63**, sp2 (mar 2011).

[37] A. E. Bauer, C. J. Conselice, P. G. Pérez-González, R. Grützbauch, A. F. L. Bluck, F. Buitrago y A. Mortlock, Monthly Notices of the Royal Astronomical Society **417**, 1 (oct 2011).

[38] D. G. Gilbank, M. D. Gladders, H. K. Yee y B. C. Hsieh, Astronomical Journal **141**, 3 (2011).

[39] S. Heinis, V. Buat, M. Béthermin, J. Bock, D. Burgarella, A. Conley, A. Cooray, D. Farrah, O. Ilbert, G. Magdis, G. Marsden, S. J. Oliver, D. Rigopoulou, Y. Roehlly, B. Schulz, M. Symeonidis, M. Viero, C. K. Xu y M. Zemcov, Monthly Notices of the Royal Astronomical Society **437**, 2 (2013).

[40] N. Reddy, M. Dickinson, D. Elbaz, G. Morrison, M. Giavalisco, R. Ivison, C. Papovich, D. Scott, V. Buat, D. Burgarella, V. Charmandaris, E. Daddi, G. Magdis, E. Murphy, B. Altieri, H. Aussel, H. Dannerbauer, K. Dasyra, H. S. Hwang, J. Kartaltepe, R. Leiton, B. Magnelli y P. Popesso, Astrophysical Journal **744**, 2 (jan 2012).

[41] R. J. Bouwens, G. D. Illingworth, P. A. Oesch, M. Franx, I. Labbé, M. Trenti, P. Van Dokkum, C. M. Carollo, V. González, R. Smit y D. Magee, Astrophysical Journal **754**, 2 (aug 2012).

[42] Y. Koyama, T. Kodama, K. I. Tadaki, M. Hayashi, M. Tanaka, I. Smail, I. Tanaka y J. Kurk, Monthly Notices of the Royal Astronomical Society **428**, 2 (jan 2013).

[43] S. de Barros, D. Schaerer y D. P. Stark, Astronomy & Astrophysics **563**, A81 (mar 2012).

[44] J. S. Speagle, C. L. Steinhardt, P. L. Capak y J. D. Silverman **15**, 1988 (2014).

[45] F. Bertola, Putting galaxies on the scale (2002).

[46] V. Springel, S. D. M. White, A. Jenkins, C. S. Frenk, N. Yoshida, L. Gao, J. Navarro, R. Thacker, D. Croton, J. Helly, J. A. Peacock, S. Cole, P. Thomas, H. Couchman, A. Evrard, J. Colberg y F. Pearce, Nature **435**, 7042 (jun 2005).

[47] J. Diemand, M. Kuhlen, P. Madau, M. Zemp, B. Moore, D. Potter y J. Stadel, Nature **454**, 7205 (aug 2008).

[48] D. et al Spergel, The Astrophysical Journal Supplement Series **148**, 175 (2003).

[49] M. Hamuy, M. M. Phillips, N. B. Suntzeff, R. A. Schommer, J. Maza, R. C. Smith, P. Lira y R. Aviles, The Astronomical Journal **112**, 2438 (dec 1996).

[50] S. Perlmutter, G. Aldering, G. Goldhaber, R. A. Knop, P. Nugent, P. G. Castro, S. Deustua, S. Fabbro, A. Goobar, D. E. Groom, I. M. Hook, A. G. Kim, M. Y. Kim, J. C. Lee, N. J. Nunes, R. Pain, C. R. Pennypacker, Quimby, R, C. Lidman, R. S. Ellis, R. G. Mcmahon, P. Ruiz-Lapuente, N. Walton, B. Schaefer, B. J. Boyle, A. V. Filippenko, T. Matheson, A. S. Fruchter, N. Panagia9, H. J. M. Newberg y W. J. Couch, the Astrophysical Journal **517**, 565 (1999).

[51] A. G. Riess, L.-g. Strolger, J. Tonry, S. Casertano, H. C. Ferguson, B. Mobasher, P. Challis, A. V. Filippenko, S. Jha, W. Li, R. Chornock y R. P. Kirshner, Camera págs. 665–687 (2004).

[52] N. Jarosik, C. L. Bennett, J. Dunkley, B. Gold, M. R. Greason, M. Halpern, R. S. Hill, G. Hinshaw, A. Kogut, E. Komatsu, D. Larson, M. Limon, S. S. Meyer, M. R. Nolta, N. Odegard, L. Page, K. M. Smith, D. N. Spergel, G. S. Tucker, J. L. Weiland, E. Wollack y E. L. Wright, Astrophysical Journal, Supplement Series **192**, 2 (2011).

[53] A. V. Kravtsov, O. Y. Gnedin y A. A. Klypin págs. 482–497 (2004).

[54] B. Willman, J. J. Dalcanton, D. Martinez-delgado, A. a. West, M. R. Blanton, D. W. Hogg, J. C. Barentine, H. J. Brewington, M. Harvanek, S. J. Kleinman, J. Krzesinski, D. Long, E. H. Neilsen, A. Nitta y S. a. Snedden, The Astrophysical Journal **626**, 2 (2005).

[55] D. B. Z. V. Belokurov, N. W. Evans, M. I. Wilkinson, D. M. B. M. J. Irwin, S. Hodgkin, J. M. Irwin, S. V. G. Gilmore, B. Willman, H. J. Newberg, . M. F. R. F. G. Wyse, P. C. Hewett, N. Cole, . T. C. B. E. F. Bell, . B. Y. C. M. Rockosi, . D. P. S. E. K. Grebel, R. Lupton, J. C. Barentine, H. Brewington, J. Brinkmann y D. L. M. Harvanek, S. J. Kleinman, J. Krzesinski,, Observatory **7**, 2 (2006).

[56] D. B. Zucker, V. Belokurov, N. W. Evans, M. I. Wilkinson, M. J. Irwin, T. Sivarani, S. Hodgkin, D. M. Bramich, J. M. Irwin, G. Gilmore, B. Willman, S. Vidrih, M. Fellhauer, P. C. Hewett, T. C. Beers, E. F. Bell, E. K. Grebel, D. P. Schneider, H. J. Newberg, R. F. G. Wyse, C. M. Rockosi y B. Yanny, The Astrophysical Journal **643**, Cmd (2006).

[57] V. Belokurov, D. B. Zucker, N. W. Evans, J. T. Kleyna, S. Koposov, S. T. Hodgkin, M. J. Irwin, G. Gilmore, M. I. Wilkinson, M. Fellhauer, D. M. Bramich, P. C. Hewett, S. Vidrih, J. T. A. De Jong, J. A. Smith, H. W. Rix, E. F. Bell, R. F. G. Wyse, H. J. Newberg, P. A. Mayeur, B. Yanny, C. M.

Rockosi, O. Y. Gnedin, D. P. Schneider, T. C. Beers, J. C. Barentine, H. Brewington, J. Brinkmann, M. Harvanek, S. J. Kleinman, J. Krzesinski, D. Long, A. Nitta y S. A. Snedden **31** (2006).

[58] S. M. Walsh, H. Jerjen y B. Willman págs. 83–86 (2007).

[59] S. E. Koposov, J. Yoo, H. W. Rix, D. H. Weinberg, A. V. MacCiò y J. M. Escudé, Astrophysical Journal **696**, 2 (2009).

[60] K. Shimasaku, M. Fukugita, M. Doi, M. Hamabe, T. Ichikawa, S. Okamura, M. Sekiguchi, N. Yasuda, J. Brinkmann, I. Csabai, S.-I. Ichikawa, Z. Ivezić, P. Z. Kunszt, D. P. Schneider, G. P. Szokoly, M. Watanabe y D. G. York, The Astronomical Journal **122**, 3 (sep 2001).

[61] M. Doi, M. Fukugita y S. Okamura, Monthly Notices of the Royal Astronomical Society **264**, 4 (oct 1993).

[62] O. Lahav, A. Naim, L. Sodre Jr y M. C. Storrie-Lombardi, Monthly Notices of the Royal Astronomical Society **283**, 207 (1996).

[63] R. G. Abraham, F. Valdes, H. K. C. Yee y S. van den Bergh, The Astrophysical Journal **432**, 75 (sep 1994).

[64] A. Sandage (1961).

[65] J. H. J., Nature **138**, 3499 (nov 1936).

[66] G. De Vaucouleurs, Symposium - International Astronomical Union **58**, 1 (aug 1974).

[67] A. Sandage, The Astrophysical Journal **202**, 563 (dec 1975).

[68] J. Kormendy págs. 113–288. (1982).

[69] S. van den Bergh, *Galaxy Morphology and Classification* (Cambridge University Press, Cambridge, England, 1998).

[70] M. S. Longair, *Galaxy Evolution - Longair*, Vol. 36 (2011).

[71] L. W. Marco Barden, Hans-Walter Rix, Rachel S. Somerville, Eric F. Bell, Boris Hauler, Chien Y. Peng, Andrea Borch, Steven V. W. Beckwith, John A. R. Caldwell, Catherine Heymans, Knud Jahnke, Shardha Jogee, Daniel H. McIntosh, Klaus Meisenheimer, Sebastian F. S y C. Wolf, Astrophysical Journal **635**, 959 (dec 2005).

[72] D. H. McIntosh, E. F. Bell, H.-W. Rix, C. Wolf, C. Heymans, C. Y. Peng, R. S. Somerville, M. Barden, S. V. W. Beckwith, A. Borch, J. A. R. Caldwell, B. Hausler, K. Jahnke, S. Jogee, K. Meisenheimer, S. F. Sanchez y L. Wisotzki, The Astrophysical Journal **632**, 1 (oct 2005).

[73] I. Trujillo, I. Ferreras y I. G. de la Rosa, Monthly Notices of the Royal Astronomical Society **415**, 4 (2011).

[74] I. Damjanov, P. J. McCarthy, R. G. Abraham, K. Glazebrook, H. Yan, E. Mentuch, D. Le Borgne, S. Savaglio, D. Crampton, R. Murowinski, S. Juneau, R. G. Carlberg, I. Jørgensen, K. Roth, H. W. Chen y R. O. Marzke, Astrophysical Journal **695**, 1 (2009).

[75] C. Mancini, E. Daddi, A. Renzini, F. Salmi, H. J. McCracken, A. Cimatti, M. Onodera, M. Salvato, A. M. Koekemoer, H. Aussel, E. L. Floc'h, C. Willott y P. Capak, Monthly Notices of the Royal Astronomical Society **401**, 2 (jan 2010).

[76] R. J. Williams, R. F. Quadri, M. Franx, P. Van Dokkum, S. Toft, M. Kriek y I. Labbé, Astrophysical Journal **713**, 2 (2010).

[77] M. Franx, P. G. van Dokkum, N. M. F. Schreiber, S. Wuyts, I. Labbé y S. Toft, The Astrophysical Journal **688**, 2 (2008).

[78] S. R. Nagy, D. R. Law, A. E. Shapley y C. C. Steidel, Astrophysical Journal Letters **735**, 1 (2011).

[79] P. Cassata, M. Giavalisco, Y. Guo, A. Renzini, H. Ferguson, A. M. Koekemoer, S. Salimbeni, C. Scarlata, N. A. Grogin, C. J. Conselice, T. Dahlen, J. M. Lotz, M. Dickinson y L. Lin, Astrophysical Journal **743**, 1 (2011).

[80] E. Daddi, A. Renzini, N. Pirzkal, A. Cimatti, S. Malhotra, M. Stiavelli, C. Xu, A. Pasquali, J. E. Rhoads, M. Brusa, S. di Serego Alighieri, H. C. Ferguson, A. M. Koekemoer, L. A. Moustakas, N. Panagia y R. A. Windhorst, The Astrophysical Journal **626**, 2 (2005).

[81] Ignacio Trujillo, Natascha M. Förster Schreiber, Gregory Rudnick, Marco Barden, Marijn Franx, Hans-Walter Rix, J. A. R. Caldwell, Daniel H. McIntosh, Sune Toft, Boris Häussler, Andrew Zirm, Pieter G. van Dokkum, Ivo Labbé, Alan Moorwood, Huub Röttgering, y L. van Starkenburg, The Astrophysical Journal **650**, 18 (2006).

[82] I. Trujillo, C. J. Conselice, K. Bundy, M. C. Cooper, P. Eisenhardt y R. S. Ellis, Monthly Notices of the Royal Astronomical Society **382**, 1 (2007).

[83] S. Toft, P. van Dokkum, M. Franx, I. Labbe, N. M. Forster Schreiber, S. Wuyts, T. Webb, G. Rudnick, A. Zirm, M. Kriek, P. van der Werf, J. P. Blakeslee, G. Illingworth, H. Rix, C. Papovich y A. Moorwood, The Astrophysical Journal **671**, 1 (dec 2007).

[84] A. W. Zirm, A. van der Wel, M. Franx, I. Labbe, I. Trujillo, P. van Dokkum, S. Toft, E. Daddi, G. Rudnick, H. Rix, H. J. A. Rottgering y P. van der Werf, The Astrophysical Journal **656**, 1 (2007).

[85] F. Buitrago, I. Trujillo, C. J. Conselice, R. J. Bouwens, M. Dickinson y H. Yan, The Astrophysical Journal **687**, 2 (nov 2008).

[86] P. G. van Dokkum, M. Franx, M. Kriek, B. Holden, G. D. Illingworth, D. Magee, R. Bouwens, D. Marchesini, R. Quadri, G. Rudnick, E. N. Taylor y S. Toft, The Astrophysical Journal **677**, 1 (apr 2008).

[87] P. G. Van Dokkum, M. Kriek y M. Franx, Nature **460**, 7256 (2009).

[88] P. G. van Dokkum, K. E. Whitaker, G. Brammer, M. Franx, M. Kriek, I. Labbé, D. Marchesini, R. Quadri, R. Bezanson, G. D. Illingworth, A. Muzzin, G. Rudnick, T. Tal y D. Wake, The Astrophysical Journal **709**, 2 (feb 2010).

[89] M. Akiyama, Y. Minowa, N. Kobayashi, K. Ohta, M. Ando y I. Iwata págs. 1–28 (2007).

[90] E. R. Carrasco, C. J. Conselice y I. Trujillo, Monthly Notices of the Royal Astronomical Society **2259**, no (apr 2010).

[91] D. Szomoru, M. Franx, P. G. van Dokkum, M. Trenti, G. D. Illingworth, I. Labbé, R. J. Bouwens, P. A. Oesch y C. M. Carollo, The Astrophysical Journal **714**, 2 (may 2010).

[92] A. van der Wel, H.-w. Rix, S. Wuyts, E. J. McGrath, A. M. Koekemoer, E. F. Bell, B. P. Holden, A. R. Robaina y D. H. McIntosh, The Astrophysical Journal **730**, 1 (mar 2011).

[93] A. van der Wel, B. P. Holden, A. W. Zirm, M. Franx, A. Rettura, G. D. Illingworth y H. C. Ford **5**, 48 (2008).

[94] D. R. Law, C. C. Steidel, A. E. Shapley, S. R. Nagy, N. A. Reddy y D. K. Erb, The Astrophysical Journal **745**, 1 (jan 2012).

[95] V. Petrosian, Astrophysical Journal **209**, L1 (1976).

[96] L. C. MICHAEL R. BLANTON, JULIANNE DALCANTON, DANIEL EISENSTEIN, JON LOVEDAY, MICHAEL A. STRAUSS, MARK SUBBARAO, DAVID H. WEINBERG, JOHN E. ANDERSON, JR., JAMES ANNIS, NETA A. BAHCALL, MARIANGELA BERNARDI, J. BRINKMANN, ROBERT J. BRUNNER, SCOTT BURLES, G. R. K. FRANCISCO J. CASTANDER, ANDREW J. CONNOLLY, ISTVA N CSABAI, MAMORU DOI, DOUGLAS FINKBEINER, SCOTT FRIEDMAN, JOSHUA A. FRIEMAN, MASATAKA FUKUGITA, JAMES E. GUNN, G. S. HENNESSY, ROBERT B. HINDSLEY, DAVID W. HOGG, TAKASHI ICHIKAWA,

ZELJKO IVEZIC, STEPHEN KE, R. C. N. D. Q. LAMB, R. FRENCH LEGER, DANIEL C. LONG, ROBERT H. LUPTON, TIMOTHY A. MCKAY, AVERY MEIKSIN, ARONNE MERELLI, JEFFREY A. MUNN, VIJAY NARAYANAN, MATT NEWCOMB, C. S. SADANORI OKAMURA, RUSSELL OWEN, JEFFREY R. PIER, ADRIAN POPE, MARC POSTMAN, THOMAS QUINN, CONSTANCE M. ROCKOSI, DAVID J. SCHLEGEL, DONALD P. SCHNEIDER, KAZUHIRO SHIMASAKU, WALTER A. SIEGMUND, STEPHEN SMEE, YEHUDA SNIR, CHRIS STOUGHTON, N. Y. ALEXANDER S. SZALAY, GYULA P. SZOKOLY, ANIRUDDHA R. THAKAR, CHRISTY TREMONTI, DOUGLAS L. TUCKER, ALAN UOMOTO, DAN VANDEN BERK, MICHAEL S. VOGELEY, PATRICK WADDELL, BRIAN YANNY y D. G. YORK págs. 2358–2380 (2001).

[97] N. Yasuda, M. Fukugita, V. K. Narayanan, R. H. Lupton, I. Strateva, M. A. Strauss, Ž. Ivezić, R. S. J. Kim, D. W. Hogg, D. H. Weinberg, K. Shimasaku, J. Loveday, J. Annis, N. A. Bahcall, M. Blanton, J. Brinkmann, R. J. Brunner, A. J. Connolly, I. Csabai, M. Doi, M. Hamabe, S.-I. Ichikawa, T. Ichikawa, D. E. Johnston, G. R. Knapp, P. Z. Kunszt, D. Q. Lamb, T. A. McKay, J. A. Munn, R. C. Nichol, S. Okamura, D. P. Schneider, G. P. Szokoly, M. S. Vogeley, M. Watanabe y D. G. York, The Astronomical Journal **122**, 3 (sep 2001).

[98] G. Rodighiero, E. Daddi, I. Baronchelli, A. Cimatti, A. Renzini, H. Aussel, P. Popesso, D. Lutz, P. Andreani, S. Berta, A. Cava, D. Elbaz, A. Feltre, A. Fontana, N. M. Förster Schreiber, A. Franceschini, R. Genzel, A. Grazian, C. Gruppioni, O. Ilbert, E. Le Floch, G. Magdis, M. Magliocchetti, B. Magnelli, R. Maiolino, H. McCracken, R. Nordon, A. Poglitsch, P. Santini, F. Pozzi, L. Riguccini, L. J. Tacconi, S. Wuyts y G. Zamorani, The Astrophysical Journal **739**, 2 (oct 2011).

[99] F. Bigiel, A. Leroy, F. Walter, E. Brinks, W. J. G. de Blok, B. Madore y M. D. Thornley, The Astronomical Journal **136**, 6 (dec 2008).

[100] L. J. Tacconi, R. Neri, R. Genzel, F. Combes, A. Bolatto, M. C. Cooper, S. Wuyts, F. Bournaud, A. Burkert, J. Comerford, P. Cox, M. Davis, N. M. Förster Schreiber, S. García-Burillo, J. Gracia-Carpio, D. Lutz, T. Naab, S. Newman, A. Omont, A. Saintonge, K. Shapiro Griffin, A. Shapley, A. Sternberg y B. Weiner, The Astrophysical Journal **768**, 1 (apr 2013).

[101] P. Madau y M. Dickinson, Annual Review of Astronomy and Astrophysics **52**, 1 (aug 2014).

[102] R. C. Kennicutt **36**, 189 (1998).

[103] A. E. Bauer, N. Drory y G. J. Hill, Astrophysics and Space Science Proceedings **1**, 202409 (2007).

[104] F. Salmi, E. Daddi, D. Elbaz, M. T. Sargent, M. Dickinson, A. Renzini, M. Bethermin y D. Le Borgne, Astrophysical Journal Letters **754**, 1 (2012).

[105] A. A. Dutton, F. C. Van Den Bosch y A. Dekel, Monthly Notices of the Royal Astronomical Society **405**, 3 (apr 2010).

[106] P. S. Behroozi, C. Conroy y R. H. Wechsler, The Astrophysical Journal **717**, 1 (jul 2010).

[107] D. W. Hogg **1**, 3 (1999).

[108] T. Dahlen, B. Mobasher, S. M. Faber, H. C. Ferguson, G. Barro, S. L. Finkelstein, K. Finlator, A. Fontana, R. Gruetzbauch, S. Johnson, J. Pforr, M. Salvato, T. Wiklind, S. Wuyts, V. Acquaviva, M. E. Dickinson, Y. Guo, J. Huang, K. H. Huang, J. A. Newman, E. F. Bell, C. J. Conselice, A. Galametz, E. Gawiser, M. Giavalisco, N. A. Grogin, N. Hathi, D. Kocevski, A. M. Koekemoer, D. C. Koo, K. S. Lee, E. J. McGrath, C. Papovich, M. Peth, R. Ryan, R. Somerville, B. Weiner y G. Wilson, Astrophysical Journal **775**, 2 (2013).

[109] S. Weinberg, *Gravitation And Cosmology: Principles And Applications Of The General Theory Of Relativity* (1972).

[110] D. W. Weedman, *Cambridge astrophysics series Quasar astronomy* (1986).

[111] Phillip James Edwin Peebles, *Principles of Physical Cosmology .pdf* (1993).

[112] M. L. HUMASON, N. U. MAYALL y A. R. SANDAGE **61**, 181 (1956).

[113] J. B. Oke y A. Sandage **154** (1968).

[114] D. W. Hogg, I. K. Baldry, M. R. Blanton y D. J. Eisenstein págs. 1–5 (2002).

[115] J. B. Oke y J. E. Gunn **266**, 713 (1983).

[116] M. Giavalisco, H. C. Ferguson, A. M. Koekemoer, M. Dickinson, D. M. Alexander, F. E. Bauer, J. Bergeron, C. Biagetti, W. N. Brandt, S. Casertano, C. Cesarsky, E. Chatzichristou, C. Conselice, S. Cristiani, L. Da Costa, T. Dahlen, D. de Mello, P. Eisenhardt, T. Erben, S. M. Fall, C. Fassnacht, R. Fosbury, A. Fruchter, J. P. Gardner, N. Grogin, R. N. Hook, A. E. Hornschemeier, R. Idzi, S. Jogee, C. Kretchmer, V. Laidler, K. S. Lee, M. Livio, R. Lucas, P. Madau, B. Mobasher, L. A. Moustakas, M. Nonino, P. Padovani, C. Papovich, Y. Park, S. Ravindranath, A. Renzini, M. Richardson, A. Riess, P. Rosati, M. Schirmer, E. Schreier, R. S. Somerville, H. Spinrad, D. Stern, M. Stiavelli, L. Strolger, C. M. Urry, B. Vandame, R. Williams y C. Wolf, The Astrophysical Journal **600**, 2 (jan 2004).

[117] H.-w. Rix, M. Barden, S. V. W. Beckwith, E. F. Bell, A. Borch, J. A. R. Caldwell, K. Jahnke, S. Jogee, D. H. Mcintosh, K. Meisenheimer, C. Y. Peng, S. F. Sanchez, R. S. Somerville, L. Wisotzki y C. Wolf **152**, 163 (2004).

[118] R. A. Windhorst, S. H. Cohen, N. P. Hathi, P. J. Mccarthy, R. E. Ryan, H. Yan, I. K. Baldry, S. P. Driver, J. A. Frogel, D. T. Hill, L. S. Kelvin, A. M. Koekemoer, M. Mechtley, R. W. O. Connell, A. S. G. Robotham, M. J. Rutkowski, M. Seibert, A. N. Straughn, R. J. Tuffs, B. Balick, H. E. Bond, H. Bushouse, D. Calzetti, M. Crockett, M. J. Disney, M. A. Dopita, D. N. B. Hall, J. A. Holtzman, S. Kaviraj, R. A. Kimble, J. W. Mackenty, M. Mutchler, F. Paresce y A. Saha, Astrophysical Journal **27** (2011).

[119] M. Davis, P. Guhathakurta, N. P. Konidaris, J. A. Newman, M. L. N. Ashby, A. D. Biggs, P. Barmby, K. Bundy, S. C. Chapman, A. L. Coil, C. J. Conselice, M. C. Cooper, D. J. Croton, P. R. M. Eisenhardt, R. S. Ellis, S. M. Faber, T. Fang, G. G. Fazio, A. Georgakakis, B. F. Gerke, W. M. Goss, S. Gwyn, E. S. Laird, E. L. Floc, L. Lin, J. M. Lotz, P. J. Marshall, D. C. Martin y A. J. Metevier, Astrophysical Journal **660**, 1 (2007).

[120] N. Scoville, R. G. Abraham, H. Aussel, J. E. Barnes, A. Benson, A. W. Blain, D. Calzetti, A. Comastri, P. Capak, C. Carilli, J. E. Carlstrom, C. M. Carollo, J. Colbert y E. Daddi **172**, 38 (2007).

[121] A. M. Koekemoer, H. Aussel, D. Calzetti, P. Capak, M. Giavalisco, J. Kneib, H. J. Mccracken, R. Massey, B. Mobasher, A. Leauthaud, O. L. Fe, J. Rhodes, N. Scoville y P. L. Shopbell, Astrophysical Journal **172**, 196 (2007).

[122] A. Lawrence, S. J. Warren, O. Almaini, A. C. Edge, N. C. Hambly, R. F. Jameson, P. Lucas, M. Casali, A. Adamson, S. Dye, J. P. Emerson, S. Foucaud, P. Hewett, P. Hirst, S. T. Hodgkin, M. J. Irwin, N. Lodieu, R. G. Mcmahon, C. Simpson, I. Smail, D. Mortlock y M. Folger **1617**, 1599 (2007).

[123] M. Cirasuolo, R. J. Mclure, J. S. Dunlop, O. Almaini, S. Foucaud, I. Smail, K. Sekiguchi, C. Simpson, S. Eales, S. Dye, M. G. Watson, M. J. Page y P. Hirst **595**, 585 (2007).

[124] R. E. Williams, B. Blacker, M. Dickinson, W. V. D. Dixon, H. C. Ferguson, A. S. Fruchter, M. Giavalisco, R. L. Gilliland, I. Heyer, R. Katsanis, Z. Levay, R. A. Lucas, D. B. McElroy, L. Petro, M. Postman, H.-M. Adorf y R. Hook, The Astronomical Journal **112**, 1335 (oct 1996).

[125] A. Babul y M. J. Rees, Monthly Notices of the Royal Astronomical Society **255**, 346 (1992).

[126] D. H. W. JAMES S. BULLOCK,ANDREY V. KRAVTSOV, The Astrophysical Journal **20**, 140 (1993).

[127] A. E. Shapley, C. C. Steidel, M. Pettini, K. L. Adelberger y D. K. Erb, The Astrophysical Journal **651**, 2 (nov 2006).

[128] I. Iwata, A. K. Inoue, Y. Matsuda, H. Furusawa, T. Hayashino, K. Kousai, M. Akiyama, T. Yamada, D. Burgarella y J.-M. Deharveng, The Astrophysical Journal **692**, 2 (feb 2009).

[129] C. Stoughton, R. H. Lupton, M. Bernardi, M. R. Blanton, S. Burles, F. J. Castander, A. J. Connolly, D. J. Eisenstein, J. A. Frieman, G. S. Hennessy, S. Kent, P. Z. Kunszt, B. C. Lee, A. Meiksin, R. B. Hindsley, J. A. Munn, H. J. Newberg, R. C. Nichol, T. Nicinski, J. R. Pier, G. T. Richards, M. W. Richmond, D. J. Schlegel, J. A. Smith, M. A. Strauss, M. Subbarao, A. S. Szalay, A. R. Thakar, D. L. Tucker, D. E. V. Berk, B. Yanny, J. K. Adelman, J. E. Anderson, S. F. Anderson, J. Annis, N. A. Bahcall, J. A. Bakken, M. Bartelmann, S. Bastian, A. Bauer, E. Berman, H. Bo, W. N. Boroski, S. Bracker, C. Briegel, J. W. Briggs, J. Brinkmann, R. Brunner, L. Carey, M. A. Carr, B. Chen, D. Christian, P. L. Colestock, J. H. Crocker, P. C. Czarapata, J. Dalcanton, A. F. Davidsen, J. E. Davis, W. Dehnen, S. Dodelson, M. Doi, T. Dombeck, M. Donahue, N. Ellman, B. R. Elms, M. L. Evans, L. Eyer, X. Fan, G. R. Federwitz, S. Friedman, M. Fukugita, R. Gal, B. Gillespie, K. Glazebrook, J. Gray, E. K. Grebel, M. Haldeman, B. Greenawalt, G. Greene, J. E. Gunn, E. D. Haas, P. B. Hall, M. Hamabe, B. Hansen, F. H. Harris, H. Harris, M. Harvanek, S. L. Hawley, J. J. E. Hayes, T. M. Heckman, A. Helmi, A. Henden, C. J. Hogan, D. W. Hogg, D. J. Holmgren, J. Holtzman, C.-h. Huang, C. Hull, S.-i. Ichikawa, T. Ichikawa, D. E. Johnston, G. Kauffmann, R. S. J. Kim, T. Kimball, E. Kinney, M. Klaene, S. J. Kleinman, A. Klypin, G. R. Knapp, J. Korienek, J. Krolik, D. Q. Lamb, R. F. Leger, S. Limmongkol, C. Lindenmeyer, R. G. Kron, J. Krzesin, D. C. Long, C. Loomis, J. Loveday, B. Mackinnon, E. J. Mannery, P. M. Mantsch, B. Margon, P. Mcgehee, T. A. Mckay, B. Mclean, K. Menou, A. Merelli, H. J. Mo, D. G. Monet, O. Nakamura, V. K. Narayanan, T. Nash, E. H. Neilsen, P. R. Newman, A. Nitta, M. Odenkirchen, N. Okada, S. Okamura, J. P. Ostriker, R. Owen, A. G. Pauls, J. Peoples, R. S.

Peterson, D. Petravick, A. Pope, R. Pordes, M. Postman, A. Prosapio, T. R. Quinn, R. Rechenmacher, C. H. Rivetta, H.-w. Rix, C. M. Rockosi, R. Rosner, K. Ruthmansdorfer, D. Sandford, D. P. Schneider, R. Scranton, M. Sekiguchi, G. Sergey, R. Sheth, K. Shimasaku, S. Smee, S. A. Snedden, A. Stebbins, P. Szkody, G. P. Szokoly, S. Tabachnik, C. Stubbs, Z. Tsvetanov, A. Uomoto, M. S. Vogeley, W. Voges, P. Waddell, S.-i. Wang, M. Watanabe, D. H. Weinberg, R. L. White, S. D. M. White, B. Wilhite, D. Wolfe, N. Yasuda, D. G. York, I. Zehavi, W. Zheng y S. E. T. Al págs. 485–548 (2002).

[130] S. J. E. GUNN, CARR, ROCKOSI, M. M.C. SEKIGUCHI, BERRY, ELMS, DE HAAS, Z‹.IVEZIC, KNAPP, LUPTON R., K. B. E. G. G. PAULS, Astronomical Journal págs. 3040–3081 (1998).

[131] S. D. P. Fukugita M. , Ichikawa T, Gunn J. E. , Doi M., Shimasaku K. **111**, 4 (1996).

[132] D. W. Hogg, D. P. Finkbeiner, D. J. Schlegel y J. E. Gunn (2001).

[133] J. A. Smith, D. L. Tucker, S. Kent, M. W. Richmond, M. Fukugita, T. Ichikawa, S.-i. Ichikawa, A. M. Jorgensen, A. Uomoto, J. E. Gunn, M. Hamabe, M. Watanabe, A. Tolea, A. Henden, J. Annis, J. R. Pier, T. A. McKay, J. Brinkmann, B. Chen, J. Holtzman, K. Shimasaku y D. G. York, The Astronomical Journal **123**, 4 (2002).

[134] G. R. K. Robert Lupton, James E. Gunn, Zeljko Ivezic **238** (2001).

[135] J. R. Pier, J. A. Munn y R. B. Hindsley, Data Processing págs. 1559–1579 (2003).

[136] E. Wright, Publications of the Astronomical Society of the Pacific **118**, 850 (2006).

[137] E. Bertin y S. Arnouts, Astronomy and Astrophysics Supplement Series **117**, 2 (jun 1996).

[138] G. Bruzual y S. Charlot, Monthly Notices of the Royal Astronomical Society **344**, 4 (2003).

[139] C. Maraston, Monthly Notices of the Royal Astronomical Society **362**, 3 (2005).

[140] C. Conroy y J. E. Gunn, Astrophysical Journal **712**, 2 (2010).

[141] P. Kroupa, Monthly Notices of the Royal Astronomical Society **322**, 2 (apr 2001).

[142] G. Chabrier págs. 763–795 (2003).

[143] E. E. Salpeter, The Astrophysical Journal **121**, 161 (jan 1955).

[144] D. Calzetti **20**, 682 (2000).

[145] J. A. Cardelli, G. C. Clayton y J. S. Mathis págs. 245–256 (1989).

[146] M. Kriek y C. Conroy, Astrophysical Journal Letters **775**, 1 (2013).

[147] B. M. Tinsley y J. E. Gunn, The Astrophysical Journal **203**, 1 (1976).

[148] G. Bruzual A. y G., The Astrophysical Journal **273**, 105 (1983).

[149] A. Renzini y A. Buzzoni (1986), págs. 195–235.

[150] Alberto Buzzoni, The Astrophysical Journal Supplement Series págs. 817–869 (1989).

[151] G. Bruzual A. y S. Charlot, The Astrophysical Journal **405**, 538 (mar 1993).

[152] G. Worthey **95**, 107 (1994).

[153] C. Maraston, Monthly Notices of the Royal Astronomical Society **300**, 3 (1998).

[154] C. Leitherer, D. Schaerer, J. D. Goldader, R. M. Gonza, L. E. Z. Delgado, D. F. O. O. Kune, D. Devost y T. M. Heckman, ApJS , 123 (1999).

[155] M. Fioc y B. Rocca-Volmerange **3**, 1996 (1997).

[156] A. Vazdekis, Astrophysics and Space Science **276**, 2-4 (1999).

[157] S. K. Yi, Y.-c. Kim y P. Demarque, Young págs. 259–261 (2003).

[158] R. Jimenez, J. MacDonald, J. S. Dunlop, P. Padoan y J. A. Peacock, Monthly Notices of the Royal Astronomical Society **349**, 1 (2004).

[159] D. L. Borgne, B. Rocca-Volmerange, P. Prugniel, A. Lancon, M. Fioc y C. Soubiran **897**, 881 (2004).

[160] R. P. Schiavon, The Astrophysical Journal Supplement Series **171**, 1 (2007).

[161] P. Coelho, G. Bruzual, S. Charlot, A. Weiss, B. Barbuy y J. W. Ferguson, Monthly Notices of the Royal Astronomical Society **382**, 2 (2007).

[162] C. Conroy, J. E. Gunn y M. White (2009).

[163] M. Mollá, M. L. García-Vargas y A. Bressan, Monthly Notices of the Royal Astronomical Society **398**, 1 (2009).

[164] R. Kotulla, U. Fritze, P. Weilbacher y P. Anders, Monthly Notices of the Royal Astronomical Society **396**, 1 (2009).

[165] S. Faber, Astronomy & Astrophysics **20**, 361 (1972).

[166] E. Bica, Astronomy & Astrophysics **195**, 76 (1988).

[167] C. Boisson, M. Joly, J. Moultaka, D. Pelat y M. S. Roos, Population (English Edition) **870**, 850 (2000).

[168] R. Cid Fernandes, L. Sodré, H. R. Schmitt y J. R. S. Leão, Monthly Notices of the Royal Astronomical Society **325**, 1 (2001).

[169] B. M. Tinsley, The Astrophysical Journal **222**, 14 (1978).

[170] C. Leitherer y T. M. Heckman, The Astrophysical Journal Supplement Series **96**, 9 (1995).

[171] G. Bruzual y S. Charlot, Bruzual.Org , version (2003).

[172] R. Cid Fernandes, A. Mateus, L. Sodré, G. Stasińska y J. M. Gomes, Monthly Notices of the Royal Astronomical Society **358**, 2 (2005).

[173] C. Conroy, Annual Review of Astronomy and Astrophysics **51**, 1 (aug 2013).

[174] S. Charlot y A. G. Bruzual, The Astrophysical Journal **367**, 126 (jan 1991).

[175] G. E. Miller y J. M. Scalo, The Astrophysical Journal Supplement Series **41**, 513 (nov 1979).

[176] P. Kroupa **X**, 1 (feb 2001).

[177] G. Kauffmann, T. M. Heckman, S. D. M. White, S. Charlot, C. Tremonti, J. Brinchmann, G. Bruzual, E. W. Peng, M. Seibert, M. Bernardi, M. Blanton, J. Brinkmann, F. Castander, I. Cs\textbackslash' abai, M. Fukugita, Z. Ivezic, J. A. Munn, R. C. Nichol, N. Padmanabhan, A. R. Thakar, D. H. Weinberg y D. York, Mon. Not. R. Astron. Soc **341**, December (2003).

[178] F. Mannucci y G. Cresci **1**, 1 (nov 2010).